Université Lille 1 - Sciences et Technologies

Laboratoire de Mécanique de Lille (UMR CNRS 8107)

Ecole Doctorale régionale Sciences Pour l'Ingénieur Lille Nord-de-France

Année 2016 - N° d'ordre : 42138

THESE

Pour obtenir le grade de

Docteur de L'Université Lille 1 - Sciences et Technologies

Discipline : Génie Civil

Présentée par

Taogen LIU

Étude expérimentale et interprétation micro-mécanique du comportement mécanique des argiles synthétiques

Soutenue publiquement le 04 Octobre 2016 devant le jury composé de :

M. Frederic SKOCZYLAS	**Président**
M. Albert GIRAUD	**Rapporteur**
M. Pierre DELAGE	**Rapporteur**
M. Marc MAINGUY	**Examinateur**
M. Wanqing SHEN	**Examinateur**
M. Wei WANG	**Examinateur**
M. JianFu SHAO, Professeur, Université Lille 1	**Directeur de Thèse**

Acknowledgement

This research work was carried out in the ER4 group at the Laboratoire de Mécanique de Lille (LML). I would like to express my deepest gratitude to all those people who have helped and encouraged me in the successful completion of my doctoral study.

First and foremost, I would like to give my most sincere appreciations to my supervisor, Prof. SHAO Jianfu, a respectable and resourceful scholar, who welcomed me in his lab, gave me the opportunity to develop this experience abroad, and made me further achieve more knowledges on my research field and also broaden my outlook. Over the past four years, with the help of his patient guidance, stimulating discussion and encouragement, I have obtained lots of research experience to successfully complete this thesis, which is also very useful for my future works.

I would like to thanks the members of jury: Mister President: SKOCZYLAS Frederic, Mister Rapporteurs: DELAGE Pierre and GIRAUD Albert, Mister Examiners: MAINGUY Marc, SHEN Wangqin and WANG Wei, to participate in the ceremony of my thesis defense.

Also I would like to express my thanks to Dr. XIE Shouyi and SECQ Jean. With their help, some technological problems commonly encountered into the experiment device can be quickly resolved so that the experimental works can be normally and orderly developed. Here I'd like to specially express my gratitude to Dr. XIE Shouyi to discuss with and teach me some very useful technical skill and experience in experiment.

I would like to express my appreciation to Dr. WANG Wei, my supervisor at my master period. He was the person to be willing to accept me as his student when I came to participate the Postgraduate Entrance Reexamine of Hohai University, and help me obtain the opportunity to contact my supervisor SHAO Jianfu. I'm very appreciate for him to only participate at my doctor thesis defense from China. I wish you will have a big success in your work and a happy family in your life.

I would like to thank ZENG Tao and his wife- WANG Fei, LIU Zaobao and his wife- XUE Dan, SHEN Wanqin, WU Qier, JIA Yun, BIAN Hanbin, ZHANG Xiaotian, HUANG Yun, YANG He, ZHEN Yuanyuan, ZHANG Yu, LI Minyao, ZHEN Lifeng, YAO Ci, LIANG Yue, CHEN Wei, HAN Bei, CAO Yajun. Their give me a lot of useful assistance to overcome those obstacles occurring at my research works and my daily life. I have to give more great appreciation to Dr. ZENG Tao, Dr. LIU Zaobao and SHEN Wanqin to help and guide me to obtain lots of experiences and skills to complete this work.

I would like to thank ZHANG Xiang and Zhang Yulong, my two colleagues in office D100. Many inspirations origin from chatting over a cup of coffee or tea with them.

With an amicable environment, I can focus more attentions on my research work.

I have to give a great appreciation to my family who are my father LIU Jinyi, my mother LI Shuying, my three sisters, LIU Hui, LIU Li and LIU Hongxia, and my twin sister LIU Taohong, for your unconditional support and encouragement during my academic career and my life. In this big family, I can truly feel your love and care in obscurity, which makes me have a happy childhood and teach me to how to be a successful man, to get into the complex society, and to teach me to cherish these person around me.

Most importantly, to my wonderful and pretty wife, LI Ling, and my cute son, LIU Hugo-Runqiu. We arrived at France together before four years ago. In my daily life, your tireless effort without any complaint make me have a warm family that give me enormous important helps to release my psychological stress and my physical tireless. You support my decision to study at abroad and stand with me at any time as I want. Your warm heart and your sincere love make me have an upward positive attitude to face everything that I have encountered. You make my life become more rich and colorful with our son birth. No words can express how grateful I am for your love and support. I would like to say that I love you forever, till the end of the world.

Last but not least, I would like to express my sincere gratitude to the Chinese Scholarship Council for providing financial support for my research and living expenses in France.

Thank you very much again…

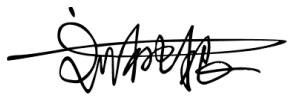

October 19, 2016 in Lille

Contents

Contents III

Résumé 1

Abstract 3

General introduction 5

Chapter 1 Synthetic clay obtained by consolidation at high range of pressure ... 11

1.1 Introduction 11

1.2 Materials 13

1.2.1 Illite 14

1.2.2 Sand 15

1.3 Experimental design 16

1.3.1 Mineralogical composition 16

1.3.2 Consolidation pressure 16

1.3.3 Compaction time 18

1.4 Development of high-pressure oedometer 19

1.4.1 Pneumatic pressure oedometer 20

1.4.2 Hydraulic pressure oedometer 21

1.5 Testing procedure 22

1.5.1 Preparation of remodeled synthetic clay 23

1.5.2 Consolidation procedure 24

1.6 Consolidation results.....25

1.6.1 Compaction deformation 25

1.6.2 Compaction modulus Es.....26

1.6.3 Porosity n.....28

1.6.4 Consolidation coefficient Cv 34

1.6.5 Permeability 35

1.7 Conclusion 38

Chapter 2 Hydro-mechanical behaviors of synthetic clay in triaxial compression 41

2.1 Introduction.....41

2.2 Sample characterization 43

2.3 Experimental methods 44

2.3.1 Triaxial testing equipment.....44

2.3.2 Experimental procedure 45

2.3.3 Permeability measurement.....46

2.4 Experimental results.....51

2.4.1 Mechanical behaviors 51

2.4.2 Permeability evolution 54

2.5 Discussion.....57

2.5.1 Mechanical behavior.....57

2.5.2 Volumetric strain evolution.....60

2.5.3 Permeability 63

2.6 Conclusions 64

Chapter 3 Laboratory investigation of synthetic clay for the offshore marine petroleum engineering-Angola 67

3.1 Introduction 67

3.2 Development of testing device 68

3.3 Preparation of synthetic clay 69

3.3.1 Mineralogical compositions 69

3.3.2 Consolidation test 69

3.4 Compression test 73

3.4.1 Oedometric test 74

3.4.2 Conventional triaxial compression 79

3.4.3 Conventional triaxial compression test after oedometric loading 82

3.4.4 Velocity of elastic wave 85

3.5 Conclusion 86

Chapter 4 Modelling of poromechanical behaviors of synthetic clay 89

4.1 Introduction 89

4.2 Micromechanical-based macroscopic model 90

4.3 Identification of model parameters 94

4.3.1 Physical parameters 95

4.3.2 Elastic parameters 95

4.3.3 Plastic parameters 96

4.4 Parameter sensitivity analyzation 96

4.4.1 Macroscopic yield criterion 96

4.4.2 Stress-strain responses and strength properties 100

4.5 Experimental validation 102

4.5.1 Synthetic clays--"*Gx"* 103

4.5.2 Synthetic clays--"*Tx"* 108

4.6 Conclusion 113

Chapter 5 Conclusions and Perspectives 115

5.1 General conclusions 115

5.2 Perspectives 117

Appendix 1: Representative consolidation curves for the synthetic clays "*GxNx*" 119

Appendix 2: Consolidation coefficient for synthetic clays "*GxNx*" 121

Appendix 3: Representative photos for the synthetic clays "*GxNx*" after consolidation test 122

Appendix 4: Photos of the synthetic clay "*Gx*" through *SEM* 123

Appendix 5: Photos of the synthetic clay "*Gx*" through *CT* scan 125

References 127

Résumé

La roche argileuse, constitué par des minéraux comme l'argile, le quartz et la calcite, etc., est un milieu poreux typique sous enquête dans le monde entier dans l'ingénierie pétrolière, le stockage souterrain de déchets et de la science de l'exploitation minière. Il est important de caractériser les roches argileuses par des approches multi-échelles depuis son comportement mécanique et les propriétés physiques sont étroitement liées à la microstructure et les compositions minéralogiques. La présente thèse est consacrée à l'enquête micromécanique des argiles synthétiques artificielles obtenues par des essais de consolidation à haute pression dans le laboratoire avec la composition minérale et de la porosité sous contrôle pour réduire au minimum l'affection de la complexité des microstructures comme dans la nature argilo roches. essais de compression triaxiale avec des cycles de chargement-déchargement sont effectuées pour caractériser les comportements mécaniques et les propriétés de transport des fluides des argiles synthétiques. Le dispositif et les méthodes expérimentales développées sont ensuite utilisées pour caractériser la couche de roche argileuse morts-terrains dans une ingénierie pétrolière en Angola. Les données expérimentales permettent enfin l'application et la validation d'un modèle constitutif micromécanique à base de caractériser et de prédire les comportements mécaniques des argiles synthétiques.

Mot-clé: argile synthétique; consolidation; essai de compression triaxial; chemin de chargement; mesure d'ondes ultrasonores; mécanismes de déformation; modèle micromécanique

Abstract

Clayey rock, constituted by such minerals as clay, quartz and calcite, etc., is a typical porous medium under investigation worldwide in petroleum engineering, underground waste storage and mining science. It is important to characterize the clayey rocks by multi-scale approaches since its mechanical behavior and physical properties are closely related to its microstructure and mineralogical compositions. The present thesis is devoted to micromechanical investigation of the man-made synthetic clays obtained by high pressure consolidation tests in laboratory with mineral composition and porosity under control to minimize the affection of microstructural complexity as in nature clayey rocks. Triaxial compression tests with loading-unloading cycles are carried out to characterize both the mechanical behaviors and fluid transport properties of the synthetic clays. The developed experimental device and methods are then used to characterize the overburden clayey rock layer in a petroleum engineering in Angola. The experimental data finally allow the application and validation of a micro-mechanics based constitutive model to characterize and predict the mechanical behaviors of the synthetic clays.

Keyword: synthetic clay; consolidation; triaxial compression test; loading path; ultrasonic wave measurement; deformation mechanisms; micromechanical model

General introduction

Clayey rock is a typical porous medium that have been under investigation worldwide in petroleum engineering, underground waste storage and mining science. For example, clayey rocks are usually served as the cap rock in petroleum engineering and mining engineering, and to act as the hosted reservoir rock for shale gas development. In underground radioactive waste disposal, clayey rocks also serve as the geological barriers in many countries in Europe. Especially in the French and Belgium concept, it also works as an engineering material together with the waste canister to constraint the radioactive wastes in the buffer. Due to these applications, it is very necessary to give a complete investigation of the physical and mechanical properties of clayey rocks.

The clayey rock is a porous heterogeneous material constituted by such minerals as clay, quartz and calcite, etc (Robinet et al., 2012). Its mechanical behavior and physical properties are closely related to its microstructure and mineralogical compositions. Thus, it is important to characterize the clayey rocks by multi-scale approaches (Zhang, 2011; Bai et al., 2013; Shen et al., 2012 and 2013; Shen and Shao, 2016a; Abou-Chakra et al., 2009; Shen, 2011). Towards this direction, former attempts have been made and achievements have been reported both in constitutive modeling and experimental characterization of the clayey rocks by multi-scale methods. Those achievements have confirmed that the multi-scale methods are promising and executable in approaching the clayey rocks. The micromechanical models can take into account the microstructural and mineralogical characteristics of porous media and thus can give a reasonable prediction of the mechanical behaviors of the clayey rocks in question. However, since the clayey rock is a nature raw material, its microstructures and mineralogical compositions are divergent and complex due to the variation of the sedimentary history and field geological evolutions. These nature complex properties cause uncertainty in calibrating and verifying the micromechanical models. In these circumstances, well-controlled laboratory experiments are necessary to obtain data for calibration and verification of micromechanical models.

The present doctoral thesis is devoted to producing synthetic clayey rocks in laboratory with mineralogical composition and porosity under control, and characterizing the physical properties and mechanical behaviors in order to calibrate and verify the developed micromechanical models. Within this purpose, a high pressure oedometer device is firstly developed to realize the high-pressure consolidation process at great depth beneath the earth. The effect of mineral composition is also investigated in laboratory to take into account the mineralogical variations with depth in the clay formation. Then, an auto-servo and -compensational hydro-mechanical testing system is developed to characterize the mechanical and transport properties of the synthetic clay. Afterwards, a specific mineral composition and testing condition is designed similar to the in situ conditions of an Angola reservoir to obtain the synthetic clay and

to investigate its physical and mechanical behaviors as well as the variation of passing-through ultrasonic wave velocities with its mechanical states. Finally, a micro-mechanical based numerical modeling is realized and verified on the mechanical behaviors of the synthetic clay. The following gives a general introduction of the present thesis.

In Chapter 1, consolidation of synthetic clay is investigated by a self-developed high-pressure oedometer. Originated from the consolidation theory (Terzaghi, 1943; Rendulic, 1935; Biot, 1941 & 1943), various experimental investigations have been reported on the determinations of consolidation properties in soils (Devapriya et al, 1976; Skempton 1969; Hamilton, 1976; Vasseur, 1995; Di Maio et al., 2004; Dutta and Mishra, 2015; Lee and Schackelfor, 2005; Hossam et al., 2009; Marcial et al., 2002; Bai and Su, 2012; Park et al., 2016) and the consolidation theory have been progressively enriched (Donald, 1940; Biot, 1955; Monte and Krizek, 1976; Coussy, 1995; Bennethum, 1997; Chen, 1997). A great majority of contributions so far have focused on low stress consolidation (σ_v <1MPa). Very few data are available for σ_v greater than 5MPa (Brooker and Ireland, 1965; Karig and Hou, 1992; Shang et al., 2014; Ferrari and Laloui, 2013). Moreover, the microscopic characteristics of soil are much less investigated such as the mineral composition and distribution, pore properties, size and shape of particle or aggregate, and so on. At the same time, it is well known that the compaction and permeability properties of soil (undisturbed soil and synthetic clay) are intensively depended on mineralogical compositions (De Magistris et al, 1998; Malkawi et al., 1999; Lado and Ben-Hur, 2004; Lee and Shackelfor, 2005; Mishra et al., 2011). With these considerations, a specific high-pressure consolidation device is developed to realize high pressure consolidation of synthetic clay to simulate consolidation process of clay formation deep in the earth taking into account effect of the mineralogical variations.

The “Argiles du Bassin Mediterraneen” (ABM) illite and GA39 sand are used as the mineral composition of the synthetic clay. Five mass proportion between sand and illite are chosen to investigate the influence of mineral composition on consolidation properties of synthetic clay. According to the slurry mixture method, the added content of saline water is suggested to be closed to the liquid limit of the mixture. With the help of the “VMI” device, the synthetic clay in slurry can be obtained. Then, the slurry mixture is used to carry out the consolidation test with consolidation pressure of about 35MPa. The multistage loading scheme is adopted, and the compaction time for each stage of consolidation is chosen as the time for completion of primary consolidation. Two developed oedometric devices are designed, and their individual characteristics are introduced in detail. The compaction deformation of synthetic clay at each stage of consolidation are discussed. The influence of mineral composition on consolidation properties are also discussed, such as consolidation coefficient, compaction modulus, permeability and porosity. It is found that the compaction modulus of synthetic clay

commonly increases with increase of consolidation pressure and is related to mineral composition. The porosity decreases with increase of consolidation pressure. The total reduction of porosity of synthetic clay is strongly dependent on mineral composition. The optimum (lowest) porosity of synthetic clay progressively transfers from the synthetic clay "G5" with a high content of sand to the synthetic clay "G2" with a low content of sand with increase of consolidation pressure.

In Chapter 2, mechanical behavior and permeability of these consolidated synthetic clays are investigated by a self-developed auto-servo and auto-compensational hydro-mechanical coupled testing system. Mechanical and transport behaviors of clayey rocks have been widely investigated worldwide by laboratory tests. It has been confirmed that for clayey rocks or soils, mineral composition and water content have great influence on mechanical behavior of clayey material (Zhang, 2011; Zhang et al., 2012; Hu et al., 2014; Bornert et al., 2010; Sone and Zobak, 2010). Also, the mechanical and transport behaviors of clayey rock/soil are very sensitive to stress level (Badrul Alam et al., 2014; Liu et al., 2015 and 2016; Davy et al., 2007; Zhang and Rothfuchs, 2004; Monfared et al., 2011). Accordingly, we propose to investigate the mechanical behavior of synthetic clay by the hydro-mechanical coupled triaxial compression test. The triaxial testing equipment and experimental procedure are firstly introduced. Permeability of synthetic clay is also performed. The influences of confining pressure and mineral composition on mechanical behavior as well as permeability of synthetic clay are experimentally investigated and discussed. It is found that the mechanical behavior of synthetic clay strongly depend on confining pressure. Most synthetic clays present a perfectly plastic flow after a nonlinear hardening phase. There also exists a continuously plastic hardening characteristic for the synthetic clay with a relative high content of sand at a relatively high confining pressure. The mechanical behavior of synthetic clay is also considerably dependent on mineral composition. In common, the initial elastic modulus and strength of synthetic clay increases with increase of sand content as well as confining pressure. The volumetric strain of synthetic clay are associated to both confining pressure and mineral composition. The volumetric dilatancy is more important at low confining pressure than higher one. Finally, two plastic mechanisms are used to interpret the evolution of both volumetric strain and permeability of synthetic clay.

Chapter 3 is devoted to give a laboratory investigation for the offshore marine petroleum engineering in Angola. The current effective vertical pressure of the argillite interested and the mass proportion between clay phase mainly consisted of illite and another solid phases are chosen as the controlling index for preparation of synthetic clay, instead of porosity. The prepared slurry mixture is then used to carry out consolidation test to obtain the experimental material for the subsequent triaxial compression tests. The experimental results related to consolidation test is then briefly introduced. After that, those obtained synthetic clay samples are subjected to different

triaxial compression tests to investigate the dependency of mechanical behavior and microstructure evolution of synthetic clay on loading path and loading rate. Three types of triaxial compression tests are performed, which are the oedometric test, conventional triaxial compression test, and conventional triaxial compression test after oedometric loading, respectively. The velocities of P- and S-wave are also measured to give an indication to estimate the microstructural evolution of synthetic clay during loading process. Based on the experimental results obtained from the conventional triaxial compression test, the initial elastic modulus and strength of synthetic clay are strongly dependent on confining pressure as well as loading path. Comparing the experimental results obtained from the oedometric test with those of the conventional triaxial compression test, the mechanical behavior of synthetic clay depends on loading path and loading rate. At the same time, the evolutions of velocities of P- and S-wave are also dependent on confining pressure and loading path. In view of the experimental results obtained from the conventional triaxial compression test, the dependency of mechanical behavior and microstructure evolution of synthetic clay on loading path and confining pressure can be confirmed again. The difference of mechanical behavior such as strength, elastic modulus, ductility/brittleness and so on between the argillite and the synthetic clay is significant, which may be related to many effect factors, for instant, porosity, mineral composition, pre-consolidation pressure, physical-chemical action, etc.

As an extension of the above experimental investigations, Chapter 4 is devoted to using the above obtained experimental results for the synthetic clays to verify the suitability of the micromechanical-based macroscopic elastoplastic criterion. The development of micromechanics, which is originally applied to composite materials, provides a rigorous mathematical framework to translate microscopic properties of each composite phases, through homogenization theories, into macroscopic constitutive relations of mass transport phenomena and poromechanical deformation of porous media (Auriault and Sanchez-Palencia, 1977; Dormieux et al, 2003; Shen and Shao, 2016b; Shen et al, 2013; Zeng et al., 2014; Ghorbandeigi et al, 2016). In view of those proposed micromechanical model, the influences of microstructure properties such as mineral composition, porosity and discontinuous surface on mechanical behavior of material can be taken into account. Consequently, a micromechanical-based model proposed by Shen et al. (2013) is used to reproduce or predict the mechanical behavior of the synthetic clays in the former experimental programs. A brief introduction on the model is given, accompanied with an in-detail illustration on parameter identification. Based on the model, the influence of both mineral composition and pore on mechanical behavior of material can be reflected through the two modelling parameters: porosity and volumetric fraction of effective inclusion, which are explicitly contained into the macroscopic yield criterion. It is particularly observed that the plasticity criterion is more sensitive to porosity than volumetric fraction of inclusion, combined with the discussion on parameter sensitivity analyzation. Comparisons between the model

predictions and experimental results show that the model can't well reproduce the mechanical behavior of the synthetic clays studied with consideration on mineral composition, porosity and loading path. In the light of the observation on the two microphotographs obtained from two different synthetic clay samples, the assumption on porosity adopted by the model is incorrect for these synthetic clays. Some discussion on the model are detailed narrated in this Chapter. Finally, it's necessary in next work to propose a more suitable micromechanical model to take into account the mechanical behavior of synthetic clay with different loading paths, different mineral composition, and different porosity at different scales. At present, instead of proposing a more suitable yield criterion with consideration on the above mentioned considerations, the model with some simple improvements such as a non-unique set of parameters identified from the experimental result of the oedometric test, a unique clay matrix porosity for the five synthetic clays without consideration on meso-pore is used to reproduce the mechanical behavior of the synthetic clays studied.

Finally, in Chapter 5, some general conclusions are made based on the findings of the doctoral thesis. Also, some perspectives on future work are given closely related to the problems raised throughout the research to well further the study of synthetic clay.

Chapter 1 Synthetic clay obtained by consolidation at high range of pressure

1.1 Introduction

The argillaceous materials commonly manifest not only a large compressibility but also a low permeability. Significant interests to investigate the physical-mechanical properties of both undisturbed/remodeled clay soils and synthetic clay composites have been concentrated by lots of scholars to analyze and resolve some practical problems with relevant to application of geotechnical engineering such as geological disposal of radioactive nuclear waste, exploitation of gas/petroleum, mining science and foundation treatment. Enormous research achievements on these materials have been obtained experimentally since recent several decades. The great majority of these contributions have mainly focused on investigating both the basically physical properties and the compaction/swelling behaviors of these argillaceous materials, and these properties of this type of material show a complex correlation with some factors such as mineral composites, temperature, degree of saturation, pore fluid composition, consolidation pressure and so on.

For instant, experimental studies show that the pore liquid composition has a significant effect on the volumetric change on bentonites by several researchers (Di Maio et al, 2004; Lee and Shackelford 2005; Dutta and Mishra, 2015; Yilmaz and Marschalko, 2014), and the change is mainly related to the interaction between clay mineral and cation. An increase in pore solution concentration causes a reduction in compressibility of both artificial mixtures and natural soils reconstituted through the work performed by Di Maio et al. (2004) and the effect is intrinsically depended on the type of clay mineral. Various attempts to analyze the effects of exchangeable cations on the volume change properties of engineered clay barriers have been based on the diffuse double layer theory, as proposed in the pioneering works of Bolt (1956), and Sridharan and Jayadeva (1982).

Apart from that, the pore liquid composition has been confirmed to have a remarkable influence on the hydraulic conductivity of clay material (Lee and Shackelfor, 2005; Scalia et al, 2013; Xue et al, 2012; Mishra et al, 2011 and 2009; Shackelford et al, 2010; Ahn and Jo, 2009). Among of them, some empirical expresses have been proposed to predict the hydraulic conductivity of clayey soils (Fan et al, 2014). A very interesting observation obtained from Lee and Shackelfor (2005) has shown that the difference in hydraulic conductivity for two geosynthetic clay liners respectively containing a high and low qualities of bentonite firstly decrease and then increase significantly with increasing concentration of calcium chlorite solution relative to that based on water

taken as the penetration media. The effect of the salt in the pore liquid composition on the properties of the bentonites depends on the salt type, salt concentration and initial compaction condition of clay material.

As the activity of cation in solution are sensitive to the change of temperature, whereas the activity of cation affects the action of exchange of cation. Delage et al. (2000) have studied the effect of temperature on consolidation coefficient, thermal flows and hydraulic conductivity of boom clay, and observed that the consolidation does not change significantly with increased temperature through fast heating test due to the opposite effect of increasing permeability and decreasing porosity, and the hydraulic and thermal transfers are uncoupled, finally, a unique relationship between the intrinsic permeability and the porosity is established with no dependence on temperature. Hossam et al. (2005, 2007, 2009) have systematically studied the influence of heat on thermal conductivity, thermal consolidation, thermal induced volume changes and thermally induced excess pore water pressures under drained heating condition of soft Bangkok clay, and a full-scale embankment test is used to obtained the heat transfer results to assess the validity of their laboratory test results. Lots of studies concerned to the effect of heat on consolidation behavior have been progressively enriched to get in-depth knowledge in such aspect (Hupers and Kopf, 2009; Park et al, 2016; Kim et al, 2012; Bai and Su, 2012).

It should be stressed that the investigations on taking account of the consolidation pressure effect on argillaceous material is considered as the principally foundational subject in classical soil mechanics. Accordingly, abundant achievements on this topic have been acquired (Di Maio et al 2004; Li et al, 2006; Baille et al, 2010, Marcial et al, 2002, Li, 1999). In addition, some of them focus on trying to relate their macroscopic observations to the clays' microscopic properties, such as microstructure (Li et al 2006, Djeran-Maigre et al, 1998) and micro water-clay links (Bolt, 1956; Marcial et al, 2002; Tripathy and Schanz, 2007). Delage (2007) had studied systematically the results obtained by various authors by using most often scanning electron microscope observations, mercury intrusion pore size distribution measurements (MIP) and X-Ray diffractometry to interpret how the hydration mechanisms occurring at the level of the clay particles inside the aggregates help interpreting existing MIP data, and with the help of these techniques the microstructure of compacted bentonites is confirmed to be made up of aggregates with two classes of pores: inter-aggregates pore and intra-aggregate pores.

However, only a few consolidation compression tests of clays at pressure higher than 5.0MPa, which is approximately equivalent to the vertical stress at the depth of overburden layer of about 250m, have been reported so far (Shang et al, 2014; Marcial et al., 2002; Baille et al, 2010; Al-Mukhtar et al, 1999; Tripathy and Schanz, 2007; Karig and Hou, 1992; Ferrari and Laloui, 2013). Although almost all the above available studies also focused on the consolidation properties of natural clay material

with relatively high consolidation pressure (for instant, about 35MPa for Karig and Hou, 30MPa for Baille, 15MPa for Shang), few available data have been processed to investigate systematically the influence of proportion of mass among essential mineral compositions due to the difficulty or expensive investment for analyzation on clayey material studied. Meanwhile, there have lots of incontrollable factors for the natural argillaceous geomaterials and it's very impossible to control preciously and exactly some essentially physical characteristics for the studied materials. That gives rise to some unpredictable changes to disturbing the researching purpose.

Consequently, taking into account the above discussion, an extensional and further investigation on the evolution of synthetic clay material on a wide range of consolidation pressure, and the influence of mass proportion among various mineral compositions on consolidation properties of the synthetic clay materials are to be carried out. In the light of this, the one-dimensional consolidation tests are conducted on five different synthesis clay soils with high consolidation pressure of about 35MPa. The main works in this chapter are performed as follows.

The basically physical characteristics of two solid phases which are used to consist of the five types of synthetic clays are first presented. Afterwards, a testing program applied to conduct the high pressure consolidation test on these synthetic clays has been proposed, in which the maximal consolidation pressure has arrived at about 35MPa. The duration for each level of consolidation pressure is decided by the time where the primary consolidation of material has been completed. Based on the consolidation testing program proposed, two consolidation equipment have then been designed and their performances are introduced in detail. Subsequently, an additional procedure for how to prepare the synthetic clay is introduced. After that, the procedure about how to conduct the high pressure consolidation test is exhaustively elaborated. The relationship between settlement compaction with time at each level of consolidation pressure for the five different synthetic clays is listed and discussed.

In terms of experimental results, the characteristics related to the consolidation process of synthetic clay such as consolidation coefficient, compaction modulus, permeability and porosity are determined and discussed. Comparing these characteristics of these synthetic clays, the influence of composition (proportion of mass between sand and illite) on consolidation properties of these studied materials are discussed. Finally, some conclusions related to the multistage consolidation test are summarized.

1.2 Materials

Argillaceous rocks or soils can be considered as an abundant existence and wide distribution geomaterials in natural. Based on experimental investigations by means of the microscopic scanning technologies such as SEM, XRD, FIB, TEM (Robinet, 2006; Yven et al, 2007; Srodori et al, 2001) and chemical analyzation (Nyakairu et al, 2001),

they are commonly constituted of clay mineral, quartz, calcite and minor mineral, etc. Accordingly, as one of the three commonest clay minerals, illite is chosen to take the place of the clay minerals contained into the natural clayey rocks/soils in the preset research work, and the basic physical characters of illite will be then presented thereinafter.

Meanwhile, both calcite and quartz commonly exist in the form of either granule or aggregation dispersed into material. In present, in order to obtain a comprehensive knowledge on the mineral compositions of the synthetic material studied and for the reason of simplicity, the sand GA39 is then chosen as the substitution of both quartz and calcite without consideration on the remaining minor minerals such as oxide, in which the vast majority of mineral composition is quartz. The chosen sand with a specific granulometric distribution will be introduced in what follows.

It's well known that both the underground water and the surface water are not only composed of the distilled water, but they commonly contains various mineral salts. That's due to the existence of water-soil/rock interaction such as dissolution and hydration. However, the solution compositions contained inside the natural solute are very complex. Thus, it's difficult to prepare the chemical solution similar with the natural solution on the condition of experimental investigation at laboratory. With that in mind, the saline solution with concentration of sodium chloride being of 3.5% is firstly taken as the mixed solution for the preparation of the synthetic clay slurry to reduce the swelling effect of clay mineral. The concentration is set to be identical to that of sea water. The obtained experimental results which will be presented in the later section and chapter may be valuable for engineering application, especially for the offshore marine petroleum engineering.

1.2.1 Illite

Table 1.1 Basically physical properties of illite

<table>
<tr><td colspan="5">percentage of chemical compound in oxide form</td><td rowspan="5"></td><td colspan="2">particle</td><td>Liquid limit</td></tr>
<tr><td>SiO_2</td><td>Al_2O_3</td><td>Fe_2O_3</td><td>MgO</td><td>K_2O</td><td rowspan="3">Maximal diameter</td><td rowspan="3">Assumed density</td><td>0.46</td></tr>
<tr><td>45.6%</td><td>21.3%</td><td>7.8%</td><td>3.5%</td><td>5.7%</td><td></td></tr>
<tr><td>CaO</td><td>TiO_2</td><td>Na_2O</td><td>MnO</td><td>P_2O_5</td><td></td></tr>
<tr><td>5.5%</td><td>0.9%</td><td>0.4%</td><td>0.06%</td><td>0.3%</td><td>$45um$</td><td>2.7 g/cm^3</td><td></td></tr>
</table>

The illite is provided by the company "Argiles du Bassin Mediterraneen" abbreviated as ABM. The illite has been dried through a rotational tempered steel dryer heated by gas and the temperature does not surpass 100℃. It has been packed into a sealed bag with weight being of 25Kg. The diameter of the powdery particle is less than 45μm. The major chemical compounds in oxide form and the percentage of weight among them are shown into Table 1.1. The chemical formula of the illite is expressed as

$(K, H_3O)Al_2(SiAl)O_{10}(H_2O, OH)_2$. However, the density of the illite can't be found from the furnished technical document, whereas, an indirectly calculated density is given through the dried test, which will be presented below.

1.2.2 Sand

The sand employed is the GA39 sand produced by the company SIBELCO, which is mainly consisted of the following mineral compositions in oxide form: $SiO_2(98.81\%)$, $Al_2O_3(0.478\%)$, $K_2O(0.283\%)$, $CaO(0.014\%)$, $Fe_2O_3(0.035\%)$. The percentage of weight for each oxide expressed into the parentheses represents its average value. The average particle gradation can be obtained through screening test with seven different sieves mesh sizes: 250, 200, 160, 125, 100, 80, 74μm. The refusal curve shown in Figure 1.1 can be modeled by a logarithmic normal distribution function of grain size (Blondel, 2014).

$$f(d) = \frac{1}{2} - \frac{1}{2} * erf\left(\frac{ln\left(\frac{d}{d_{50}}\right)}{S\sqrt{2}}\right) \tag{1.1}$$

in which the $d_{50} = 108\mu m$ represents the average diameter of grain and corresponds to the accumulative mass of the refusal or passable particles being equal to a half of mass of the sand used. And then, the $S = 0.25 \pm 0.02$ is the standard deviation, the symbol "*erf*" represents the error function.

The range of density of the sand grain locates into the interval $[2.63, 2.66] g/cm^3$. The Mohs hardness of it is about 7 and the apparent density under dry condition is identical to $1.5\ g/cm^3$.

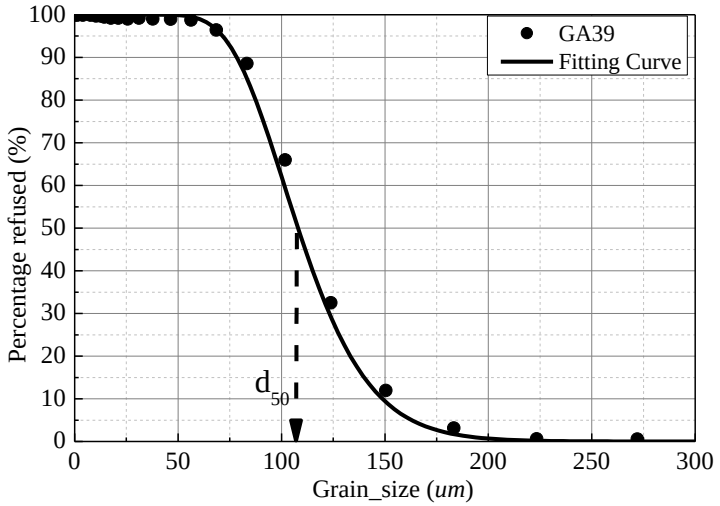

Figure 1.1 Grain-size distribution curve for the sand GA39 (SEBELCO)

1.3 Experimental design

1.3.1 Mineralogical composition

As we know, the time for completion of consolidation (primary consolidation and secondary consolidation) of soil depends, to a great extent, on the hydraulic conductivity of the soil studied. The hydraulic conductivity is directly related to the pores/cracks structure of soil. The structure is often dependent on mineral composition, apart from other factors. For example, when the content of sand increases, the permeability of synthetic soil can be in general significantly improved. The compaction deformation, compaction time, permeability, and pore properties such as pore size and distribution of soil, are also associated to mineral composition. Consequently, choosing a reasonable design on mass proportion among different mineral compositions for the preparation of synthetic clay is very important and useful for the application of geotechnical engineering. In order to take into account the variation of mineral composition in the clayey rock layer along with depth and to deeply investigate the effect of mineral composition on consolidation properties of synthetic clay, five different mass proportions between illite and sand are then chosen for the preparation of synthetic clay, which are 15:85, 30:70, 45:55, 60:40 and 75:25, respectively. In Table 1.3, the design on mass proportion among different mineral compositions for the five synthetic clays are listed.

Table 1.2 Proportion among sand, illite and saline water for the five different synthetic clays studied

Species	Mass proportion of composition
	fine sand : Illite : saline water (FS : IC : SW)
G1	15 : 85 : 50
G2	30 : 70 : 50
G3	45 : 55 : 50
G4	60 : 40 : 40
G5	75 : 25 : 40

1.3.2 Consolidation pressure

In the classical soil mechanics, the external surcharge per unit square meter for the consolidation test of soil at laboratory usually ranges from several kilo-newtons to thousands of kilo-newtons. Only for few super-high buildings, the additional load conducted on the subgrade soil/rock layer can reach to or over tens of thousands of kilo-newton per unit square meter. Meanwhile, the buried depth for some underground engineering structures such as the geological disposal of nuclear waste have reached over 1000m, where the crustal stress or gravity stress can arrive at several mega-pascal

or much higher. The gravity/crustal stress is significantly greater than those applied for the consolidation test in the classical soil mechanics. Accordingly, consolidation test at a large range of pressure should be performed to experimentally provide some available data for some special underground engineering. In view of the above considerations, the consolidation pressure is set to be up to 35MPa, the buried depth corresponding to such high pressure can be more than1000m.

Meanwhile, the prepared synthetic clay slurry which will be used to conduct the uniaxial consolidation test can be considered as one kind of porous synthetic composite with water content close to the liquid limit of the mixture. One remarkable feature of the slurry mixture is that it has a significant compressibility. Accordingly, if the consolidation pressure of 35MPa is conducted by only one-step, there may exist some unpredictable problems.

Technologically speaking, oedometric device must have enough stiffness to keep the imposed pressure be constant, even if the compaction deformation of the slurry mixture is significant. Moreover, in order to prevent the synthetic clay slurry excluding from consolidation chamber and blocking up the drainage passage of the permeable stone or the porous metal plate placed at both ends of the sample, the diameter for the permeable stone or the porous metal plate should be very small.

In the case of rapid loading for the consolidation pressure with a relatively high pressure, the excessive hydrostatic pore pressure has no sufficient time to dissipate, so that the liquefaction effect may occur. Due to the difference of the specific surface area between illite and sand particles, the liquefaction may lead to the delamination between sand and illite caused by the difference of buoyance between two solid phases.

According to the above-mentioned analyzations, it is very necessary to adopt the multistage loading scheme for the consolidation test of the prepared synthetic clay mixture at large range of pressure. The multistage loading scheme for the five different synthetic clays is presented in Table 1.2.

Table 1.3 Multistage loading scheme for uniaxial consolidation test

Species	Consolidation pressure(MPa)											
	S1	S2	S3	S4	S5	S6	S7	S8	S9	S10	S11	S12
G1	0.3	0.7	1.1	1.6	3.3	4.7	8.2	12.7	17.7	22.7	27.7	34.8
G2	0.3	0.7	1.1	1.6	3.3	4.7	8.2	12.7	17.7	22.7	27.7	34.8
G3	0.7	2.5	4.7	8.2	12.7	17.7	22.7	27.7	34.8			
G4	0.3	0.7	1.6	3.3	4.7	8.2	12.7	17.7	22.7	27.7	34.8	
G5	0.3	0.7	1.1	1.6	3.3	4.7	8.2	12.7	17.7	22.7	27.7	34.8

1.3.3 Compaction time

The compaction curves, i.e., $e - P_{cs}$ and $e - lg(P_{cs})$, are commonly used to analyze the compressibility of soil, where the P_{cs} is the consolidation pressure. The e is void ratio where the compaction deformation of soil due to the application of the consolidation pressure P_{cs} has completely finished. The compaction deformation can be commonly divided into two parts: one attributed to the primary consolidation and the other contributed to the secondary consolidation. Generally speaking, the time for completion of the secondary consolidation of soil, if the soil has, is significantly greater than the primary consolidation one. When the content of illite increases, the time for completion of the primary consolidation of synthetic clay will significantly increase, not to speak of the secondary consolidation.

Consequently, the compaction time of synthetic clay at each stage of consolidation is firstly chosen as the time to make sure that the primary consolidation of synthetic clay can be confirmed to have completed. The time is mainly determined based on the Taylor's method, i.e., the compaction deformation versus square-root coordinate axis of time curve ($\delta_{sc} - \sqrt{t}$) as shown in Figure 1.2. The δ_{sc} represents the compaction deformation, the t is the any time of consolidation process.

According to this method, it requires to identify the fitting line (L_1) to the initial linear portion on the curve of $\delta_{sc} - \sqrt{t}$. By means of the first interception point $\delta_{sc}^{0\%}$ of the fitting line L_1 with the vertical coordinate δ_{sc} and the slope k_{sc}^0 of the fitting line, the other fitting line (L_2), passing through the interception point $\delta_{sc}^{0\%}$ and with the slope of 1/1.15 times of that of the line L_1, i.e., $k_{sc}^{90} = k_{sc}^0/1.15$, is used to identify the second intersection point ($t_{90\%}$, $\delta_{sc}^{90\%}$) between the line L_2 and the compaction curve $\delta_{sc} - \sqrt{t}$, where the consolidation degree at this intersection point is of $U = 90\%$. The compaction deformation and the time for completion of primary consolidation can be then calculated. An important point is that the method gives a visualization of consolidation process as the test proceed. The schematic illustration about the method is shown in Figure 1.2.

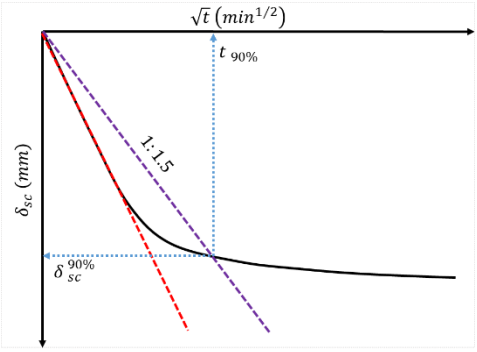

Figure 1.2 Schematic illustration of the Taylor's method

Alternatively, through the Taylor's method, the consolidation coefficient C_v can be calculated based on the following equation:

$$C_v = \frac{0.848 * H^2}{t_{90\%}} \quad (1.2)$$

where H represents the initial length of drainage path of sample. The H equals to $1/2\,H_0$ for the double-drainage condition and to H_0 for the one-drainage condition, in which the H_0 is the initial length of sample before application of the consolidation pressure. The $t_{90\%}$ corresponds to the time when the consolidation degree of sample has achieved to $U_{90\%} = 90\%$ as shown in Figure 1.2.

Secondly, for the five different synthetic clays studied, the time for completion of the primary consolidation corresponding to the same consolidation pressure differs from each one. Taking consolidation time-consuming into account, the mass proportion between sand and illite of 30:70 is firstly chosen as the reference standard to decide the compaction time for each stage of consolidation for the remaining four synthetic clays. On the one hand, only the content of illite inside the synthetic clay "*G1*", in which the mass proportion between sand and illite is 15:85, is higher than the reference "*G2*" one. The compaction time for each stage of consolidation for the synthetic clay "*G1*" is thus completely controlled based on the time for completion of the primary consolidation. On the other hand, for the three synthetic clays "*G3*", "*G4*" and "*G5*", the compaction time at the same level of consolidation pressure is made be identical to the reference one as much as possible, in order to make the compaction deformation of synthetic clay become less insignificant.

1.4 Development of high-pressure oedometer

As abundant experimental achievements on consolidation at low range of pressure have been obtained, therefore, consolidation pressure less than 0.1MPa is not paid our attentions. As mentioned in previous section, the consolidation pressure imposed on the synthetic clays is so high that the pressure should be carried out by the multistage loading scheme. Meanwhile, the compaction deformation of synthetic clay is very significant. Accordingly, the developed consolidation device should have the performance to maintain the applied pressure stability, and the device should also have an ability to provide a super-high pressure for consolidation test. Meanwhile, it is also very interesting to further investigate the mechanical behavior of the compacted synthetic clay with various loading paths at triaxial compression condition.

Consequently, a specific oedometric device differing from the classical oedometer is designed to satisfy the above-mentioned requirements. The device is made up of two separated independent parts, one is mainly used to perform the consolidation test with a relatively low consolidation pressure in order to keep the imposed pressure be

constant at overlarge deformation condition as shown in Figure 1.3, and the other is used to provide a super-high consolidation pressure at small deformation condition as shown in Figure 1.4. In what follows, the two devices are introduced in detail, respectively.

1.4.1 Pneumatic pressure oedometer

The pneumatic pressure oedometer is shown in Figure 1.3, which is a self-designed uniaxial consolidation device. The oedometer contains two identical and independent consolidation cells, each of which is composed of loading system, computer recording system, drainage seepage system, vacuum system and consolidation chamber.

The inner diameter of the consolidation chamber is about 37mm with the length of about180mm, and the maximal height of the filled-in sample can be arrive at about 110mm. The compaction deformation of sample is recorded by two *LVDT*s (*Linear Variable Differential Transformer*) with measurement range of 50mm and accuracy of 0.01mm, which are both mounted in parallel with the loading piston placed at the both ends of sample as shown in Figure 1.3. Inasmuch as the *LVDT* is placed outside, it's very convenient to adjust the *LVDT*, when the journey of it is insufficient to monitor the displacement of sample.

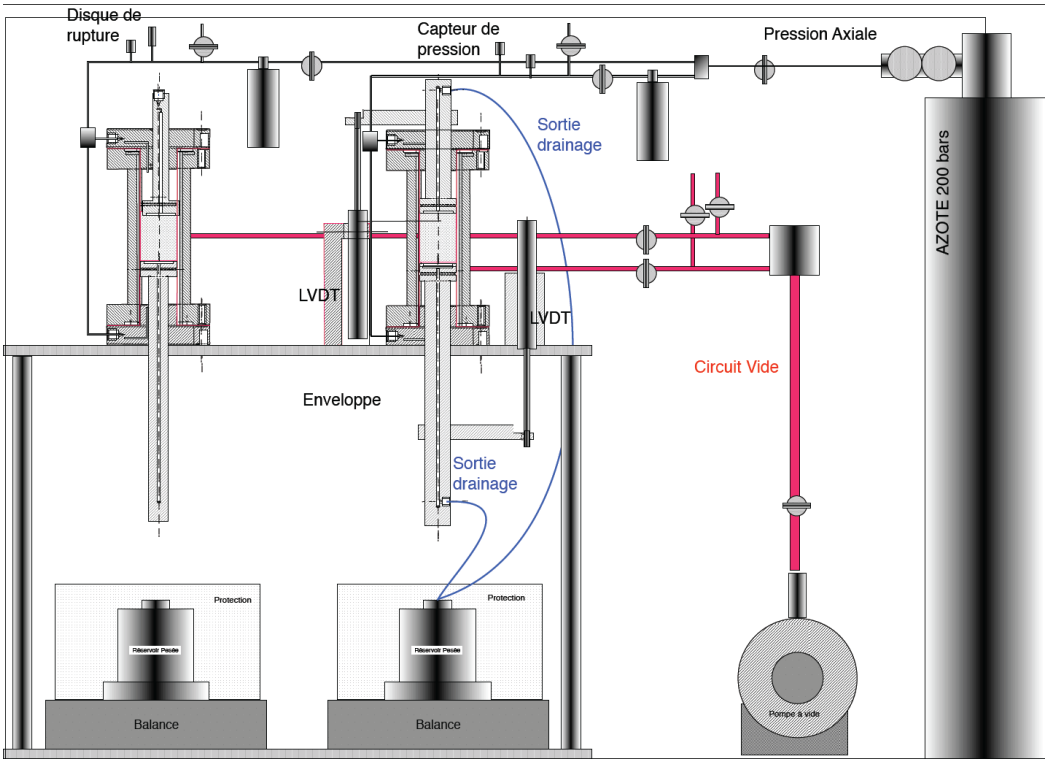

Figure 1.3 Schematic drawing of pneumatic pressure consolidation device

The consolidation pressure is provided through a gas steel cylinder. The inner pneumatic pressure of an unused gas steel cylinder is common about 20MPa. A

pneumatic pressure regulator is installed at the outlet of the gas steel cylinder, which is used to regulate the output pneumatic pressure. The output pneumatic pressure is then imposed on one or two ends of sample. The pressure is surveyed through a gas pressure sensor with measurement range of 50MPa and accuracy of 0.1MPa.

The vacuum system is used to expel the air between the internal wall of the consolidation chamber and the rubber jacket in order to make the rubber jacket closely stick to the internal wall of the consolidation chamber. The main aim is to reduce the possibility of wrinkle of the rubber jacket during the compaction process. Since the wrinkle of rubber jacket can lead to consolidation test being unsuccessful.

The water expelled from sample can access into the drainage passage installed into the loading piston through numbers of fine drainage holes assembled at the end of the loading piston adjacent to the end of sample. The water is collected by a bottle. A balance is used to weigh the mass of the expelled water. In some cases, the evolution of mass of the expelled water can be used to indirectly evaluate the variation of porosity of sample during the consolidation process.

Due to reason that the consolidation pressure is provided by the gas steel cylinder, the imposed pressure can be thus maintained stability, even if the compaction deformation of sample is very large. That’s to say the pneumatic pressure oedometer has enough stiffness. However, the gas sealing problem of the device is not at present resolved well. When the pneumatic pressure imposed is more than 5.0MPa, the gas can infiltrate into the zone of consolidation chamber where the sample is placed. The leakage of gas into the consolidation chamber will lead sample to undergoing the desiccation. The initial complete saturated soil will become a partial saturated soil. Therefore, the consolidation test with consolidation pressure less than 2.5MPa is firstly chosen to carry out for the five synthetic clays by means of the device. The main objectives are to obtain a formed sample with a relatively low compaction deformation instead of a flowage sample.

After that, the formed sample is placed into the consolidation chamber of the hydraulic pressure oedometer in order to conduct the subsequent consolidation test with higher pressure, which will be immediately presented in next section.

1.4.2 Hydraulic pressure oedometer

The hydraulic pressure oedometer is shown in Figure 1.4, which is also a self-designed uniaxial consolidation device developed by the *LML* organism. The device is composed of loading system, computer recording system, drainage/seepage system and consolidation chamber.

The inner diameter of the compaction chamber is about 37mm but slight more than the pneumatic pressure one, and the length of the compaction chamber is about 140mm. The maximal height of the filled-in sample can be up to 100mm. The compaction deformation of sample is recorded through a *LVDT* with measurement range of 10mm

and accuracy of 0.01mm, which is mounted the loading piston parallel with axial direction of sample as shown in Figure 1.4. The *LVDT* is also placed outside and can be easily adjusted.

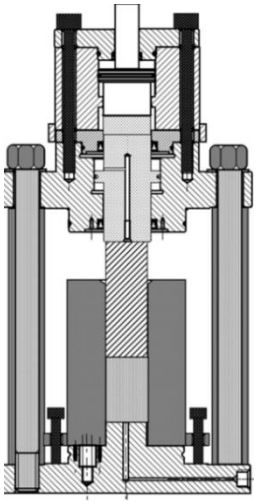

Figure 1.4 Schematic drawing of hydraulic pressure transmission consolidation device

The consolidation pressure is provided by the oil hydraulic pump Gilson®. The pump has a maximal capacity of generated pressure of 60MPa. The injected fluid of oil ranges from $5.0*10^{-4}$ to 5.0ml/min. The pump has the ability to elevate the hydraulic pressure to the desired value without an automatic servo-control function. The disadvantage of the pump can be overcome by manual operation in order to avoid the consolidation pressure excessing the desired value. The deviator chamber is used to transmit hydraulic pressure to mechanical pressure manifested through a loading piston. The deviator chamber can be also used as a constituted part of the triaxial compression testing device. For the consolidation device, the maximal consolidation pressure imposed on sample can reach to 100MPa. At present, the pressure is only imposed on one end of sample.

The water can be also expelled from the both ends of sample through the drainage passage of the pedestal and the interval between the internal wall of consolidation chamber and the loading piston. The advantage of the device is that it can provide a super-high consolidation pressure for consolidation test at small deformation condition.

1.5 Testing procedure

The consolidation testing procedure is not similar with the one in soil mechanics (Lambe, 1951). The whole testing procedure can be divided into two phases. The first phase is about the preparation of the synthetic clay slurry mixtures, and the second phase is associated to the consolidation test conducted on the slurry mixtures.

1.5.1 Preparation of remodeled synthetic clay

As mentioned before, five different synthetic clays are chosen to investigate the influence of mineral composition on consolidation properties of synthetic clay. Before we proceed to carry out consolidation test, the preparation of synthetic clay should be firstly done to obtain the material for consolidation test.

Based on the scheme on mass proportion among different mineral compositions as listed into Table 1.3, mass of the sand and the illite are weighted, and then they are placed into a stainless stock-pot without stirring. The slurry mixture method is adopted for the preparation of the synthetic clay slurry mixture, according to which the added content of saline water is suggested to be close to the liquid limit of the mixture. The mass proportion among the sand, illite and saline water for each type of synthetic clay is listed into Table 1.3.

We use the stirring apparatus to obtain the slurry mixture, and then the prepared slurry mixtures are used to conduct the uniaxial consolidation test. The stirring apparatus, named as the *VMI* laboratory mixture apparatus, is showed in Figure 1.5. It consists of a high performance motor with velocity varying from 50 to 3600rmp/min. The velocity of 250rmp/min is adopted to obtain the synthetic clay mixture.

Figure 1.5 VMI high-speed colloidal mixer

The mass of the synthetic clay mixture before and after the stirring test is measured in order to monitor the mass loss of water. The maximum of mass loss of water is less than 2.3g for all prepared synthetic clay mixtures. After that, the synthetic clay slurry with a known mass is applied to conduct the consolidation test, and then it is putted into the consolidation chamber of the pneumatic pressure oedometer. Based on the mass loss of

water, initial mass of sample and mass proportion, the mass of sand and illite contained into sample can be calculated. The initial mass of sample is listed into Table 1.4.

Table 1.4 Initial mass of each synthetic clay sample

Species	*G1*		*G2*		*G3*		*G4*		*G5*	
Sample	N01	N02	N01	N02	N01	N02	N02	N03	N01	N02
Mass (g)	199.2	204.5	187.3	180.6	219.7	180.8	241.1	235.0	218.7	213.3

After that, the sample is then applied to carry out the uniaxial consolidation test successively conducted on the pneumatic pressure oedometer and the hydraulic pressure oedometer. The consolidation procedure is introduced below.

1.5.2 Consolidation procedure

The consolidation test with low consolidation pressure is firstly performed on the pneumatic pressure oedometer. Except for the synthetic clay "*G3*", an initial consolidation pressure of 0.3MPa is applied, and then the consolidation pressure continuously increases with a constant augmentation of about 0.4MPa up to the value of 1.6MPa as listed into Table 1.2. After the primary consolidation of sample with the consolidation pressure of 1.6MPa has completed, the pneumatic pressure is removed step by step from the 1.6MPa to zero, until the rebounded deformation of sample becomes insignificant. The rebounded deformation of sample at each stage of unloading is also measured, which will be used to obtain the length of sample for each stage of consolidation and unloading by means of the back-calculated method.

The pre-consolidated synthetic clay sample is then taken out from the pneumatic pressure oedometer, and then the sample is placed into the consolidation chamber of the hydraulic pressure oedometer. In this device, the consolidation pressure also increases from 0.3 to 1.6MPa step by step as similar with the procedure performed on the pneumatic oedometer as much as possible. Such procedure is to get a close contact between the lateral surface of sample and the internal wall of consolidation chamber, and to make the sample with consolidation pressure of 1.6MPa at the hydraulic pressure oedometer be approximately identical to that at the pneumatic pressure oedometer. Subsequently, the consolidation pressure increases from 1.6 to 34.8MPa according to the designed project as listed in Table 1.2. The Vaseline is smeared around the internal wall of consolidation chamber of the two oedometers to reduce the friction as much as possible.

It can be seen that the loading scheme for the two samples "*G3N01*" and "*G3N02*" differs from those for the remaining samples, when the consolidation pressure is less than 4.7MPa. That's due to that we try to test the sealing capability of the pneumatic pressure consolidation device. When the pneumatic pressure arrives at 4.0MPa, the gas

leakage into sample occurs. In the case of the occurrence of gas leakage, the gas pressure is then immediately removed out till zero. After that, in the hydraulic pressure oedometer, the consolidation pressure of 1.6MPa is directly imposed on the two samples, and then augments to 4.7MPa.

1.6 Consolidation results

1.6.1 Compaction deformation

In this section, the curves of compaction deformation with square-root of time for each stage of consolidation, i.e., $\delta_{sc} - \sqrt{t}$, obtained from the sample "*G2N01*" (*FS:IC*=30:70), are shown in Figure 1.6. Meanwhile, the curves of compaction deformation versus logarithm of time are also shown in order to check whether the primary consolidation of sample for each stage of consolidation has completed or not again. Some parameters on consolidation properties of synthetic clay are determined only in terms of the Taylor's method. The comparison and difference between the two methods are not our research emphases. Both $\delta_{sc} - \sqrt{t}$ and $\delta_{sc} - lg(t)$ relationships for the five synthetic clays are presented in Figure.A. 1.

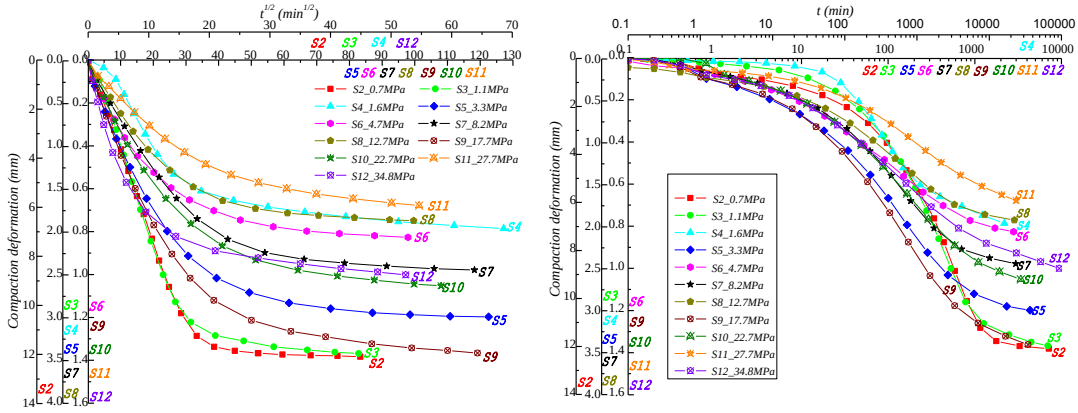

(a) Typical δ_{sc} versus $\sqrt{t}$ curves *(b) Typical δ_{sc} versus $lg(t)$ curves*

Figure 1.6 Compaction deformation-time curves for each stage of consolidation obtained from the sample G2N01: (a) Typical $\delta_{sc} - \sqrt{t}$ curves; (b) Typical $\delta_{sc} - lg(t)$ curves

From Figure 1.6, the primary consolidation of the synthetic clay "*G2*" can be confirmed to have completed. It can be seen that the time for completion of primary consolidation for most stages are within 3days. The compaction deformation for the first two stages "*S2*" and "*S3*", especially for the stage "*S2*", is obviously greater than the others, even if the increment of consolidation pressure has only had 0.4MPa considerably less than 2.0 or 5.0MPa. Such significant compaction deformation at the first two stages may be related to pore size and porosity of synthetic clay. In order to estimate the influence of mineral composition on consolidation properties and to investigate the evolution of compressibility of synthetic clay, the compaction modulus, porosity, consolidation coefficient and permeability are then discussed in the next several sections.

1.6.2 Compaction modulus E_s

In soil mechanics, the compaction modulus E_s is commonly used to estimate the compressibility of material, which is defined as the ratio of increment of stress $d\sigma_v$ with increment of strain $d\varepsilon_v$ under the complete confined compression condition. The calculation on the compaction modulus can be described as:

$$E_s = \frac{d\sigma_v}{d\varepsilon_v} = \frac{\Delta P_{cp}}{\frac{\Delta H}{H_0}} \tag{1.3}$$

where the $\Delta P_{cp} = P_{cp}^{i+1} - P_{cp}^{i}$ is increment of pressure; the $\Delta H = H_i - H_0$ is compaction displacement produced by the increment of pressure. The H_0 is the initial length of sample before the ΔP_{cp} is imposed, and the H_i represents the final length of sample where the compaction deformation of sample has fully finished.

In present, the measured compaction deformation corresponding to each stage of consolidation due to the increment of consolidation pressure is appropriately taken as the ΔH. The E_s for each stage of consolidation can be thus determined based on Eq.1.3, which represents its average value at the interval of consolidation pressure $[P_{cp}^{i},\ P_{cp}^{i+1}]$.

In Figure 1.7(a), we show consolidation pressure as a function of compaction modulus ($E_s - P_{cp}$) for the five synthetic clays. Meanwhile, for the sake of convenience for analyzation on the influence of mineral composition on compaction modulus, the evolutions of compaction modulus with sand content at the same consolidation pressure are also shown in Figure 1.7(b), in which the sand content is defined as the mass ratio between sand and the summation of sand and illite.

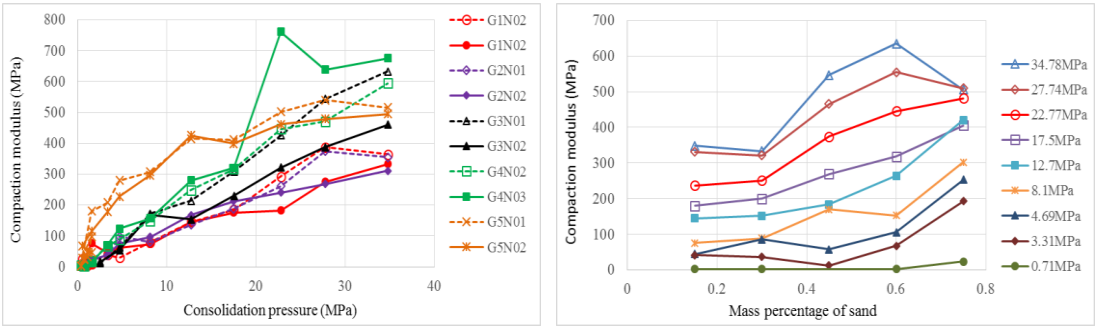

(a) Evolution of compaction modulus with consolidation pressure

(b) Evolution of compaction modulus with sand content

Figure 1.7 Evolution of compaction modulus: (a) with consolidation pressure; (b) with sand content

The following main remarks can be issued from Figure 1.7. Firstly, the compaction

modulus generally increases with increase of consolidation pressure. Secondly, the evolutions of compaction modulus with consolidation pressure obtained from the two samples classified into the same group are similar with each other, and the difference between them is not obvious. The abnormal point on the curve of compaction modulus with consolidation pressure for the sample "*G4N03*" at which the imposed consolidation pressure is 22.7 MPa is due to the mistake that the loading piston has reached to its journey (25mm) but the compaction deformation of the sample associated to the primary consolidation has not completed. Thirdly, the compaction modulus generally increases with increase of sand content. Fourthly, the influence of sand content on compaction modulus is simultaneously dependent on consolidation pressure. As the consolidation pressure increases, the maximum of compaction modulus occurs at the synthetic clay "*G5*" with sand content of 0.75 and then transforms to the synthetic clay "*G4*" with sand content of 0.6; and the minimum firstly appears at the synthetic clay "*G3*" with sand content of 0.45 and then transforms to the synthetic clay "*G1*" with sand content of 0.15, finally, towards to the synthetic clay "*G2*" with sand content of 0.3.

The evolution of compaction modulus can be interpreted through the following aspects: consolidation pressure; mineral composition; pore size and porosity; thickness of adsorbed water film.

In general, the pore size decreases with augmentation of content of clay mineral in material. Since the mixture solution and the mineral components contained into the five synthetic clays are fully identical with each one, the difference among the five synthetic clays is only caused by the mass proportion between sand and illite. Firstly, although the added content of saline water for the five synthetic clays is different among them, the effect of the content of saline water on the thickness of adsorbed water film around clay mineral particle can be ignored. The thickness of adsorbed water film can be considered to be controlled by the imposed external force and skeleton structure of material without consideration on any other effect factors such as temperature.

When the content of illite is more than a critical value, the skeleton structure of the synthetic clay can be then considered to be totally constructed by the clay phase. Accordingly, the compaction behavior of argillaceous soil is related to the pore compaction manifested through the expulsion of both the gravity water and the adsorbed water produced by the reduction of distance between two clay platelets, with a slight volume compaction induced by the re-arrangement of clay mineral particle. On the contrary, when the content of sand is more than another critical value, the skeleton structure of the synthetic clay can be then considered to be constructed by the sand phase. Accordingly, the compaction behavior of sandy soil is also related to the pore compaction manifested through the expulsion of gravity water mainly caused by the re-arrangement of sand particle, with few compaction contributed to the reduction of distance between two clay platelets. Between the two critical values, the skeleton

structure of synthetic clay can be then considered to be constructed by the two solid phases, and the dominance on skeleton structure of material controlled by sand or illite is up to the mass proportion between them.

Combined with the above discussions, after the pre-consolidation phase with consolidation pressure of 0.3MPa, the skeleton structure of synthetic clay can be considered to have formed, with a relatively large size of pore and high porosity where the influence of the resistant force related to the Van der Waal force on compaction of synthetic clay can be ignored. With further increase of consolidation pressure, taking the argillaceous material into consideration, when the pore size decreases to a certain value, the resistance force begins to have an effect on the compaction deformation of synthetic clay, especially for the synthetic clay with high content of illite. Before the value, the pore compaction is mainly attributed to the expulsion of gravity force and re-arrangement of clay particle. After that, as we know, the resistant force commonly increases in the form of exponential function with diminution of the distance between two clay platelets. The compaction will become more difficult so that the compaction modulus presents an accelerating/linear growth mode. However, for the sandy material at a relatively low consolidation pressure, the compaction deformation of material is less than the argillaceous material due to that it's more difficult to compact the skeleton structure constituted by the sand phase. With further increase of consolidation pressure, the area of contact surface between two sand particles increases progressively, that will lead to a non-linear increase of compaction modulus due to plastic deformation caused by the shear slip along contact surface and rotation of sand grain. When consolidation pressure is over than a critical value, the compaction attributed to the shear slip and rotation of particle becomes insignificant. That leads to the augmentation of the contact surface becoming inconspicuous. A role played by the adsorbed water film will become more and more important. Meanwhile, at the same consolidation pressure, especially for low pressure, the compaction deformation of synthetic clay is, to a great extent, dependent on its initial porosity or the pore size.

1.6.3 Porosity n

Geologists commonly quantify porosity-vertical stress relation by expressing porosity as a function of the buried depth from the earth surface (Athy,1934; Magara, 1980). Based on the distribution of weight per unit volume of overburden layer along with the vertical orientation, the vertical stress at arbitrary depth of underground can be thus approximately calculated.

In terms of initial void ratio e_0 and compaction deformation, the variation of void ratio of material can be determined by applying the following express:

$$e_1 = -\frac{\Delta H}{H_0}(1+e_0)+e_0\ , n_1 = \frac{e_1}{1+e_1} = \frac{(1+e_0)*\Delta H+e_0*H_0}{(1+e_0)*(\Delta H+H_0)} \qquad (1.4)$$

in which the e_1 is the void ratio where the compaction deformation of sample due to increment of pressure has completed.

It is impossibility to obtain the initial void ratio of sample, we approximately estimate the void ratio of sample at each stage of consolidation based on a back-calculated method. An assumed density for the illite mineral of about $2.7 g/cm^3$ is adopted. The density can be considered to be reasonable according to the dried test briefly illustrated below. Meanwhile, we consider that the compressibility of mineral particle can be ignored during the compaction process.

With the help of the dried test performed on some synthetic clays samples undergone triaxial compression, porosity of sample can be easily determined based on the mass difference of sample before and after the dried test, and sample's volume. Because the sample has been completely saturated through the constant head permeability test. Alternatively, with the incompressibility assumption on mineralogical particle, the porosity can be also determined by means of an estimated density for the illite mineral. Compared the two values on porosity obtained from the two methods, the density of the illite mineral can be determined. The obtained experimental results on pore volume for the four tested samples are listed into Table 1.5.

Table 1.5 Comparisons between the measured pore volume based on dried test and the estimated pore volume in terms of density

Sample	FS:IC	Wet mass (g)	Volume (mm^3)	Dry mass (g)	Pore volume (mm^3)	
					Drying test	density(2.7g/cm3)
G2N01	30:70	126.05	55.17	111.15	14.9	14.03
G2N02	30:70	122.59	54.61	108.85	13.74	13.20
G3N01	45:55	158.35	68.58	142.47	15.88	15.81
G4N02	60:40	184.67	81.59	166.53	19.91	19.82

Based on the compaction deformation at each stage of consolidation and the dimension of sample disassembled from the consolidation chamber after consolidation test, the length of sample at each stage of consolidation (including the unloading stage) can be determined by a back-calculated method. In Figure 1.8, we show consolidation pressure and sand content as functions of porosity for the five different synthetic clays, respectively.

From Figure 1.8(a), the porosity of synthetic clay generally decreases with increasing consolidation pressure. At the first several stages of consolidation, the reduction of porosity is higher than those at the middle and later stages, especially for the synthetic clay with a high content of clay. For instant, the porosities for the two synthetic clays "*G1*" and "G2" are both about 0.5 after application of consolidation pressure being of

0.3MPa. When consolidation pressure is up to 1.56MPa, the porosities for them are about 0.37. The diminution of porosity is about 0.13. Instead of that, the reduction of porosity for the synthetic clay "*G5*" has only about 0.01, from 0.35 to 0.34. The decreasing rate of porosity for most synthetic clays progressively decreases with increase of consolidation pressure instead of a constant rate for the synthetic clay "*G5*".

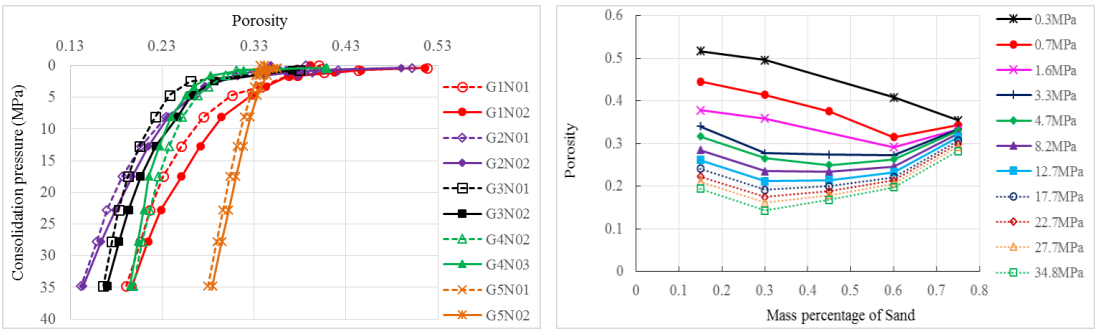

(a) Consolidation pressure *(b) Sand content*

Figure 1.8 Porosity evolution: (a) with consolidation pressure; (b) with sand content

From Figure 1.8(b), the synthetic clay "*G5*" has the lowest porosity, when the consolidation pressure is 0.3MPa. After that, the lowest porosity occurs at the synthetic clay "*G4*", when the consolidation pressure equals to 0.7 and 1.6MPa. We should illustrate that the porosity of the synthetic clay "*G3*" is determined at the consolidation pressure of 2.5MPa rather than 3.3MPa. Therefore, the synthetic clay "*G3*" has the lowest porosity, when the consolidation pressure locates into the interval [3.3, 4.7]MPa. Finally, when the consolidation pressure is equal to or more than 8.2MPa, the synthetic clay "*G2*" has the lowest porosity. Consequently, the lowest porosity progressively transfers from the synthetic clay with a high content of sand to the synthetic clay with a low content of sand, accompanied with increase of consolidation pressure. There exists an optimal mass proportion among mineralogical compositions for the studied synthetic clay, and the optimum value is also related to consolidation pressure.

For each type of synthetic clay, Figure 1.9 shows void ratio (e) as a function of consolidation pressure, where the evolution of compaction displacement with compaction time are also presented. In order to quantitatively describe the influences of both mineralogical composition and consolidation pressure on void ratio of synthetic clay, the void ratio is firstly fitted as a function of consolidation pressure by a power function as shown in Figure 1.9. The power function can be expressed as follows:

$$e = A * \sigma_v^{-B} \tag{1.5}$$

in which σ_v represents consolidation pressure; A and B are two coefficients, and depend on mineralogical composition, A reflects the distance between the original point and the curve described by the power function, and B controls the kinetic of void

ratio.

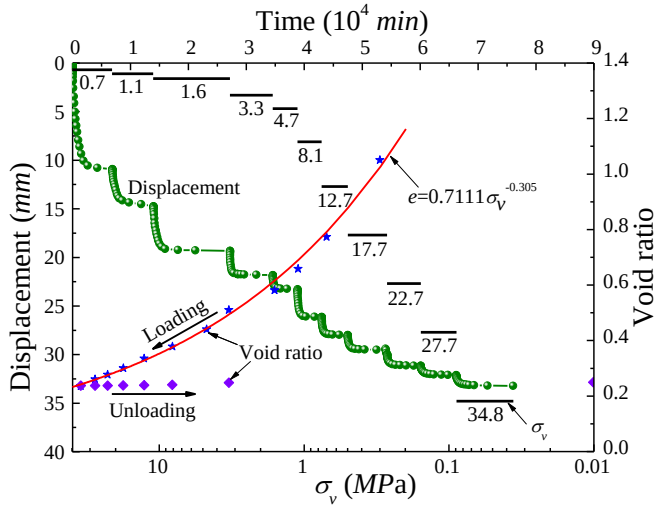

(a) Synthetic clay "*G1N01*"

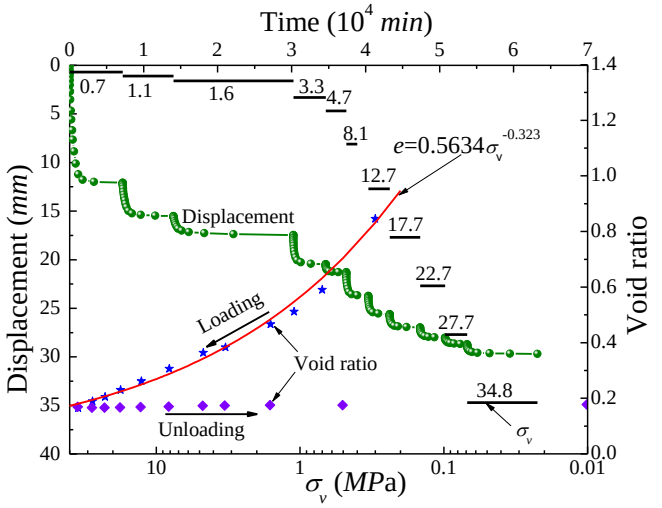

(b) Synthetic clay "*G2N01*"

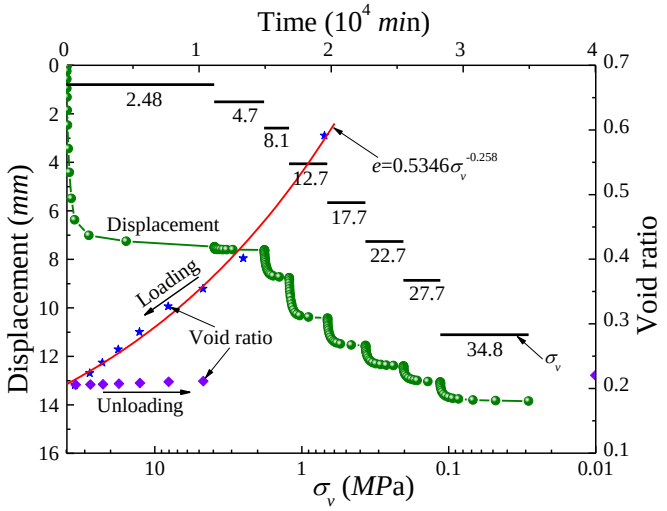

(c) Synthetic clay "*G3N02*"

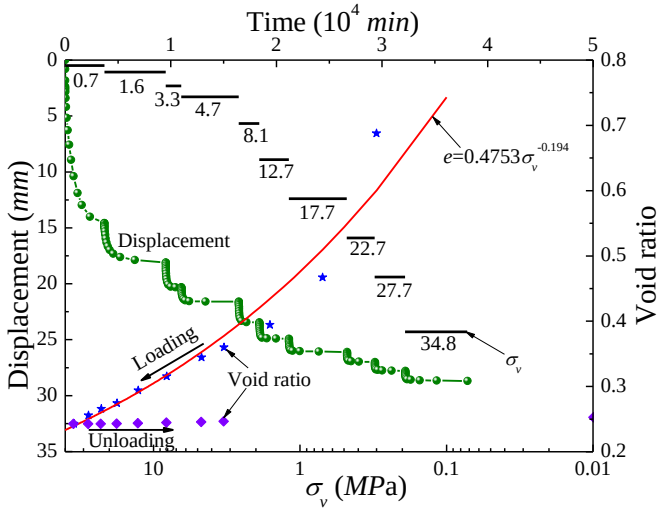

(d) Synthetic clay "*G4N02*"

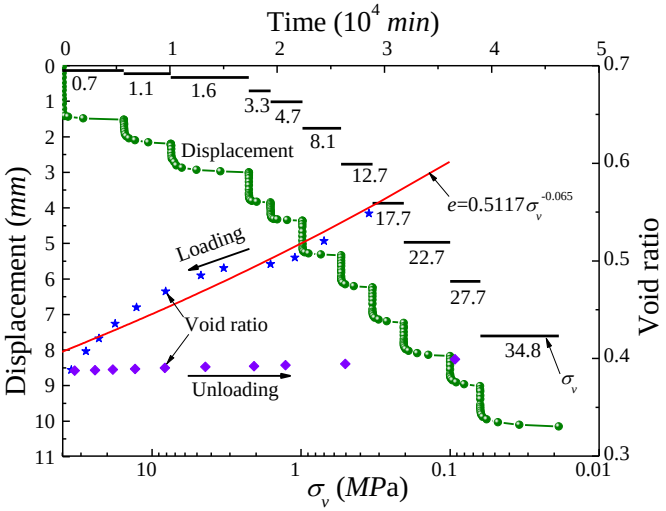

(e) Synthetic clay "*G5N02*"

Figure 1.9 Displacement vs time and void ratio vs pressure of synthetic clay

Table 3. Values of the two coefficient *A* and *B* for the five synthetic clays

Coefficient	*G1*	*G2*	*G3*	*G4*	*G5*
A	0.7111	0.5634	0.5346	0.4753	0.5177
B	0.305	0.323	0.258	0.194	0.065
R^2	0.9944	0.9833	0.9899	0.9485	0.9230

The identified values of the two coefficients A and B, and the coefficient of determination R^2 for the five synthetic clays are listed into Table 3. According to the value of the coefficient of determination, the adopted power function has a good performance to describe the evolution of void ratio of synthetic clay with consolidation

pressure, especially for the synthetic clay with high content of clay such as "*G1*". The drawback of the power function is that two asymptotic states described by the function respectively corresponding to consolidation pressure of zero and positive infinite are not consistent with any soil one in practice.

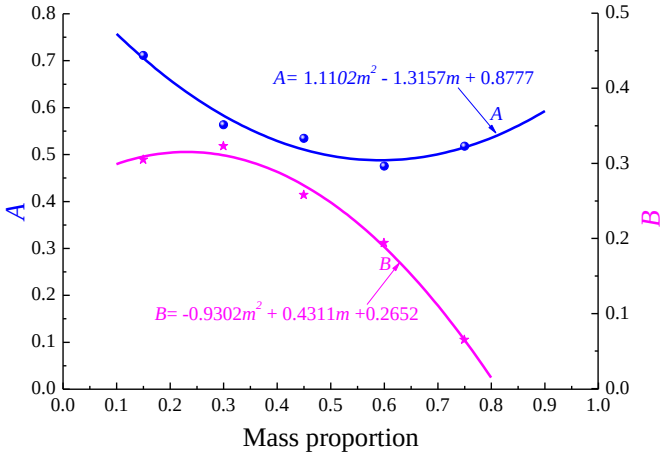

Figure 1.10 Relationships between coefficient A/B and sand content represented by *m*

By means of the two coefficients, a quadratic polynomial is used to get the correlation between the two coefficients and sand content. Figure 1.10 presents both the coefficient A and B as a function of sand content. Based on the above procedures, the void ratio of synthetic clay can be thus expressed as function of both consolidation pressure and sand content as follows:

$$e = f(m) * P_c^{g(m)} \tag{1.6}$$

where $f(m)$ and $g(m)$ respectively represent the coefficient A and the B one, in which m represents the mass proportion between illite and sand. Here, $A = f(m) = 1.1102m^2 - 1.13157m + 0.8777$ with $R^2 = 0.9642$, and $B = g(m) = -0.9302m^2 + 0.4311m + 0.2652$ with $R^2 = 0.9919$.

We could see through Eq.1.6 that when consolidation pressure is low, the effect of A on void ratio is stronger than the B one; whereas with increasing consolidation pressure, the effect of A will become lower than the B one. Thus, the least void ratio of synthetic clay at high consolidation pressure is controlled by the location of the peak point of the function $g(m)$. As presented in Figure 1.8(b), when the consolidation pressure is more than 8.1MPa, the void ratio of the synthetic clay "*G2*" has the least value among the five synthetic clays. The prediction given by the Eq.1.6 and experimental data for the five synthetic clays are shown in Figure 1.11. A relative good agreement between them can be observed.

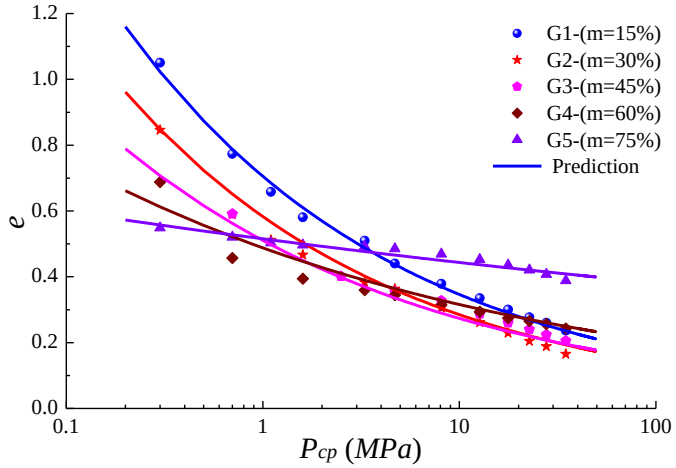

Figure 1.11 Comparison between model predictions and experimental data

1.6.4 Consolidation coefficient C_v

In previous section, we have briefly introduced the Taylor's method and used it to judge whether the primary consolidation of synthetic clay have completed or not. In terms of Eq.1.2, the consolidation coefficient at each stage of consolidation can be obtained. In Figure 1.12, we show consolidation pressure as a function of consolidation coefficient C_v for the five synthetic clays. To clearly observer the evolution of consolidation coefficient, the consolidation coefficient for the five synthetic clays are separately drawn through three subfigures. The value of consolidation coefficient corresponding to each stage of consolidation in accord with the Figure 1.12 is listed into Table .A.1.

For the three synthetic clays "*G1*", "*G2*" and "*G3*", the consolidation coefficient firstly increases and then continuously decreases with increase of consolidation pressure. Whereas, the consolidation coefficient for the two synthetic clays "*G4*" and "*G5*" increases with augmentation of consolidation pressure. It can be observed again that the high pressure consolidation test has repeatability.

The effect of mineralogical composition on consolidation coefficient is significant. For instant, the consolidation coefficient for the synthetic clay "*G5*" is about $1*10^{-6}m^2/s$, but for the synthetic clay "*G1*" it is about $1*10^{-8}m^2/s$. The difference between them reach to two orders of magnitude.

In order to explain the variation of consolidation coefficient, it's necessary to recognize that the consolidation coefficient is a deduced physical variable rather than a directly measured one. The consolidation coefficient is defined as a function of coefficient of hydraulic conductivity K_f, compaction modulus E_s, and weight of interstitial fluid per unit volume γ_f, which can be expressed by Eq.1.7.

$$C_v = \frac{K_f * E_s}{\gamma_f} \tag{1.7}$$

It's well known that the permeability of soil during the uniaxial compaction process commonly decreases with increase of consolidation pressure due to volume compaction of pore caused by pore structure collapse. In contrary to the permeability, the compaction modulus generally increases with increase of consolidation pressure. Through Eq.1.7, when the declining rate of permeability is greater than the growth rate of compaction modulus, the consolidation coefficient will manifest a decreasing tendency, vice versa. Accordingly, the interpretation on the evolution of consolidation coefficient for the two synthetic clays "*G4*" and "*G5*" can be given that the declining rate of permeability is less than the growth rate of compaction modulus. For the three synthetic clays "*G1*", "*G2*" and "*G3*", the declining rate of permeability is firstly less than the raising rate of compaction modulus, and then the circumstance turn into its opposition direction.

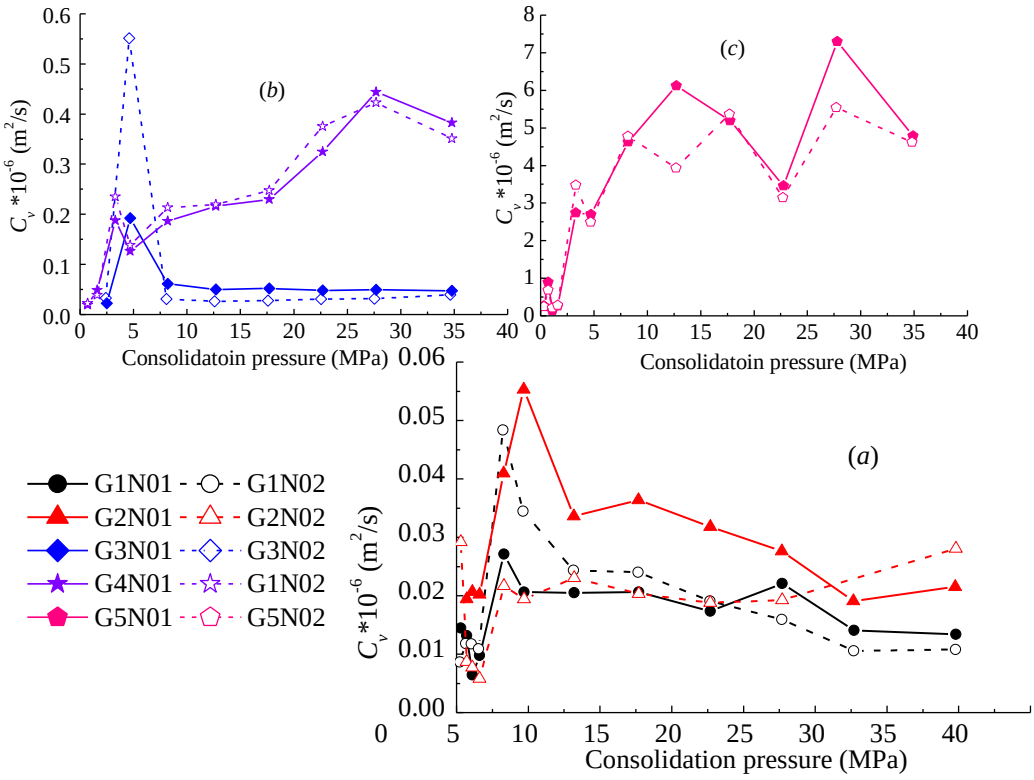

Figure 1.12 Evolution of consolidation coefficient with consolidation pressure for the five synthetic clays

1.6.5 Permeability

Apparently, the consolidation coefficient is not a directly measurable variable but is obtained based on the Taylor's method. A question is thus proposed by us whether the Taylor's method is appropriate for the determination of consolidation coefficient for the synthetic clays studied. In what follows, we discuss the applicability of the method for

determination of consolidation coefficient of synthetic clay through estimating the coefficient of hydraulic conductivity K_{fc} or the coefficient of permeability k_{fc}. The relationship between the two coefficients can be expressed as follows:

$$K_{fc} = \frac{k_{fc} * \gamma_f}{\eta_f} \tag{1.8}$$

in which the η_f the kinematic coefficient of viscosity of interstitial fluid.

We firstly calculate the permeability k_{fc} of synthetic clay based on Eq.1.7, and then the evolution of it with consolidation pressure are presented. After that, based on the experimental data obtained from the constant head permeability test at hydrostatic pressure state, the permeability (k_{hc}) of sample can be determined. Comparisons of permeability obtained from the two methods are used to indirectly verify the applicability of the Taylor's method for the synthetic clays.

In order to distinguish the permeability obtained from the two methods, the permeability based on the Taylor method is hereafter named as the consolidation permeability k_{fc}, and the permeability obtained by the constant head permeability test is called as the hydraulic permeability k_{fh}.

1.6.5.1 Evaluation by Taylor's method

We assume that the consolidation coefficient C_v determined based on the Taylor's method for the synthetic clays studied is applicable. The compaction modulus E_s of sample corresponding to each stage of consolidation can be considered to be reasonable due to insignificant compaction deformation related to secondary consolidation. Accordingly, in terms of Eq.1.7, the k_{fc} can be determined and listed into Table 1.6.

Table 1.6 Permeability of synthetic clay for each stage of consolidation pressure

Sample	Permeability k_{fc}*10^{-18} (m^2)										
	S2	S3	S4	S5	S6	S7	S8	S9	S10	S11	S12
G1N01	4.87	0.98	1.04	0.70	0.69	0.26	0.14	0.09	0.07	0.03	0.03
G1N02	4.09	1.39	1.59	1.06	0.57	0.33	0.16	0.11	0.08	0.04	0.03
G2N01	6.28	2.70	1.29	1.14	0.56	0.41	0.27	0.17	0.10	0.05	0.06
G2N02	2.86	1.40	0.52	0.56	0.26	0.24	0.12	0.09	0.08	x	0.09
G3N01	2.01	x	0.36	0.23	0.17	0.11	0.09	0.07			
G3N02	2.12	x	0.19	0.18	0.12	0.10	0.08	0.09			
G4N02	6.37	2.50	2.81	1.42	1.25	0.87	0.72	0.73	0.94	0.64	
G4N03	6.99	3.30	3.42	1.15	1.39	0.81	0.79	0.49	0.67	0.53	
G5N01	36.5	3.99	2.57	12.5	9.20	14.3	14.0	11.9	6.56	12.8	8.83
G5N02	27.1	4.57	5.94	19.5	10.9	16.1	9.24	13.4	6.81	11.6	8.88

From Table 1.6, the following main remarks can be issued. Firstly, the k_{fc} for most synthetic clays decreases with augmentation of consolidation pressure, except for the synthetic clay "*G5*" for which the k_{fc} slightly changes after the first stage (S2). Secondly, the difference of k_{fc} between the first stage and the last one for the three synthetic clays "*G1*", "*G2*" and "*G3*" can reach to two orders of magnitude, one order of magnitude for the synthetic clay "*G4*", and only about four times for the synthetic clay "*G5*". Thirdly, the effect of mineral composition on k_{fc} is very significant. Taking the k_{fc} at the last stage of consolidation as an example, the k_{fc} of synthetic clay remarkably increases with augmentation of sand content. For instant, when the mass proportion between sand and illite is 15:85 (the synthetic clay "*G1*"), the k_{fc} locates at 10^{-20} order of magnitude, but 10^{-18} for the synthetic clay G5 (75:25).

We can deduce that there may exist two critical mass proportions between sand and illite (represented through the two parameters $m_{\%}^{1}, m_{\%}^{2}$, and $m_{\%}^{1} < m_{\%}^{2}$) to decide whether the interconnecting pore systems of synthetic clay is constructed by illite or sand. When the proportion is less than $m_{\%}^{1}$, the interconnecting pore systems for fluid seepage are constructed by illite phase. The sand particles are separated from each one and are surrounded well by the illite particles. In contrast, in the case of the proportion higher than $m_{\%}^{2}$, the interconnecting pore systems are dominated by sand phase. Entre the interval $[m_{\%}^{1}, m_{\%}^{2}]$, there exists a transition where the pore systems of synthetic clay are dependent on the two solid phases.

1.6.5.2 Permeability through constant head test

A direct way to measure the permeability of synthetic clay is to carry out the constant head permeability test performed only at hydrostatic pressure state. That is used to verify the reasonability of consolidation coefficient determined through the Taylor's method. The hydraulic head at the both ends of sample is set to be 0.6MPa.

In here, an implicit assumption is adopted by us. The assumption is that the influence of rebound deformation due to the unloading of consolidation pressure on permeability of synthetic clay can be ignorable. Since the rebound deformations of synthetic clay are not significant which can be confirmed through experimental data. Meanwhile, the effect of volumetric compaction due to application of confining pressure on permeability of synthetic clay can be also considered to be insignificant. Accordingly, the permeability of synthetic clay is dominantly decided by the state of the last loading stage of consolidation. The permeability determined by the constant head test for the synthetic clays are listed into Table 1.7.

As one can see from Table 1.7, the differences between the consolidation permeability and the hydraulic permeability for the sample tested are not obvious. Consequently, we could consider that the Taylor's method for the determination of consolidation coefficient is at present available and acceptable for the studied synthetic clays. Due to the absence of available data on the permeability of synthetic clay at each stage of

consolidation, we should state that the availability of the indirect method for verification on permeability of synthetic clay can be only confirmed for the last stage of consolidation. It's very interesting to directly measure the permeability of synthetic clay at each stage of consolidation and to further verity the availability of the Taylor's method for the determination on consolidation coefficient.

Table 1.7 Permeability of synthetic clay obtained by the constant head test and the Taylor's method

Sample	Constant head permeability test		Consolidation test
	Confining pressure (MPa)	Hydraulic permeability k_{fh} (m^2)	Consolidation permeability k_{fc} (m^2)
G1N01	4	$1.08*10^{-19}$	$3.67*10^{-20}$
G1N02	9	$5.32*10^{-20}$	$3.22*10^{-20}$
G2N01	4	$9.56*10^{-20}$	$6.00*10^{-20}$
G2N02	9	$2.18*10^{-20}$	$9.00*10^{-20}$
G3N02	9	$6.01*10^{-20}$	$9.00*10^{-20}$
G4N02	4	$4.51*10^{-19}$	$6.40*10^{-19}$
G4N03	9	$2.69*10^{-19}$	$5.30*10^{-19}$
G5N01	9	$4.17*10^{-18}$	$8.80*10^{-18}$
G5N02	4	$5.53*10^{-18}$	$8.90*10^{-18}$

1.7 Conclusion

In this chapter, in light of the research background and purpose, sand and illite are chosen as the basic constituents of the synthetic clays studied. In order to investigate the effect of mineralogical composition on consolidation properties of synthetic clay, five different mass proportions between sand and illite are considered. Due to the characteristic of large deformation of the synthetic clay slurry, a multistage loading scheme is performed to achieve to the desired consolidation pressure. Meanwhile, two self-designed oedometers are used to carry out the uniaxial consolidation test. The compaction time for each stage of consolidation is mainly based on the time for completion of primary consolidation. Based on experimental results, we have investigated the compaction modulus, porosity, consolidation coefficient and permeability of synthetic clay and the evolutions of them with consolidation pressure. The following main remarks can be issued.

(1) The compaction modulus increases with augmentation of consolidation pressure and is dependent on the content of sand in synthetic clay. The extreme (minimal and maximal) value of compaction modulus depends on the consolidation pressure, thickness of absorbed water film, pore property and mineral composition.

(2) The density of illite is assumed and then verified through the dried test conducted on some saturated synthetic clay samples. After that a back-calculated method is used to obtain the porosity of sample. The porosity decreases with increase of consolidation pressure. When the consolidation pressure increases from 0.3MPa to 34.8MPa, the reduction of porosity of synthetic clay are strongly dependent on mineral composition. For instant, the reduction of porosity for the synthetic clay "*G1*" is about 0.33, but for the synthetic clay "*G5*", it has only about 0.07. The optimum porosity of synthetic clay progressively transfers from the synthetic clay "*G5*" with the highest content of sand to the synthetic clay "*G2*" with a relatively low content of sand, accompanied with increase of consolidation pressure.

(3) The consolidation coefficients for the five different synthetic clays obtained through the Taylor's method present different evolutionary modes among them. For the synthetic clays "*G1*", "*G2*" and "*G3*", the consolidation coefficient firstly increases and then decreases. For the two synthetic clays "*G4*" and "*G5*", it presents a continuously increasing trend. The variation of consolidation coefficient is directly related to permeability and compaction modulus.

(4) The permeability of synthetic clay can be calculated by means of combining the Taylor's method and the definition on consolidation coefficient. The permeability progressively decreases with increase of consolidation pressure, and is very sensitive to mineral composition. For instant, the reduction of permeability for the three synthetic clays "*G1*", "*G2*" and "*G3*" can reach to two orders of magnitude, whereas one order of magnitude for the synthetic clay "*G4*" one and 4 times for the synthetic clay "*G5*" one. The difference of permeability between the two synthetic clays "*G1*" and "*G5*" at the last stage has reached up to 100 times. Furthermore, the permeability is indirectly verified by the constant head permeability test to illustrate the applicability of the Taylor's method for the synthetic clays studied.

The uniaxial consolidation process of synthetic clay seems to be similar with the geological consolidation-sedimentation process, the physical-mechanical properties of synthetic clay are commonly reinforced due to compaction deformation of volume. However, the changes of external condition can destroy the originally equilibrium state of synthetic clay towards to build a new equilibrium state. Consequently, the mechanical behavior and permeability of synthetic clay are also of very interest to engineering application. In view of this, a series of triaxial compression tests have been performed to investigate mechanical behavior and permeability of those consolidated synthetic clay, which will be presented in the next chapter.

Chapter 2 Hydro-mechanical behaviors of synthetic clay in triaxial compression

2.1 Introduction

Argillaceous rocks are one of the most abundant sedimentary rock type containing silt- or clay-sized particles that less than 0.0625 mm and clay minerals. The overburdened rock strata adjacent to the storage layer of petroleum/gas are usually made up of the argillaceous rocks. The rocks are commonly taken as the sealed bulkhead layer to prevent petroleum/gas from escaping from the reservoir rock layer with high porosity such as limestone, sandstone. Not all fossil resources are deposited into these rocks with a good hydraulic conductivity, such as the shale rocks have also been discovered as the storage layer of oil or gas since half-century in the context of shortage of energy (Adamson et al, 2006; Kaattel and Valgma, 2005; Eseme et al., 2006; Barties et al., 2005). In recent decades, owing to abundant storage of petroleum/gas in the offshore marine regional environment, the onset of the exploitation of them has been proceeded by numbers of petroleum companies where the argillaceous rocks/soil are commonly taken as the bulkhead layer or the repository of these fossil resources (Kim et al, 2013; Liu et al., 2014).

Some previous experimental studies revealed that physical-hydromechanical properties of clayey rocks depend many factors. Due to the presence of clay element such as smectite, illite, Kaolinite, the mechanical properties of claystone are strongly influenced by the degree of saturation. A number of experimental investigations have been performed for various clayey rocks in various saturated conditions (Hu et al., 2014a; Berner et al., 2004; Charlier et al., 2013; Fityus and Buzzi, 2009; Hoxha et al., 2007; Zhang and Rothfuchs, 2004; Zhang et al., 2012; Hu et al., 2014b; Liu et al., 2015). These previous works generally show that the macroscopic failure stress decreases and the clayey rocks become more ductile when the water increases, such as the elastic modulus and failure properties. Similar investigations have examined the influence of water content on the mechanical behaviors of other types of rock materials, such as shale rocks (Vales et al, 2004; Eseme and Krooss, 2006; Masri et al., 2014), clay-bearing sandstone (Soe et al. 2010).

Meanwhile, with increasing depth beneath the earth, both mineralogical composition and pore properties of clayey rocks with different depths are commonly different among them. Pore properties and mineralogical composition have been confirmed through experimental investigations at laboratory to have a significant influence on mechanical behavior (Hu et al. 2014; Bornert et al., 2010; Zhang, 2011; Fabre and Pellet, 2006; Robinet et al., 2012). Zhang (2011, 2012) has investigated the change of mechanical

behavior of the argillite rocks drilled from three different depths of underground by mini compression tests and micro indentation tests, among which the porosity and the mineralogical composition are different. From the works, the mineralogical compositions were obtained by means of microscopic measurement technologies (X-Ray diffusion and SEM), and the experimental results have shown that the Young's modulus decreases with increasing clay content but increases with increasing both calcite and quartz as well as the failure/peak strength. Similar investigations have examined the influence of mineralogical composition on the mechanical behaviors of various clayey rocks, such as shale rocks (Oscar et al., 2014; Sone and Zoback, 2013) and mudstones (Mondol et al. 2007). In views of this and the correlation between macroscopic behaviors and microstructure, it's very necessary to investigate the physical-mechanical properties of rock at multiscale in order to in-depth recognize the deformation mechanism, such as porous structure, mineralogical composition and distribution, particle shape and so on, with the help of some visualization technologies (Bai et al., 2013; Zhang, 2011; Robinet, 2008).

Consequently, the physical-mechanical properties of rock are closely related to microstructure and mineralogical composition. Due to the drawbacks for the macroscopic theories commonly constructed through the phenomenological methodology, the macro-models are unable to take into consideration the main features at small scale, the development of micromechanics provides a rigorous mathematical frameworks to translate microscopic properties and behaviors of fluid and solid phase through multi-scale approaches into macroscopic constitutive relations to describe the macroscopic response of composite material. However, the clayey rocks are one kind of the nature geological materials. The microstructure and mineralogical compositions of the clayey rock are very complex. It's thus very difficult to get a comprehensive knowledge on the natural geological material, which will bring out some uncertainties for calibration and verification of micromechanical model. In the context of such circumstance, it's very necessary to carry out the laboratory experimental investigation with a well-controlled performance in order to obtain the related reliable experimental data for calibration and verification of micromechanical models.

As mentioned in the Chapter 1, Apart from the research works on consolidation properties of synthetic clay during the consolidation period, it's also necessary to investigate the mechanical properties of synthetic clay. In-depth knowledge of the hydro-mechanical behaviors of synthetic clay is an important issue for design, construction and stability evaluation of engineering structures. Commonly, the triaxial compression test is chosen to investigate the basic mechanical properties due to its practicability. Moreover, it's also important to investigate their permeability properties. Furthermore, the mechanical properties of material are not only influenced by the loading conditions but also the mineral composition, microstructure, saturation conditions, stress history, permeability and so on (Meerea and Mulchrone, 2003; Yang

et al, 2008).

Therefore, the conventional triaxial compression test is chosen to investigate the mechanical behaviors of the synthetic clays obtained from the consolidation test at high range of pressure. The permeability test is also carried out to estimate the evolution of permeability of synthetic clay during the process of deviatoric loading. Our main aims are concentrated on analyzing the influences of confining pressure, mineral composition and microstructure on mechanical behavior and permeability properties of synthetic clay. In view of this, in this chapter, the studied materials are firstly briefly introduced at the beginning to have an intuitive acknowledgement on them. And then, the triaxial testing equipment and the experimental procedure are illustrated in detail. Afterwards, the experimental results on mechanical and permeable behaviors of the materials studied are presented and discussed, respectively. The influence of mineral composition on the two strength parameters based on M-C criterion are discussed. Two plastic mechanisms are used to try to interpret the evolution of volumetric strain of synthetic clay and the influence of composition on the volumetric as well as effective confining pressure.

2.2 Sample characterization

Here, the studied materials will be briefly introduced to obtain an intuitive knowledge on them.

Table 2.1 Physical properties of synthetic clay samples after consolidation test

Sample	Mass (g)	Length (mm)	Diameter (mm)	Density (g/cm^3)	Porosity (%)	FS:IC (%)	PCP (MPa)
G1N01	121.95	50.20	37.01	2.26	19.86	15:85	34.8
G1N02	125.37	51.86	37.00	2.25	20.34		
G2N01	123.08	49.87	37.00	2.29	14.98	30:70	
G2N02	120.73	48.90	37.01	2.29	15.09		
G3N01	156.09	62.22	37.01	2.33	17.62	45:55	
G3N02	128.30	51.25	37.01	2.33	18.03		
G4N02	183.92	74.7	37.02	2.28	20.65	60:40	
G4N03	178.56	72.33	37.03	2.29	20.17		
G5N01	189.37	82.15	37.00	2.14	29.48	75:25	
G5N02	185.68	79.98	37.00	2.16	29.36		
(1) FS:IC :represents the mass proportion of between fine sand and illite; (2) PCP: pre-consolidation pressure							

Firstly, the studied materials contain five different synthetic clays, in each of which the

mass proportion between sand and illite is set to be a specific known value. Secondly, the synthetic clay samples are obtained through the uniaxial consolidation test conducted on the prepared synthetic clay mixture in slurry with consolidation pressure of about 35MPa. Thirdly, the sand is mainly consisted of silica with purity of 98% and average diameter of particle of about 108um; the diameter of illite particle is less than 47um. Finally, the porosity of sample can be obtained accordingly to a back-calculated method.

In Table 2.1, some physical properties of sample are listed. As we can see, both the porosity and density of the two samples classified into the same group show few difference. The representative photos of sample before and after triaxial compression test respective for the five synthetic clays are presented in Figure.A. 2.

2.3 Experimental methods

2.3.1 Triaxial testing equipment

The thermo-hydro-chemical-mechanical (*THMC*) coupling test system as shown in Figure 2.1 is used to conduct the conventional triaxial compression test. The equipment has been developed by Laboratory of mechanics of Lille (*LML*). It is made up of a loading system, a data collection system and a water/gas drainage/seepage system. An important advantage for the device are the self-equilibrium confining pressure chamber. The self-equilibrium confining pressure chamber is made up of an auto-compensate cell allowing for application of confining pressure (P_c), which makes the axial pressure provided by the upper deviator chamber directly be the deviatoric pressure (P_a). The drainage/seepage passage is used to measure the permeability of the tested sample.

Three pressure pumps Gilson® are respectively used to provide deviatoric pressure, confining pressure and pore pressure. The pressure provided by the pump can reach to 60MPa. The loading mode supported by the pump includes the flow-controlling loading mode, the displacement-controlling loading mode. For the flow-controlling loading mode, the flow rate of injected fluid can vary from 5ml/min to $5*10^{-4}$ml/min. For the displacement-controlling loading mode, the displacement rate can vary in a large range, whereas an auxiliary device should be installed to monitor the displacement of sample in order to make the displacement-controlling loading mode be taken effect.

In addition, a furnace is developed to control the temperature of triaxial compression test. The temperature can be up to 120℃ and a built-in thermocouple is used. The oil named as *ENERPACK HF95Y* is used as the hydraulic pressure medium. Four pressure sensors are used to respectively monitor the confining pressure P_c, axial deviatoric pressure P_a, and two pore pressure at both ends of sample (inlet and outlet pore pressure, i.e., P_p^{in} and P_p^{out}). The outlet pore pressure (P_p^{out}) can be controlled through a relief valve with pressure range of 0~50 bar and accuracy of 1.0bar. The displacement of sample parallel to the direction of deviatoric pressure is measured by

two *LVDTs* (Linear variable differential transformer) with measurement range of 10mm and accuracy of 0.01mm. The lateral displacement of sample perpendicular with the direction of deviatoric pressure is measured by a circumferential deformation strain-ring (Lateral deformation collar) which is made up of a strain gauge pasted on a copper sheet, with measurement range of 2.9mm and accuracy of 0.01mm.

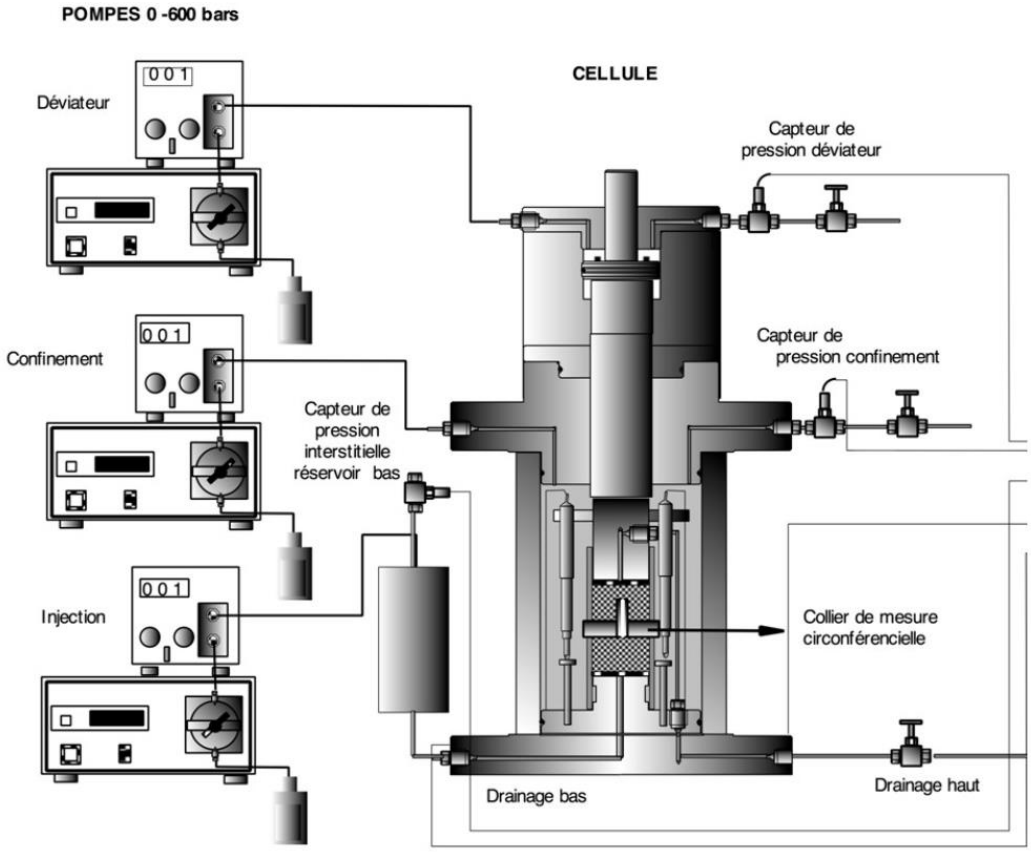

Figure 2.1 Self-equilibrium triaxial pressure chamber system

2.3.2 Experimental procedure

In order to investigate the mechanical behavior of the synthetic clays, the conventional triaxial compression tests with two different confining pressures are performed on the synthetic clay under drainage condition with pore pressure of 2MPa at room temperature $20 \pm 2℃$. The testing procedure is mainly composed of the following three stages: (1) A confining pressure of 3MPa and an average pore pressure of 2MPa are firstly imposed on sample. The pore pressures imposed at both ends of sample are set to be 2.3 and 1.7MPa. (2) Confining pressure increases to the desired value, but pore pressure remains unchanged. (3) Pore pressures imposed at both ends of sample are set to be identical, and the loading of deviatoric pressure is then carried out. The flow-controlling loading mode is adopted for the triaxial compression test.

At the first stage, the confining pressure and pore pressure simultaneously augment to the pre-compressive stress state with the flow rate of injected oil of 0.1ml/min. After

that, the pre-compressive stress state is maintained several days, until the deformation of sample remains unchanged and the sample can be confirmed to be fully saturated through the measured flow rate of the expelled water at the outlet point becoming constant. At the second stage, the confining pressure increases up to the desired value with flow rate of injected oil of 0.1ml/min. After that, the constant head permeability test is performed to measure the permeability of sample, with hydraulic head difference of 0.6MPa. At the third stage, the pore pressures at both ends of sample are set to be 2MPa. The deviatoric pressure increases through the flow-controlling loading mode with the flow rate of injected oil of 0.005ml/min and the transient pulse decay permeability test is conducted to determine the permeability of sample. The compressibility of the oil (*ENERPACK HF95Y*) is ignored so that the flow-controlling loading mode is, to a great extent, equivalent to the displacement-controlling loading mode. For the triaxial compression test, the loading rate of axial strain of sample during the loading process of deviatoric stress corresponding to the flow rate of 0.005ml/min is about $1.0*10^{-6}$/s.

The application and variation of pore pressure for the three stage start from the following purposes. The purpose at the first stage are to assure the sample to be fully saturated, and to reduce the saturated time. Since higher the confining pressure is, the lower the permeability of sample has. At the second stage, the given hydraulic head difference is applied to determine the permeability of sample only under hydrostatic stress condition (confining pressure and pore pressure). On the one hand, the measured permeability will be used to discuss the reasonability of the Taylor's method for the determination of consolidation coefficient; on the other hand, it will be used to investigate the influence of confining pressure and mineralogical composition on permeability of synthetic clay. For the last stage, the determination on permeability of synthetic clay by means of the transient pulse decay permeability method is due to the following reasons: (1) Generally, for the material with a relatively higher permeability (say $>10^{-16}m^2$), it's easily to reach the permanent flow regime inside the sample. In the contrary, it needs a long time to achieve to the steady state flow permeability for the material due to its low permeability; (2) Capability and advantages of the transient pulse decay permeability testing method, the most largely used one; (3) Avoid to the influence of different testing methods on permeability of material.

2.3.3 Permeability measurement

Triaxial compressive behavior of synthetic clay is investigated with different confining pressures. The permeability of sample only under confining pressure state is determined through the constant head permeability test and the transient pulse decay permeability test. Whereas, the permeability of sample during the process of deviatoric loading is measured only through the transient pulse decay permeability test to investigate the influence of stress/strain history on permeability of synthetic clay. In what follows, we illustrate in detail the testing procedures referring to the triaxial compression test and

the permeability test.

The constant head permeability test is a directly method for determination of permeability of sample. It differs with the transient pulse decay permeability test, an indirect measurement method proposed by Brace et al (1968). For the transient pulse decay permeability method, the permeability of sample is estimated from the pore pressure evolution with time, using an inverse numerical algorithm. First of all, the two methods for determination of permeability of sample will be firstly briefly introduced. And then, the reasons for which kind of testing method for determination of permeability of synthetic clay should be adopted, and for which kinds of stress states are chosen as the measured point are interpreted in detail.

2.3.3.1 Steady state method

The test is to determine the permeability of porous medium using a constant difference of hydraulic head. The rate of flow under laminar flow conditions through a unit cross sectional under unit hydraulic gradient is defined as the coefficient of permeability. The flow of a fluid through the porous medium is described by the Darcy's law formulated by Henry Darcy based on the results of experiments on the flow of water through beds of sand. The Darcy's law at constant elevation is a simple proportional relationship between the instantaneous discharge rate through a porous medium, the viscosity of the fluid and the pressure drop over a given distance, which can be expressed as:

$$\mathrm{Q}_{fl} = \frac{-k_{fh} * A * \left(P_p^{in} - P_p^{out}\right)}{\mu_{fl} * L} \tag{2.1}$$

where the Q_{fl} is the total discharge, units of volume per time (m^3/s); the k_{fh} the intrinsic permeability of medium (m^2); the A the cross-sectional area to flow (m^2); the μ_{fl} the viscosity of fluid (Pa*s); the term $P_p^{in} - P_p^{out}$ the total drop (Pa); the L the length over which the pressure drop is taking place (m).

For the constant head permeability test conducted on the synthetic clays, the distilled water is chosen as the interstitial fluid. A schematic illustration on the testing procedure is shown in Figure 2.2. The permeability of sample is determined when the deformation of sample at a stress state has kept stable and the total discharge of water per unit time for several continuously measurable points become constant. The reason that the constant head permeability test is only carried out under hydrostatic pressure condition will be detailed discussed below.

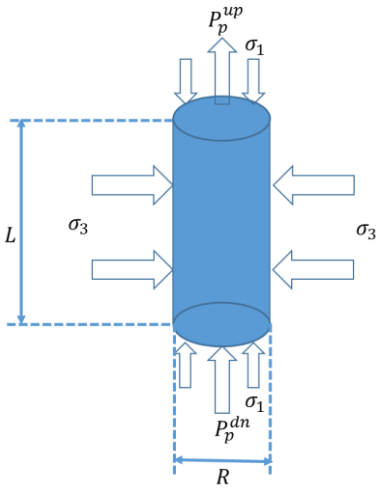

Figure 2.2 Schematic illustration of testing principle for constant head permeability test

2.3.3.2 Transient pulse decay method

The method of transient pulse decay permeability test is based on the fact that the required time for diffusion of interstitial fluid pressure in a saturated material with a relatively low permeability to achieve an equilibrium state is remarkably less than the permanent flow regime one (Larive, 2002). The method was firstly proposed by Brace et al in 1968.

In this method, the Darcy's law is considered to be valid. Based on the decay characteristics of fluid pressure, the permeability of sample is calculated. A schematic illustration on the experimental device for the transient pulse decay permeability test is shown in Figure 2.3. Lots of authors (Hsieh et al, 1981: Neuzil et al, 1981; Trimmer, 1981; Zhang et al, 2000) have been focusing their attentions on obtaining the analytical solution on permeability related to the transient pulse decay permeability test.

The experimental procedure associated to the transient pulse decay method mainly contains the following steps. The studied material is firstly saturated through a given hydraulic pressure difference at both ends of sample. After that, the pore pressures at two ends of sample are set to be identical till the distribution of interstitial fluid pressure along with the length of sample being uniform. A small augmentation of fluid pressure at time t_0 is imposed on the upstream reservoir, and the connecting pipelines entre the reservoir and the pedestal of confining pressure chamber are then immediately switched off. The fluid pressures for the upstream and downstream reservoirs at any time t are monitored by pressure sensor, which commonly depend on the permeability of material, length of fluid passage, volume of the two reservoirs and physical properties of interstitial fluid. In what follow, we will briefly introduce the principle of the method.

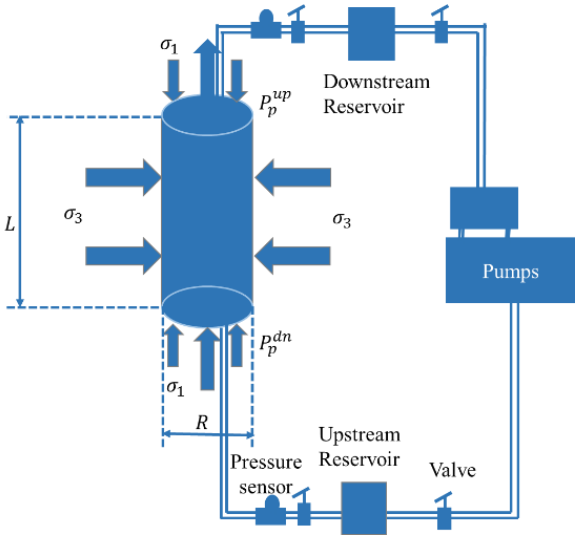

Figure 2.3 Schematic illustration of testing principle for transient pulse decay permeability test

Based on the work performed by Brace et al.(1968), the interstitial fluid pressure diffusion law can be described through the following equation:

$$\frac{\partial^2 P_p}{\partial x^2} = \frac{\mu_{fl}}{k_{fh}}\left(\partial n/\partial t + \beta n \frac{\partial P_p}{\partial t}\right) \qquad (2.2)$$

where the β is fluid compressibility (Pa^{-1}); the n is porosity of material; the fluid viscosity μ_{fl} and the permeability k_{fh}; the P_p the fluid pressure at location x in length direction of sample (Pa), and x is the distance from the ejected end of porous medium (m).

In the case of change of porosity only due to change of fluid pressure, so that the differential of porosity with time $\partial n/\partial t$ can be uniquely related to the term $\partial P_p/\partial t$ for a specific rock. The change of porosity dn due to an increase in internal pressure (initial fluid pressure) dP_p is expressed by $dn = \left(-n\beta_s dP_p - dn_e\right)$, where β_s is the compressibility of the solid matrix and dn_e is the increase in porosity due to an increase in external pressure.

Furthermore, the increase in porosity dn_e is related to the fluid pressure and it can be described through the expression $dn_e = \left(\beta_s - \beta_{eff}\right) * dP_p$ as shown by the work proposed by Walsh (1965), where β_{eff} is the effective compressibility of the material as measured on jacketed samples. Finally, the interstitial fluid pressure diffusion equation can be transformed into the following equation:

$$\frac{\partial^2 P_p}{\partial x^2} = \frac{\mu_{fl}*\beta}{k_{fh}}\left[\left(\beta_{eff} - \beta_s\right)/\beta + n(1 - \beta_s/\beta)\right]\frac{\partial P_p}{\partial t} \quad (2.3)$$

In general, the porosity n of sample compared with the volume of the upstream and downstream reservoirs is very small, and the β is much greater than both the β_{eff} and the β_s, so that the porosity effect on the change of two reservoirs can be ignored. The Eq. 2.3 can be finally simplified as Eq. 2.4 with the analysis solution on Eq. 2.4 can be expressed as Eq. 2.5.

$$\frac{\partial^2 P_p}{\partial x^2} = 0 \quad (2.4)$$

$$\left(P_p^1 - P_p^f\right) = \Delta P_p\left[\frac{V_d}{V_u} + V_d\right]e^{-s*t};\ \text{with: s} = \frac{A}{L} * \frac{k_{fh}}{\beta*\mu_{fl}}\left(\frac{1}{V_u} + \frac{1}{V_d}\right) \quad (2.5)$$

where ΔP_p is the applied augmentation of fluid pressure in the upstream reservoir at time $t = 0$, the V_u and V_d are the upper/lower reservoir volume plus the total volume occupied by those connecting pipelines entre the reservoir and the pedestal of confining pressure chamber (m^3), respectively, *A* is cross-section area, *L* is length of sample. The parameter s can be obtained through fitting the $\lg\left(\Delta P_p(t)/\Delta P_p^0\right) - t$ curve, which can be considered to be identical to the slope of the fitting line.

Due to the reason that the permeability of most synthetic clays is very low, especially for those synthetic clays with a relatively high content of clay, the transient pulse decay permeability test is thus adopted to determine the permeability k_{fh} of synthetic clay rather than the constant head permeability test during the process of deviatoric loading. That's due to the time for determination of permeability of material with a low permeability required for the diffusion of interstitial fluid pressure is apparently less than that to form a steady flow state.

We should stress that the synthetic clays present a significant rheological behavior. Thus, it requires a very long time to make the deformation of sample reach to a stable state. If the deformation of sample still changes, the effect of either compaction or dilatation of sample will make the measured permeability for the material studied become inaccurate. Consequently, it's impossible to determine the permeability of synthetic clay with a relatively low permeability at a relatively high stress level.

Furthermore, we mainly focus on investigating the short-term transient mechanical behavior of these synthetic clays rather than the long-term rheological behavior. The rheological characteristic of material under a low stress level state are commonly less evident than the high one. The lowest point of loading-unloading cycle on stress-strain curves is thus chosen to determine the permeability k_{fh} of synthetic clay. Although the obtained permeability k_{fh} can't be used to directly illustrate the influence of stress level on permeability, it can reflect the strain history effect.

For the transient pulse decay permeability test conducted on the synthetic clays, the initial equilibrium pore pressure is set to be 2.0MPa, and the transient pulse fluid pressure imposed on the inlet end of sample is of 2.4MPa.

2.4 Experimental results

2.4.1 Mechanical behaviors

The conventional triaxial compression tests with two different confining pressures (4, 9MPa) have been performed on the five synthetic clays. In Figure 2.4, we show axial, radial strain as functions of deviatoric stress $(\sigma_1 - \sigma_3)$ for the two confining pressures. The results are quite representative for the porous ductile geomaterial such as mudstone, argillite and soft soil. In here, it should be stated that the deviatoric stress imposed on the axial direction of sample is corrected in terms of the radial deformation of sample. The following main remarks can be issued.

(1) We can see that a nonlinear plastic hardening behavior can be observed from the stress-strain curves at the beginning of deviatoric loading. The nonlinear inelastic strain can be considered to relate to the collapse destruction of those pore with a relatively big diameter and the friction shear sliding along those poor contact surfaces between two particles. For the synthetic clay with high content of illite, the pore collapse can be considered to be insignificant. In this case, the majority of pores can be assumed to only exist into the clay matrix constructed by illite phase, and the sand grain can be considered to be completely surrounded by the clay phase. The pore diameter can be thus considered to be smaller than the size of solid phase. The role played by the pore collapse becomes less and less important due to a relatively high Van der Waal force, but rather the friction shear sliding mainly along the contact surface between two clay platelets. Accordingly, the mechanical behavior of synthetic clay firstly presents a nonlinear hardening phase, and then tends to a perfectly plastic flow. Instead of that, if the clay is considered as a filling phase and the skeleton structure of synthetic clay is constructed by the sand phase, so that the majority of pores are fully generated through the interval constructed by the sand particles. The pore collapse plays dominant role on plastic deformation of material, so that the stress-strain curves of synthetic clay can present a continuous hardening characteristic due to a progressive increase of contact area among grains (Malecot et al, 2010).

(2) The mechanical behavior of synthetic clay is strongly dependent upon confining pressure. At a relatively low confining pressure, the stress-strain curves for most synthetic clays present an obvious nonlinear phase at the beginning of deviatoric loading, and then a plastic flow characteristic can be observed. On the contrary, at a relatively high confining pressure, a quasi-linear phase at the beginning of deviatoric loading can be observed, and the synthetic clays with a relatively high content of sand can present a continuous hardening characteristic. With increase of confining pressure,

the effect of initial defect on nonlinear deformation of sample decreases; and the pore collapse plays more and more important role on the nonlinear deformation of sample. The strength and initial elastic modulus of synthetic clay increase with increasing confining pressure. The effect of confining pressure is generally associated with two kinds of plastic deformation mechanisms. The two mechanical mechanisms are the plastic shear mechanism (Bandis et al, 1981; Wong et al, 2001, Pereira and Freita, 1993) and the plastic pore collapse mechanism (Hayen et al 2005; Suarez-Rivera et al 1900, Fortin and Gueguen, 2007; Guenguen and Bouteca, 2004; Barden et al, 1973; Mowar et al, 1996, Zhu et al, 2010).

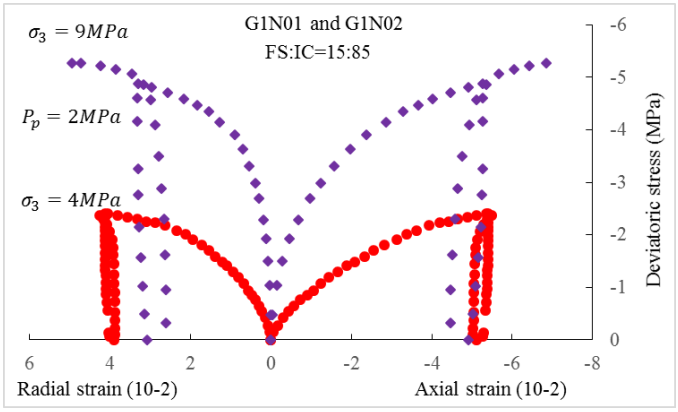

(a) Stress-strain curves of the synthetic clay G1

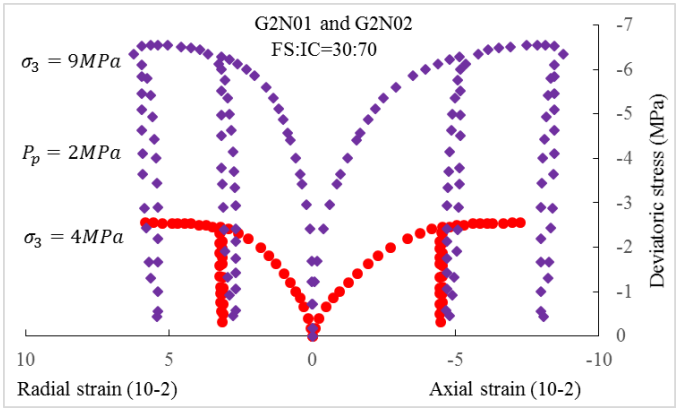

(b) Stress-strain curves of the synthetic clay G2

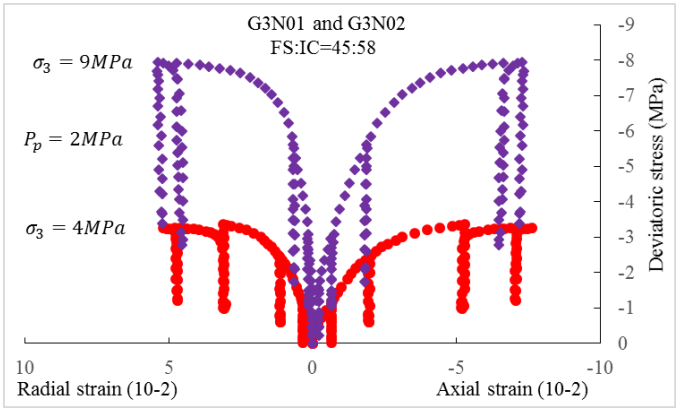

(c) Stress-strain curves of the synthetic clay G3

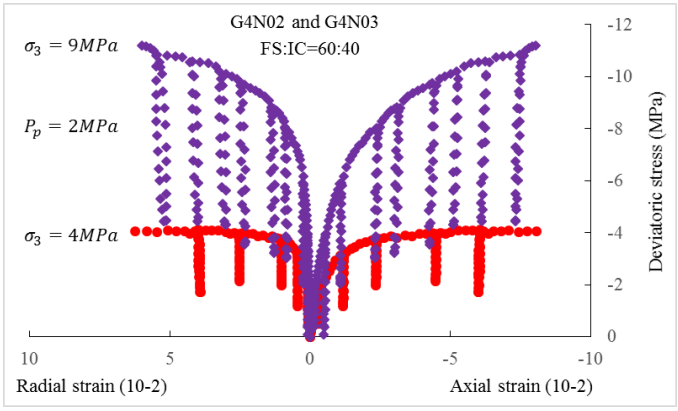

(d) Stress-strain curves of the synthetic clay G4

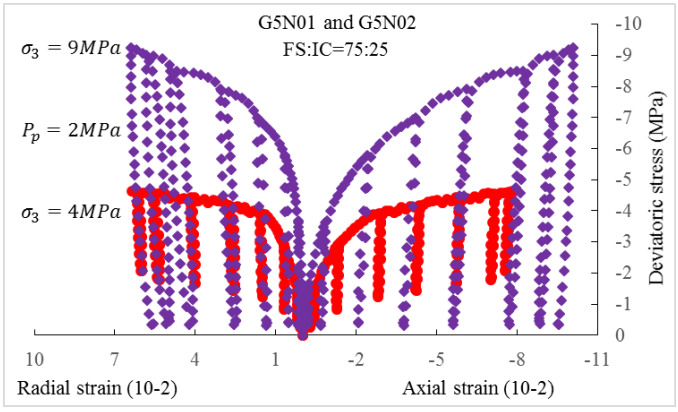

(e) Stress-strain curves of the synthetic clay G5

Figure 2.4 Stress-strain curves of triaxial compression tests of the five different synthetic clays under different confining pressures

(3) The transition from volumetric compressibility to dilatancy for the five synthetic clays is related to confining pressure. In order to clearly display the transition, only the envelope line of volumetric strain versus axial strain curves are shown in Figure 2.5.

We can see that, the transition occurs much earlier and the volumetric dilatancy at a low confining pressure is more remarkable than that at a high one. The volumetric transition is also related to the porous properties of synthetic clay. Some relative interpretations on the volumetric evolution of synthetic clay is in detail discussed in later section.

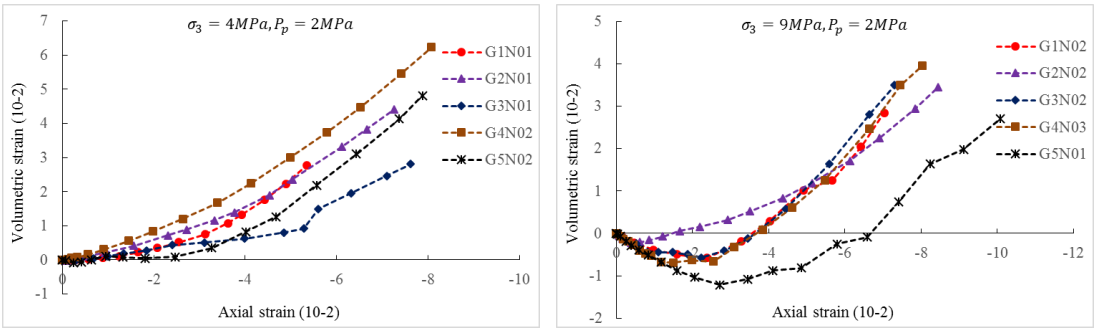

(a) Effective confining pressure of 2MPa *(b) Effective confining pressure of 7MPa*

Figure 2.5 Volumetric strain-Axial strain curves of triaxial compression tests for the five types of synthetic clay under different confining pressure: (a) Effective confining pressure of 2MPa; (b) Effective confining pressure of 7MPa.

2.4.2 Permeability evolution

As we have mentioned above, the permeability of synthetic clay is determined by using the transient pulse decay permeability test. The reason and the purpose to measure the permeability of synthetic clay have been explained before. In Figure 2.6, the development of permeability as well as volumetric strain with axial strain are shown simultaneously. The dark cycle drawn on the left figures represents the chosen point on measurement on permeability. Note that only the permeability in the axial direction of sample is measured in the present work. It's obvious to observer that the deviatoric stress-axial strain curves obtained from the same test as respectively shown in Figure 2.4 and Figure 2.6 exist some differences between them. Since the deviatoric stress as shown in Figure 2.6 is directly calculated by the initial cross-section area of sample. Therefore, the displayed range of axial strain without the correction on deviatoric stress in terms of the radial deformation of sample becomes much greater than that as shown in Figure 2.4. The purpose that we do is to reveal the variation of permeability of synthetic clay under the condition of large deformation.

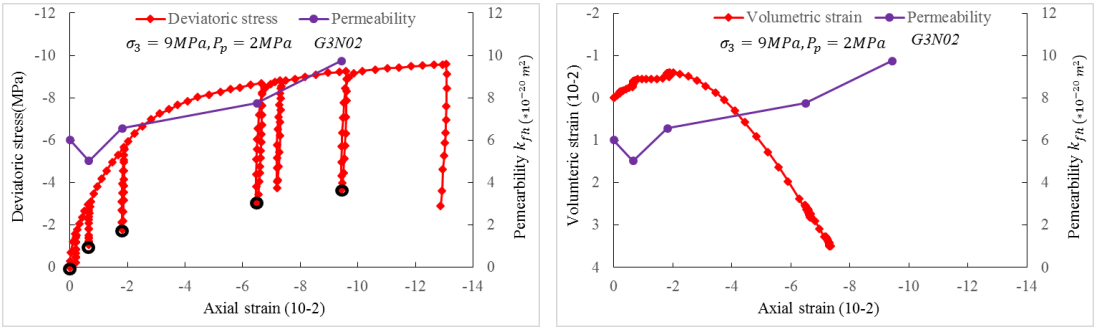

(a) Evolution of permeability of the synthetic clay G3 under effective confining pressure 7MPa

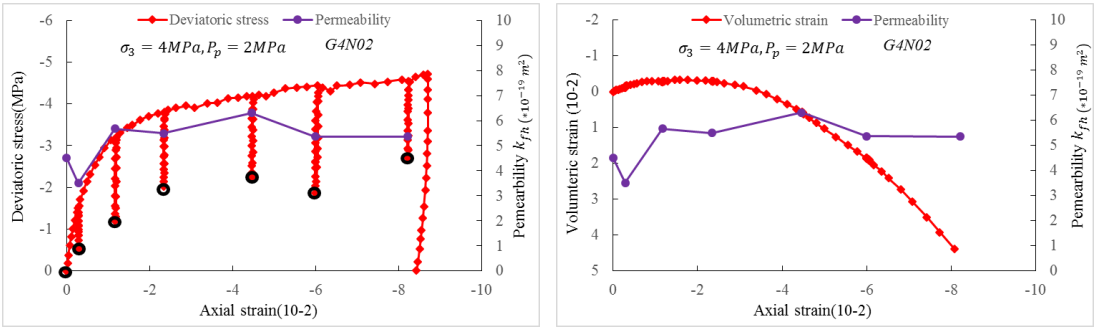

(b) Evolution of permeability of the synthetic clay G4 under effective confining pressure 2MPa

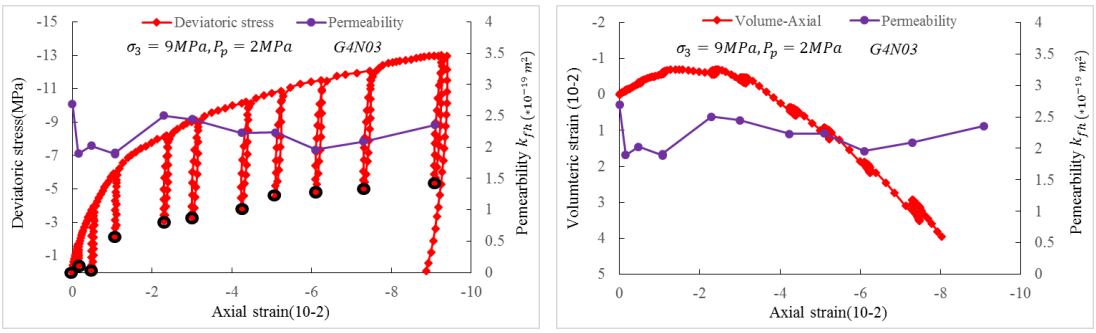

(c) Evolution of permeability of the synthetic clay G4 under effective confining pressure 7MPa

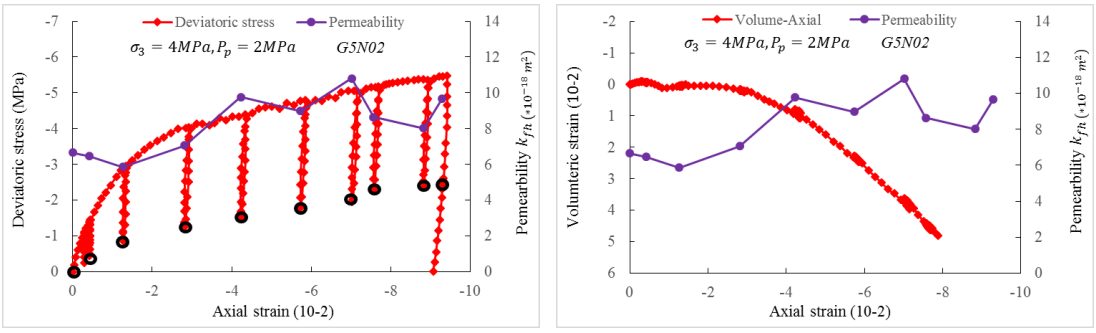

(d) Evolution of permeability of the synthetic clay G5 under effective confining pressure 2MPa

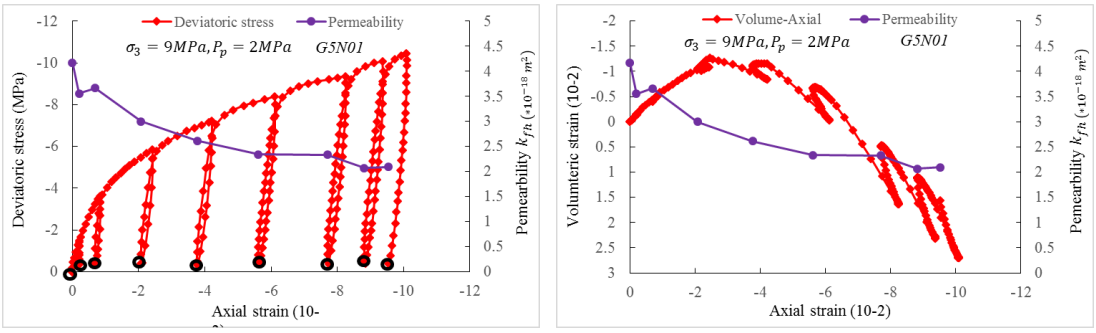

(e) Evolution of permeability of the synthetic clay G5 under effective confining pressure 7MPa

Figure 2.6 Evolution of permeability of synthetic clay with strain under different effective confining pressure

From Figure 2.6, some interesting remarks can be observed. The permeability of the

three synthetic clays at the beginning of deviatoric loading shows a reduction due to compaction of pore volume. After that, with increase of the accumulated irreversible deformations, the permeability shows a slight augmentation at close to the transition point of volumetric strain. At the phase of volumetric dilatancy, the permeability slightly increases. That's to say that the change of hydraulic conductivity of the three synthetic clays caused by the accumulated irreversible deformation are not significant.

For the synthetic clay "*G5*" with confining pressure of 9MPa, the permeability presents a continuous decrease with increase of the accumulated irreversible strain, even if the volumetric strain has transformed from compaction to dilatancy. The variation of permeability of the synthetic clay differs with the others'. In this case, the rebounded of volumetric strain of the synthetic clay "*G5*" becomes more significant due to the complete unloading of deviatoric stress accompanied with a relatively high confining pressure. On the one hand, those induced defects which may be capable to improve the permeability of synthetic clay are closed again; on the other hand, it is easier to further reproduce the pore collapse at a relatively high confining pressure, which will result in the reduction of both size and connectivity of pore. However, for the low confining pressure, the pore collapse becomes more difficult to occur than that at higher one. Accordingly, the difference on the evolution of permeability of the synthetic clay "*G5*" under the two confining pressures can be considered to be acceptable.

The synthetic clay can be considered as one type of porous medium. The permeability can be thus considered to be fully controlled by the pore properties including pore size, porosity and their connectivity. For the porous material, the plastic shear mechanism and the plastic porous collapse mechanism are usually considered as the two basically plastic deformation mechanism, which will be also in detail discussed later.

At the beginning of deviatoric loading, due to the closure of the defects including some weakness pore structure and poor contact surface between two grains. Thus, that will lead to the reduction of both porosity and its connectivity. Moreover, due to the unloading of deviatoric stress, parts of the stress induced micro-cracks will reclose again. Consequently, the permeability of synthetic clay decreases.

Commonly, the plastic porous collapse mechanism will lead to volumetric compaction of sample; on the contrary, the volumetric dilatancy is often contributed to the plastic shear mechanism due to the generation of microscopic shear crack. At the phase of volumetric compaction of sample, the plastic porous collapse mechanism may play a dominant role in volumetric deformation comparing with the plastic shear mechanism. It's natural to observer the reduction of permeability.

Whereas, at the phase of volumetric dilatancy of sample, can we assure that the permeability of the sample must present an increasing trend due to the macroscopic volumetric dilatancy of sample? The answer is not. That have been reported and confirmed through some relatively experimental results (Zhu and Wong 1997; Zhu et

al., 1997; Han et al., 2016). However, as the lithology of the synthetic clay is not completely similar with the above mentioned experimental materials such as sandstone or limestone. Accordingly, by means of those experimental researches, we try to give a possible interpretation on permeability of the synthetic clay at the phase of volumetric dilatancy. At this phase, there may have three circumstances: the first is when the augmentation of permeability induced by the microscopic shear cracks is less than the reduction generated by the shrink of pore size related to pore collapse; the second is when the porosity of sample increases, where the augmentation of porosity contributed to the increase of the microscopic shear cracks is larger than the diminution of porosity contributed to the reduction of pore size, but the pore connectivity is not improved; the third is similar with the second one, but the pore connectivity is somewhat improved in form of several times. According to the first two circumstances, the permeability of sample will then decreases. For the third circumstance, the permeability will slightly increase, if the loading of deviatoric pressure is monotonic. On the one hand, it can be considered that the pore connectivity due to volumetric dilatancy has been improved, but not significant. On the other hand, even if the dilatancy of volumetric deformation of sample (at macroscopic) is very significant such as more than 4%, whereas the pore connectivity will be further reduced due to the rebounded deformation caused by the unloading of deviatoric pressure and the secondary pore collapse caused by confining pressure during the unloading process of deviatoric pressure.

In order to well understand the variation of permeability, it's very important to monitor the evolution of pore structure of synthetic clay during the triaxial compressive process in the light of some microscopic scanning technologies. The experimental investigations on such aspect will be developed in future.

2.5 Discussion

In this section, we mainly focus on discussing the influences of mineral composition and confining pressure on mechanical behavior and permeability of synthetic clay.

2.5.1 Mechanical behavior

Here, the influence of mineral composition on mechanical behavior of synthetic clay is illustrated. For the reason of clearness, only the envelop lines of the stress-strain curves for the five synthetic clays corresponding to the same confining pressure (4 and 9MPa) are respectively presented through two subfigures as shown in Figure 2.7.

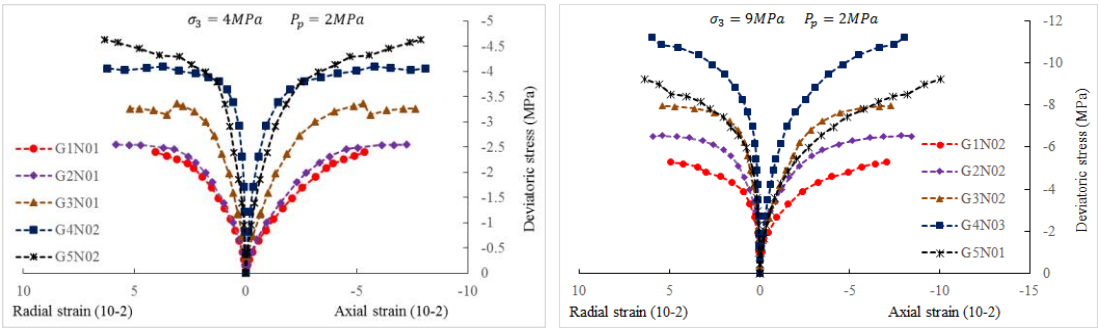

(a) Confining pressure of 4MPa *(b) Confining pressure of 9MPa*

Figure 2.7 Comparisons of stress-strain curves among the five synthetic clays at the same confining pressure

With confining pressure of 4MPa as shown in Figure 2.7(a), the strength of synthetic clay generally increases with increase of content of sand, as well as the initial elastic modulus. We can see that the stress-strain curves obtained from the two synthetic clays "*G1*" and "*G2*" are very close with each other, whereas the stress-strain curves for the three synthetic clays "*G2*", "*G3*" and "*G4*" seems to present an equidistant characteristic. However, for the two synthetic clays "*G4*" and "*G5*", the initial elastic modulus of the synthetic clay "*G5*" is less than that of the synthetic clay "*G4*". Note that the stress-strain curves of the synthetic clay G5 is below those of the synthetic clay "*G4*", when the axial strain is less than 2.5%. On the contrary, with axial strain more than 2.5%, an opposition circumstance can be observed.

With confining pressure of 9MPa as shown in Figure 2.7(b), the initial elastic modulus and strength also commonly increase with increase of content of sand. It is particularly observed that the difference of stress-strain curves for the two synthetic clays "*G1*" and "*G2*" becomes more significant than those at low confining pressure. Nevertheless, an abnormal phenomenon can be noted that the initial elastic modulus as well as the strength of the synthetic clay "*G5*" are lower than the synthetic clay "*G4*" one. That may be associated to the lithology of synthetic clay and its pore property. As we can see from Table 2.1, the initial porosity (0.29) of the synthetic clay "*G5*" is higher than the synthetic clay "*G4*" one (0.20). During the process of deviatoric loading especially at a relatively high confining pressure, it's much easier for the synthetic clay "G5"to occur the collapse failure of pore structure to make its mechanical behavior be weaker than the synthetic clay "*G4*" one.

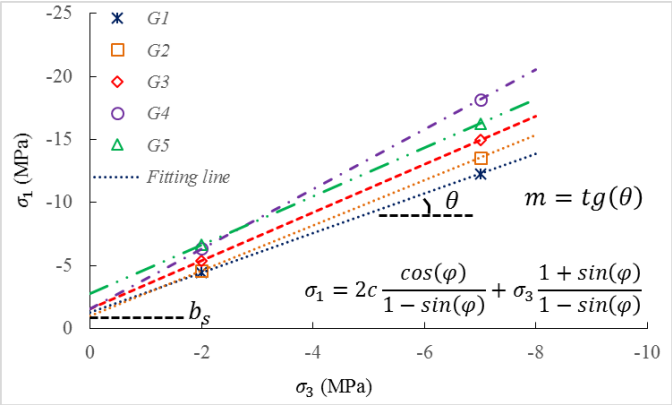

Figure 2.8 Schematic illustration on the two strength parameters based on the Mohr-Coulomb criterion, by means of the experimental results obtained from the conventional triaxial compression test with two different confining pressures

For the purpose to give a quantitatively illustration on the influence of mineral composition on mechanical properties of synthetic clay, the two strength parameters based on the Mohr-Coulomb criterion are then chosen. Due to the reason that some synthetic clays manifest a continuous hardening behavior under the condition of large deformation, it's very difficult to identify the "exact" strength or peak stress. Accordingly, we propose that the stress corresponding to the maximum of deviatoric stress is defined as the strength of synthetic clay. In the light of this, we report the pair values of failure stress as function of (effective) confining pressure in Figure 2.8. The value of the two strength parameters (friction angle $\varphi = arcsin\,(m-1)/(m+1)$ and cohesion $c = b_s\,(1-sin\varphi)/(2cos\varphi)$) for the five synthetic clays can thus be obtained based on the interception with the axial $\boldsymbol{\sigma_1}$ and the slope m of the fitting straight line as plotted in Figure 2.8, and are listed in Table 2.2.

Table 2.2 Strength parameters based on M-C criterion

Species	FS:IC (%)	Strength		Initial Porosity (%)	Internal friction angle (°)	Cohesion (*MPa*)
		Effective axial stress (*MPa*)				
		2	7			
G1	15:85	4.40	12.28	≈ 20.00	12.92	0.49
G2	30:70	4.55	13.55	≈ 15.05	16.51	0.35
G3	45:55	5.36	14.94	≈ 18.00	18.31	0.55
G4	60:40	6.32	18.17	≈ 20.00	23.98	0.51
G5	75:25	6.63	16.24	≈ 29.50	18.39	1.00

In Table 2.2, the greatest internal friction angle occurs at the synthetic clay "*G4*" instead

of the synthetic clay "*G5*", and the maximal cohesion occurs at the synthetic clay "*G5*" rather than the synthetic clays "*G1*" or "*G2*". If the pore properties such as porosity, pore size and distribution for the five synthesis clays are completely identical to each one, and the sole difference among the five synthetic clays is the different mineral composition, we may consider that the cohesion of synthetic clay will increase with augmentation of content of clay phase but in opposite for the internal friction angle, and both of the two strength parameters will finally tend to the asymptotic values identical to those of the synthesis clay only consisted of the clay phase. However, the obtained results seems to dissatisfy the above-mentioned analyzation. The reason to result in the dissatisfaction maybe be caused by the pore property of synthetic clay.

The skeleton structure for the two synthesis clays "*G1*" and "*G2*" can be considered to be constructed by the clay phase, whereas the skeleton structure for the other two synthesis clays "*G4*" and "*G5*", or at least for the last one, can be considered to be constructed by the sand phase. The skeleton structure for the synthesis clay "*G3*" can be considered to be the intermediate transition state entre the clay-phase skeleton structure and the sand-phase skeleton structure. It's reasonable to consider that the pore diameter among the five different synthetic clays is different with each one and increases with augmentation of sand content. Therefore, for the synthesis clay with a relatively high porosity and large pore size, the collapse failure of pore structure (shown in Figure.A.3 and Figure.A.4) becomes easier to occur, and it is easier to occur the separation of contact interface between sand-clay grains. That will make the synthetic clay "*G5*" have a lower strength compared to the synthetic clay "*G4*".

The pore properties have significant influences on mechanical behavior of material. Whereas, the influences are very complicated to understand well, which are commonly related to the pore properties such as pore size and distribution, pore connectivity, and porosity. The investigations on this aspect are beyond our works. We here try to discuss the influences of porosity and pore size on mechanical behavior of material. Considering the complete saturation condition, the degraded effect of pore size on mechanical behavior of synthetic clay decreases with increase of pore size due to the progressive decrease of swelling force generated due to the overlap of the absorbed water film between two clay platelets. Meanwhile, it's easier to generate the excessive hydrostatic pore pressure inside the synthetic clay with a relatively low hydraulic conductivity, where the pore diameter is commonly small. In general, the mechanical behavior of synthetic clay are usually degraded with increase of porosity. More comprehensive experimental investigations should be performed in future to further discover the influences of mineral compositions and pore properties on mechanical behavior of the synthetic clays studied.

2.5.2 Volumetric strain evolution

For the reason of comprehension and visualization, the interpretation on the volumetric

strain of these synthetic clays is then discussed here with the help of Figure 2.5 and Figure 2.9. The deformation of elastic volume induced by application of deviatoric pressure is compressed. Assuming that the pore collapse mechanism controlling the pore collapse deformation can be described through a series of ellipsoidal yield surfaces in stress space, a series of elliptic curves in the stress meridian plane; and the plastic shear mechanism controlling the friction slipping deformation can be described through a series of circular cones yield surface in stress space, a series of straight lines in the stress meridian plane.

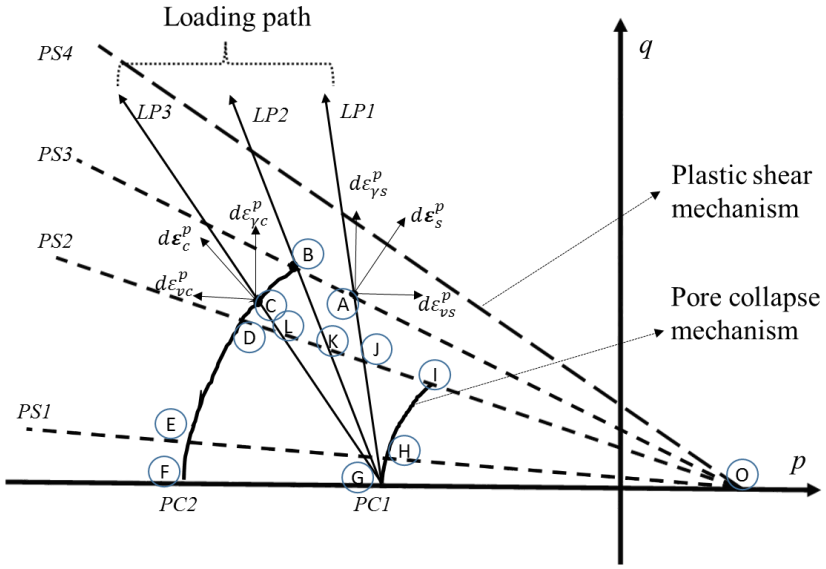

Figure 2.9 Schematic illustration of plastic shear mechanism and plastic pore collapse mechanism in meridian plane (*p, q*) with triaxial compression stress path, in which the symbol "*PC*" represents the plastic pore collapse mechanism, the "*PS*" the plastic shear mechanism, and the "*LP*" the loading path

For the synthetic clay with high content of clay, considering the formed mechanism of pore in the material, it's difficult to occur the pore collapse deformation. Thus, the pore collapse yield surface in stress space can be described by a small initial yield surface with a fast rate of plastic hardening. Meanwhile, a small initial yield surface with a small rate of plastic hardening is used to describe the evolution of plastic shear yield surface. In the case of this circumstance, after the application of confining pressure with a low value, the plastic shear yield surface can be described by the line "*PS1-OH*" and the pore collapse yield surface corresponds to the curve "*PC1-GH*". The elastic region surrounded by the zone "*OGH*" is small due to the small hardening rate of plastic shear yield surface.

At the incipience of deviatoric loading as shown in Figure 2.6, the fast hardening of pore collapse yield surface may result in the intersection point between the stress path and the plastic yield surface only occurring on the plastic shear yield surface. The

loading path for the triaxial compression test can be here described by the line "*LP1*". The plastic deformation of material is thus basically controlled by the plastic shear mechanism so that the deformation of plastic volume is expansive $d\varepsilon_{vs}^{p} > 0$.

Whereas, after the application of confining pressure with a high value, the elastic region is assumed to be described by the zone "*OGI*". The two plastic yield surfaces can be respectively described by the line "*PS2-OI*" and the curve "*PC1-GI*". At the incipience of deviatoric loading, only the pore collapse mechanism is acted and the plastic shear yield surface still extends progressively due to plastic hardening. During this process, the deformation of plastic volume of the material is compressed $d\varepsilon_{vs}^{p} < 0$. The total deformation of volume is also compressed because of compaction of deformation of elastic volume. The stress path firstly intersects only with the elliptic curve. After that, as the plastic hardening rate for the plastic pore collapse yield surface is higher than the plastic shear yield surface one, the stress path simultaneously intersects with the two plastic yield surfaces just like the line "*LP2*". At this specific point, there exist plastic volumetric compaction as well as plastic volumetric dilation. With further increase of deviatoric stress, the plastic deformation is basically controlled by the plastic shear mechanism described by the loading path line "*LP1*". The deformation of plastic volume of the material becomes thus dilatancy so that the transition from volumetric compressibility to dilatancy of material can be occur.

For the synthetic clay with high content of sand, due to the formed mechanism of pore in the material, it's very easy to occur the pore collapse deformation due to the weakness pore and low bonding force between sand and illite. Thus, the hardening rate of the plastic pore collapse yield surface can be considered to be identical with or slight less than the plastic shear yield surface one. That conception seems to be acceptable, if the influences of pore properties on mechanical behavior of material are very significant. The elastic range surrounded by the two plastic yield surfaces due to plastic hardening is directly related with confining pressure. In other words, the greater the application of effective confining pressure, the larger the elastic range becomes. Moreover, the slope of the line describing the plastic shear yield surface in stress meridian plane can be considered to be less than the slope of the line representing the asymptotic value of internal friction angle of the material. Consequently, with the application of deviatoric loading, the intersection point between the stress path corresponding to the triaxial compression test and the plastic yield surface in stress meridian plane transfers progressively from the plastic pore collapse yield surface to the plastic shear yield surface. The transition occurs much earlier and the volumetric dilatancy is more importance under low confining pressure. The deformation of plastic volume of the material transfers from compaction to dilatancy.

At confining pressure of 4MPa, the compaction of volumetric strain of the synthetic clay "*G5*" is very difficult to observe, and the deformation is less than the synthetic clay "*G4*" one. That may be interpreted that the hardening rate for the plastic pore collapse

yield surface for the synthetic clay "*G5*" is more than the synthetic clay "*G4*", as well as the hardening rate for the plastic shear yield surface; whereas, the initial elastic region for the former is less than the latter one. At a relative low confining pressure, the elastic region for the synthetic clay "*G5*" is smaller than the synthetic clay "*G4*" one, it's thus more difficult for the former to occur the volumetric compaction than the latter. At a relatively high confining pressure, the elastic region for the synthetic clay "*G5*" may be slightly lower than the synthetic clay "*G4*" or the former is identical or larger than the latter, the volumetric compaction for the former will be stronger than the latter one.

2.5.3 Permeability

The measurement on permeability of synthetic clay only at the hydrostatic stress state, obtained from the constant head permeability test, is chosen to analyze the influences of both mineral composition and confining pressure on permeability of synthetic clay. The values of permeability of the five synthetic clay samples are listed into Table 1.7. In Figure 2.10, we show the evolution of permeability with increase of sand content.

The following main remarks can be obtained: (1) the permeability of synthetic clay decreases with increase of confining pressure. It's very evident to observe that the influence of confining pressure on permeability of synthetic clay is also dependent on mineral composition. For instant, the reduction for the synthetic clay "*G1*" is larger than that of the synthetic clay "*G5*". (2) The influence of composition on permeability of synthetic clay is very significant. The permeability significantly increases with increase of sand content. For instant, the difference of permeability between the two synthetic clays "*G1*" and "*G5*" can reach to two orders of magnitude. (3) The permeability of synthetic clay is also directly related to porosity. It can be notice from Table 1.7, the permeability of the synthetic clay "G2" has the lowest value rather than the synthetic clay "*G1*" one. That may be related to porosity.

Two types of soils have been defined by us. The first set of soil is consisted of the two synthetic clays "*G1*" and "*G2*", named as the argillaceous soil; the second set one includes the two synthetic clays "*G4*" and "*G5*", or only "*G5*", named as the sandy soil. The pore properties between two types of materials are considered to be different with each other. The pore size for the argillaceous soil can be considered to be smaller than the sandy soil one due to the different formed mechanisms for the skeleton structure mainly related to the pore structure. Although it's more difficult for the argillaceous soil to reduce the pore size than the sandy soil one, the diminution of permeability of the argillaceous soil caused by the reduction of pore size can be more significant than the sandy soil one. As, corresponding to the same diminution of magnitude of pore diameter, the viscous force of fluid existing at the pore with a relatively small size increases more significantly than that at large pore, or sometimes, even if the diminution on diameter for the small pore is less than the large pore one. For all synthetic clays, the change of

pore due to increase of confining pressure from 4 to9MPa, such as the compaction of pore volume and the diminution of porosity, are not evident enough to give rise to a significant change of permeability for all synthetic clays studied.

.

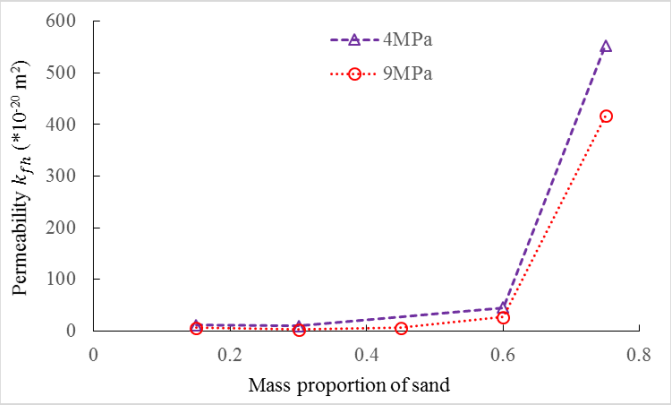

Figure 2.10 variation of permeability of synthetic clay with increase of sand content wth two different confining pressures 4 and 9MPa

2.6 Conclusions

In this chapter, we have investigated the mechanical behavior and permeability of synthetic clay in saturated and drained conditions. The conventional triaxial compression tests with two different confining pressures have been performed on the five synthetic clays. The mechanical behavior of synthetic clay strongly depends on confining pressure, such as initial elastic modulus and strength. Most synthetic clays present a plastic flow after a nonlinear hardening phase. There also exists a continuous plastic hardening characteristic for the synthetic clays with both a relatively high content of sand and confining pressure.

The mechanical behavior of synthetic clay are also considerably dependent on mineral composition. In common, both the strength and initial elastic modulus of synthetic clay are enhanced with augmentation of content of sand, and are also sensitive to confining pressure.

The variation of volumetric strain of synthetic clay is associated to confining pressure and mineral composition. The transition from volumetric compressibility to dilatancy becomes more important at low confining pressure than that at higher one.

In terms of the M-C criterion and the owner definition on strength, the two macroscopic strength parameters (cohesion and internal friction angle) are then obtained based on the experimental results of the conventional triaxial compression test with two different confining pressures. The influences of mineral composition on the two strength

parameters are briefly discussed.

The permeability of synthetic clay firstly decreases due to the volumetric compaction at the beginning of deviatoric loading, and then it almost arrives at the minimum near to the transition point of volumetric strain, after that it slightly increases at the phase of volumetric dilatancy. According to those measured values of permeability obtained from the constant head permeability test only conducted at the hydrostatic stress state, it's particularly observed that the mineral composition can affect the permeability of synthetic clay in a significant way through both porosity and pore size. It can be confirmed that the effect of pore size on permeability is obviously higher than the porosity one through the comparisons of permeability between the two synthetic clays "*G1*" and "*G4*". The permeability of synthetic clay are also dependent on confining pressure, and the influence of confining pressure on permeability depends on mineral composition.

Finally, the evolution of volumetric strain of synthetic clay with different confining pressures are discussed by means of the two plastic deformation mechanisms, i.e., the plastic shear mechanism and the plastic collapse mechanism. The transition from volumetric compressibility to dilatancy becomes more obvious at high confining pressure that at low one.

For geotechnical engineering, it's very necessary to investigate the mechanical properties of the rock interested such as the reservoir layer or the overburden rock layer adjacent to the reservoir layer. Meanwhile, the investigations on the consolidation-sedimentation of soil is also of very significance to obtain an in-depth knowledge on geological material. Furthermore, the changes of the in-situ stress field are commonly very complicated, the loading path corresponding to the conventional triaxial compression test is not sufficient to achieve a comprehensive understanding on mechanical behavior of material. In view of this, in the following chapters, we will propose to carry out a series of triaxial compression tests with different loading paths on a specific type of synthetic clay, in which the mineral compositions and the mass proportion among them are designed to be identical to the argillite in-situ, accompanied with the imposed consolidation pressure being set to be the current effective vertical pressure imposed on the argillite, in order to attempt to give a laboratory investigation for the offshore marine petroleum engineering in Angola.

Chapter 3 Laboratory investigation of synthetic clay for the offshore marine petroleum engineering-Angola

3.1 Introduction

As we have mentioned in the previous chapter, we mainly investigate the mechanical behavior of synthetic clay under various loading paths in order to assess the mechanical properties of the overburden geomaterials in-situ as much as possible. The feasible research is proposed by TOTAL to apply to the offshore marine petroleum engineering located in the South Atlantic off the western coast of Africa (Angola). The overburden rock layer adjacent to the petroleum storage layer can be considered as the argillaceous rock. In order to predict and resolve some possibly potential problems occurring at the oil exploitation process, it's necessary to investigate the mechanical properties of the argillite interested. However, in the stage of flexibility research and in the condition of difficulty to obtain the intact drilled rock core, the experimental investigations at laboratory on mechanical behavior of synthetic clay are performed to try to in advance estimate the mechanical behavior of the argillite in-situ.

Based on the experimental results on mineralogical analysis conducted on the drilled core sample of argillite, the proportion of clay component mainly constituted of illite to another mineral components mainly composed of quartz, calcite and oxide is about 70:30, and the current effective vertical pressure in situ, performed on the argillite, is about 7.8MPa. The porosity of argillite is about 21%. The mineral compositions and the effective vertical pressure are firstly chosen by us as the mainly controlled indexes to prepare the synthetic clay sample instead of porosity. And then we attempt to take advantage of the experimental investigations on mechanical behavior of the synthetic clay to give an estimation and comparison with the argillite one.

The synthetic clay slurry mixture with the mass proportion between illite and sand identical to the argillite one is firstly prepared. A multistage uniaxial consolidation test with consolidation pressure of 7.8MPa has been performed on the prepared slurry mixture to obtain the experimental material for the subsequent triaxial compression tests. The compaction time for each stage of consolidation is also based of the time for completion of primary consolidation. The time for completion of primary consolidation can be determined by means of some visualized methods such as the Taylor's method and the Casagrande method.

We mainly aim to investigate the mechanical behavior of the consolidated synthetic clay. The testing procedures and experimental results related to the uniaxial consolidated test are thus briefly illustrated in this chapter. After that, three kinds of triaxial compression tests are carried out to investigate the dependency of mechanical

behavior of synthetic clay on loading path, which are the conventional triaxial compression test, oedometric test and conventional triaxial compression test after oedometric loading, respectively.

On the one hand, by means of the inversion method, the velocity of elastic wave are widely used for lots of geological engineering such as petroleum exploitation and mining science to assess the quantity of rock mass and the distribution of different rock layers beneath earth; on the other hand, the variation of velocity of elastic wave can be often applied to estimate the evolution of elastic properties or microstructure of material during the loading process because of the correlation between the elastic properties and the velocity of elastic wave. Consequently, it's worth monitoring the evolution of velocity of elastic wave of material for experimental investigations both at laboratory and in situ. In view of this, a specific experimental cell is developed and simultaneously allows for measuring the velocities of both longitudinal and transverse elastic waves parallel with the loading direction of deviatoric stress to be used to assess the microstructure evolution of material during loading process.

The main outcomes of the experiments reported here are (1) compaction characteristic of synthetic clay, (2) influence of loading path on mechanical behavior of synthetic clay, (3) assessment on the microstructure evolution of synthetic clay in terms of elastic wave velocity, (4) given an estimation for the offshore marine petroleum engineering compared with the experimental investigations on the argillite in situ. The obtained experiment results can be used to provide some essential and fundamental data for the petroleum engineering design and formulation of the multiscale mechanical constitutive model.

3.2 Development of testing device

The autonomous and auto-compensated hydro-mechanical coupling system synthesized with the measurement on ultrasonic wave is designed by Laboratory of Mechanics of Lille (*LML*) as shown in Figure 3.1. A combination of P-wave (Longitudinal wave) and S-wave (Transverse wave) ultrasonic transducer (transmitters) with the resonant frequency of 500KHZ is installed in a special upper draining end cap in the cell, and a combination of P-wave and S-wave ultrasonic receivers is installed on face of the combination of the transmitters outside of the bottom of the cell. Each transmitter is excited independently by using a switch, as well as a high voltage and short duration electrical pulsar. The applied electrical pulse firstly transforms into mechanical pulse and then passes through sample in the form of ultrasonic wave, after that it is received by the receiver installed at the bottom of the cell. The received ultrasonic wave signal is converted back to an electrical pulse, and it is manifested as an electrical waveform using a high precision digital oscilloscope. With the end caps calibration data and the waveform received by each receiver (P-wave and S-wave), the

P-wave and S-wave arrival time can be in theory measured, and then ultrasonic velocities can be calculated based on the length of sample. The measurement of elastic wave velocity can be conducted under hydrostatic, oedometric and triaxial conditions.

The particular advantage of the system is that it allows for using the velocity to assess the evolution of the microstructure of material during loading process. The only difference between the system and the previous system as shown in Figure 2.1 in chapter 2 is the ingenious installation of the transmitting device of ultrasonic wave placed into the chamber of confining pressure.

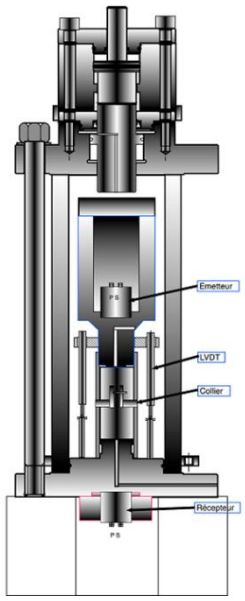

Figure 3.1 Schematic illustration of the self-equilibrium triaxial cell coupling with an ultrasonic wave cell

3.3 Preparation of synthetic clay

3.3.1 Mineralogical compositions

The basic physical properties of the mineral compositions used for the preparation of the synthesis clay are briefly introduced here. The sand GA39 has been illustrated in detail in chapter 1. The clay mineral provided by TOTAL is mainly constituted of illite with diameter of grain less than 77μm, and the density of it is about 2.68g/cm^3. The saline water with concentration of sodium chloride of 3.5% is used as the mixture solution obtained through distilled water and sodium chloride.

3.3.2 Consolidation test

In this section, we schematically introduce the experimental procedure on consolidation test, and then focus on investigating the evolution of porosity of sample during the

compaction process. Another consolidation characteristics, such as consolidation coefficient, compaction modulus and permeability, which have been discussed in detail for the five synthetic clays in chapter 1, are not discussed again. Firstly, the preparation of the synthetic clay slurry mixture is introduced. After that the slurry mixture is used to carry out the consolidation test and the testing procedure on consolidation will be briefly introduced. Finally, the evolution of porosity of sample is then discussed.

3.3.2.1 Preparation of synthetic clay in slurry

Based on the two chosen controlled indexes as mentioned above (effective vertical pressure at current, mineral composition inside argillite), the mass proportion between sand and illite for the preparation of synthetic clay is set to be 30:70. The added content of saline water is suggested to be close to the liquid limit of the mixture based on the slurry mixture method, which is equal to half of the sum mass of solid phases. In terms of the previous studied works, the added content of saline water is sufficient to make the slurry mixture have a good fluidity.

The VMI laboratory mixture apparatus as shown in Figure 1.5 is used to obtain the slurry mixture. The rotational speed of 250rmp/min for the preparation of slurry mixture is chosen again. The stirring time is about 20min. The weight of the synthetic clay slurry mixture before and after the mixing test are also measured to monitor the mass loss of water. The mass losses of water for all prepared slurry mixtures locate into the interval 1.0~2.0g. Slurry mixture with a known mass is then putted into the consolidation chamber to proceed the consolidation test. The initial mass of sample is listed into Table 3.1.

Table 3.1 Initial added mass of sample before application of consolidation pressure

Sample	*T1N01*	*T1N02*	*T1N03*	*T1N04*	*T1N05*	*T1N06*	*T1N07*	*T1N08*
Mass (*g*)	171.6	157.6	182.7	181.0	182.6	188.7	180.6	185.2

3.3.2.2 Consolidation testing procedure

Based on the previous experimental works as illustrated in chapter 1, the consolidation pressure of 7.8MPa should be imposed step by step. The consolidation pressure is thus imposed on sample by five stages with a constant increase of 1.77MPa, except for the first stage with consolidation pressure equal to 0.71MPa. The aim for the first stage is to eliminate those big cavities inside sample. The compaction test is performed through the pneumatic pressure consolidation device (Figure 1.3). Some improvements on the device have been done to deal with the sealing problem, so that the supportable pressure can reach above 8.0MPa. The loading scheme for consolidation test is listed in Table 3.2.

Table 3.2 Multistage loading scheme for consolidation test

Stage of consolidation test	S1	S2	S3	S3	S5
Consolidation pressure (MPa)	0.71	2.48	4.25	6.02	7.79

After the primary consolidation at last stage S5 has already finished, the imposed consolidation pressure is then unloaded by two stages. At the unloading process, the consolidation pressure is firstly unloaded to 4.25MPa, and then to zero. When the rebounded deformation due to the unloading of consolidation pressure becomes insignificant, the sample is then taken out from the consolidation chamber with measurements on dimension and weight of sample. After that, the triaxial compression tests are performed on these consolidated synthetic clay.

3.3.2.3 Consolidation deformation

In Figure 3.2, we show time as function of compaction deformation for each stage of consolidation obtained from the sample "*T1N08*". The compaction deformation related to the stage corresponding to the pre-compressive consolidation pressure is not presented. Similar experimental results on the compaction deformation with time for the remaining samples can be also obtained but are not displayed yet. It can be confirmed that the primary consolidation of sample at each stage of consolidation has completed.

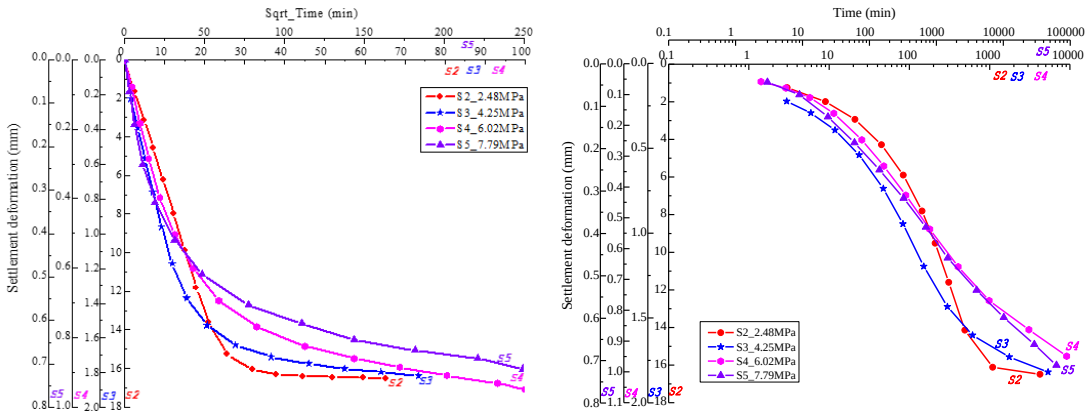

(a) Typical $\delta_{sc} - \sqrt{t}$ *curves* *(b) Typical* $\delta_{sc} - lg(t)$ *curves*

Figure 3.2 Deformation-time curves for the sample T1N08 through the uniaxial consolidation test with the multistage loading scheme: (a) Typical $\delta_{sc} - \sqrt{t}$ curves; (b) Typical $\delta_{sc} - lg(t)$ curves

When the consolidation pressure is low, the initial quasi-linear portion on the curve of compaction deformation with square-root of time becomes more significant than those with a relatively high consolidation pressure. For instant, the curve corresponding to the stage "*S2*" can be considered as a straight line before the compaction time is less than 600min, the curve for the stage "*S3*" also presents a quasi-linear feature when the

compaction time is less than 220min; for the stage S4, the linear feature can be only observed when the compaction time is less than 100min; however, for the last stage, the linear feature is not legible to be observed.

The inflection point through the curve of compaction deformation with logarithm of time becomes more difficult to be identified with increasing consolidation pressure, which is also used as an auxiliary way to confirm whether the primary consolidation of sample has completed or not. The time for completion of primary consolidation increases with augmentation of consolidation pressure. The compaction deformation for each stage of consolidation decreases with increase of consolidation pressure.

3.3.2.4 Porosity

The porosity of sample is determined in terms of the density of particle for each type of solid phase, dimension and mass of sample, mass proportion between sand and illite. The initial length and diameter (Table 3.3) of sample at each stage of consolidation are obtained based on the back-calculated method. The curves of porosity with consolidation pressure for all tested samples are shown in Figure 3.3. The diminution of porosity of sample at the stage "*S2*" with consolidation pressure increasing from 0.71 to 2.48MPa is more significant than those at the subsequent stages. The variation of porosity is mainly concentrated at the stage "*S2*".

Table 3.3 Initial length of sample at each stage of consolidation

Sample	Initial length of sample (*mm*)					Diameter (*mm*)
	S1(0.71)	*S2*(2.48)	*S3*(4.25)	*S4*(6.02)	*S5*(7.78)	
T1N01		84.71	65.34	64.33	63.35	36.04
T1N03		100.08	72.50	70.26	69.25	36.04
T1N04		95.66	68.43	66.81	65.66	36.50
T1N05		81.82	73.31	71.77	70.89	35.68
T1N06		78.15	69.51	67.81	66.99	36.07
T1N07		81.88	69.92	68.53	67.67	35.64
T1N08		87.01	70.52	68.70	67.67	35.97

Meanwhile, the porosities for all samples at the stage "*S5*" locate into the interval [0.322, 0.346]. The difference of porosity among the six samples is not obvious. Accordingly, the uniaxial consolidation test have a good repeatability. The porosities for the two samples "*T1N03*" and "*T1N04*" before the stage "*S2*" are higher than the others'. That's due to that the consolidation pressure imposed on the two samples at the stage "*S2*" is 1.91MPa without the application of the stage "*S1*". The porosity of the sample "*T1N02*" can't be obtained due to the reason that the sample is destroyed when it is taken out from the consolidation chamber, so that the measurement on dimension of sample

becomes impossible.

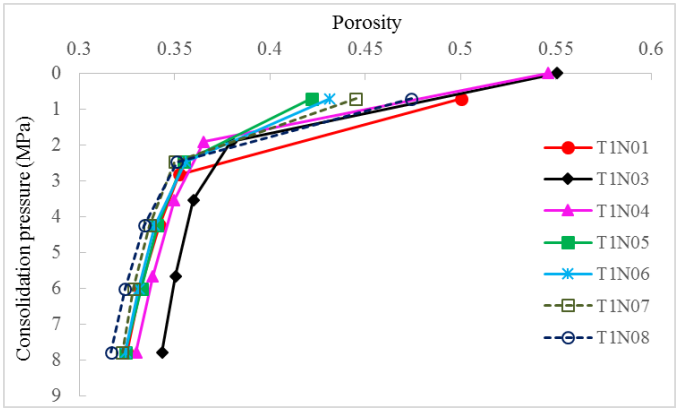

Figure 3.3 Variations of porosity of sample with consolidation pressure

3.4 Compression test

All triaxial compressive mechanical tests are realized with the help of the self-equilibrium triaxial cell accompanied with an ultrasonic wave cell. Here, only six samples are applied to carry out the triaxial compression tests. In Figure 3.4, we show a representative photo of the synthetic clay (sample "*T1N08*"). Physical properties of sample are listed into Table 3.4.

Table 3.4 Physical properties of sample after consolidation test

Sample	Physical properties				
	Length (*mm*)	Diameter (*mm*)	Mass (*g*)	Porosity	Dry density (*g/cm3*)
T1N01	62.88	36.04	135.20	0.327	1.82
T1N03	68.77	36.04	142.83	0.346	1.77
T1N04	62.33	37.04	141.19	0.333	1.80
T1N06	66.30	36.07	143.03	0.324	1.82
T1N07	67.30	35.64	141.00	0.325	1.82
T1N08	67.54	35.97	145.31	0.323	1.83

The confining pressure of 3MPa and pore pressure of 2MPa are firstly conducted on sample, which is considered as the initial stress state of sample. The initial stress state is used to saturate the tested sample, which is similar with the procedure as discussed in chapter 2. All triaxial compression tests are performed in drained conditions with pore pressure of 2MPa at room temperature 20 ± 2℃. The flow-controlling loading mode which can be considered to be equivalent to the deformation-controlling loading mode (assumption on incompressibility of oil) is chosen for application of both

confining pressure and deviatoric stress.

Figure 3.4 Representative photo of synthesis clay ("*T1N08*")

A multistage cyclic loading-unloading method is adopted for all mechanical tests. On the one hand, the permeability of the studied synthetic clay is low, which can be deduced by comparing the time for completion of primary consolidation for the two synthetic clays ("*Tx*" and "*Gx*"). If the monotonic loading is adopted instead of the multistage cyclic loading-unloading, it may give rise to the existence of excessive hydrostatic pore pressure. The deviatoric stress at the lowest point of the loading-unloading cycle of stress-strain curves is sustained about 12 hours to dissipate the possible excessive hydrostatic pore pressure. On the other hand, the elastic ultrasonic wave can be not automatically recorded. Since the emission for the P-wave and the S-wave needs to be individually switched through the manual operation. Finally, the rheological characteristic of the synthetic clay is very remarkable, whereas we mainly in present focus on investigating the short-term instantaneous mechanical behavior of the synthetic clay.

As we have illustrated at the introduction section, the conventional triaxial compression test, oedometric test and conventional triaxial compression test after oedeometric loading are performed to investigate the influence of loading path on mechanical behavior of synthetic clay. During the loading process, the elastic ultrasonic wave test is also conducted at the axial direction of sample parallel with the direction of deviatoric stress. Due to that the loading paths for the three types of triaxial compression tests are different, it's thus necessary to separately narrate the experimental procedure for each type of test as well as the experimental results, in what follows.

3.4.1 Oedometric test

3.4.1.1 Loading procedure

When the saturated state of sample have achieved and the deformation of sample at the initial pre-compressive stress state has maintained stability, both deviatoric pressure and confining pressure should increase simultaneously for the oedometric test. The confining pressure should increase to make the lateral (or radial) deformation of sample

be zero accompanied with increasing deviatoric stress. The deviatoric stress is chosen to play a dominant controlled role in the loading process in order to control the loading rate of axial strain of sample. Through monitoring the change of lateral deformation of sample, the confining pressure is then adjusted. To investigate the influence of loading rate on mechanical behavior of synthetic clay for the oedometric loading path, two different flow rates of injected oil are adopted for the two oedometric tests: 0.01ml/min corresponding to the axial strain rate of about $5.0 \times 10^{-6}\ 1/s$ for the sample "*T1N01*", and 0.005ml/min corresponding to the axial strain rate of about $5.0 \times 10^{-7}\ 1/s$ for the sample "*T1N08*".

The testing procedure for the oedometric test is given as follows. The deviatoric pressure is piloted by a computer-controlled pressure generator with the given flow rate of injected oil (0.01 or 0.005 ml/min). The confining pressure is simultaneously readjusted to make sure that the change of lateral deformation of sample keeps zero. The elastic ultrasonic wave test are also performed during the oedometric test. The multistage cyclic loading-unloading is carried out. The schematic illustration on the loading path of oedometric test in stress meridian plane $(p,\ q)$ is shown in Figure 3.5.

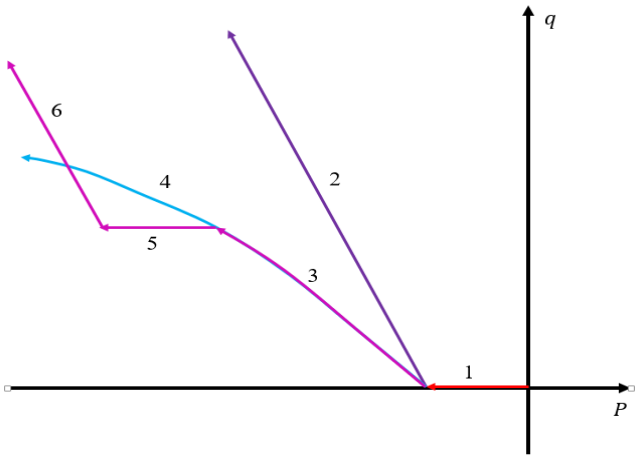

Figure 3.5 Schematic illustration of loading path in the stress meridian plane (p, q) for the three types of tests: 1) Path 1→2 represents the conventional triaxial compression test; 2) Path 1→3→4 the oedometric test; 3) Path 1→3→5→6 the triaxial compression test after oedometric loading

3.4.1.2 Experimental results

The effective axial stress versus axial strain curves obtained from the two oedometric tests are presented in Figure 3.6. The basic mechanical response of the synthetic clay under oedometric compression can be decomposed into four phases. In the first phase, a short nonlinear concave upward curve at the beginning of loading can be observed. The nonlinearity is attributed to the plastic compaction of the weakness pores and the plastic shear slip along the contact interface between two particles adjacent to those weakness pores. After that, at the second phase, a quasi-linear elastic-plastic phase is

obtained, where the effective axial stress is less than the pre-consolidation pressure. When the effective axial stress reaches to but slight less than the pre-consolidation pressure, called the pore collapse yield stress, a suddenly accelerated irreversible axial strain is produced, a plastic hardening phase. In the four phase, an accelerated increase of the contact surface between particles is produced due to the further plastic pore collapse but with a declining collapse rate, which leads to a plastic strengthening phase with a decreasing axial strain rate. The four phase can be considered to be similar to plastic consolidation in soil mechanics. The plastic deformation is clearly shown through the loading-unloading cycle on stress-strain curves.

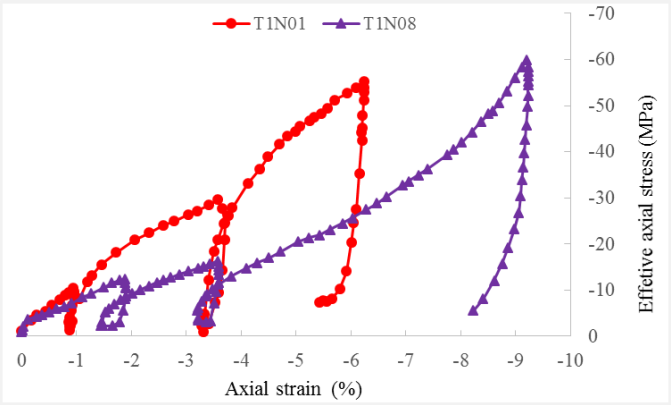

Figure 3.6 Effective axial stress versus axial strain for the two oedometric tests with different axial strain rate: (a) Circle corresponds to the axial strain rate of $5 * 10^{-6}\, 1/s$; (b) Triangle $5 * 10^{-7}\, 1/s$

The evolutions of effective lateral stress versus effective vertical stress for the two oedometric tests, i.e., σ_1 vs. σ_3, are presented in Figure 3.7. In order to clearly observe the effect of loading rate on mechanical behavior of the synthetic clay, the envelope lines of the σ_1 vs. σ_3 curves are also shown in the right side of Figure 3.7. When the imposed effective axial stress is less than the pre-consolidation pressure, the envelope lines of the two tests almost coincide with each other. After that, they separate towards to two different orientations which can be indicated by the slopes of the two curves. Combined with the experimental results as shown Figure 3.6, the mechanical behavior of synthetic clay is enhanced with increase of loading rate.

The enhanced effect on mechanical behavior of synthetic clay may be also related to the excessive hydrostatic pore pressure. The increase of excessive hydrostatic pore pressure will lead to a supplement/additional increase of confining pressure to keep the lateral strain of sample be zero. Accordingly, the applied confining pressure with a high loading rate is higher than that with a low one. Small change of the ratio between effective lateral pressure and effective axial stress can be observed, which is usually defined in soil mechanics as the coefficient of Earth pressure at rest K_{0c}. The coefficients K_{0c} for the two tests almost manifest a constant but with two different

values. In conclusion, the loading rate has an important influence on mechanical behavior of the synthetic clay.

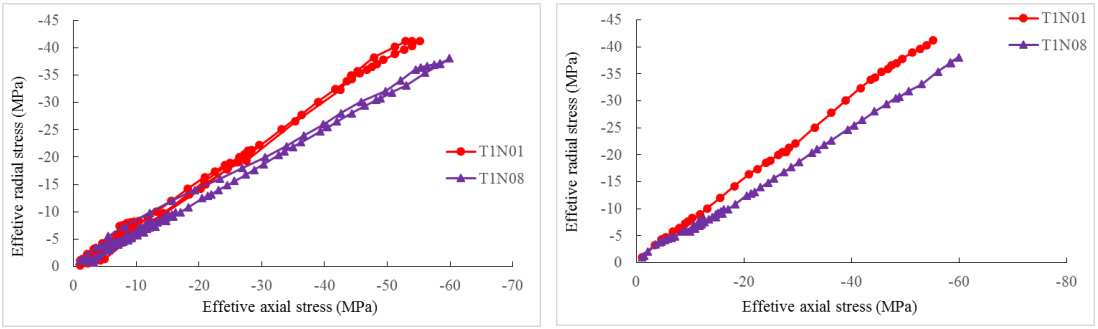

(a) Curves of multistage loading-unloading *(b) Envelope lines of loading*

Figure 3.7 Effective axial stress versus effective lateral stress for two oedometric tests with different axial strain rate

The elastic ultrasonic wave test is used to investigate the evolution of microstructure of the synthetic clay during loading process. During the loading of odeometric test, both the P- and S-wave velocities at the axial direction of sample are obtained through the measured/estimated traveltimes and the length of sample corrected by its axial strain. As the P-wave is the fastest one among all elastic waves, it's thus easy to identify the arrival time of P-wave. However, on the one hand, the S-wave is neither the fastest one nor the slowest one; on the other hand, there exist lots of interference waves such as interface wave to interrupt the identification of the arrival time of P-wave. It's usually admitted that the manual picking of S-wave-arrival time is a subjective procedure that depends greatly on the accuracy and experience of the human analyst who performs the task (Sleeman and Eck, 1999; Kurz et al., 2005).

Although it's difficult to identify the exactly arrival time of S-wave, we can choose a legible and reasonable point (crest or trough) on the receiving S-waveform curve instead of the onset point. Meanwhile, the S-waveform curves are recorded step by step with a short-time interval or a small change of deformation of sample during the loading process. Accordingly, a specific and reasonable chosen crest/trough point on one S-waveform curve will continuously occurs on its adjacent curves and regularly evolves on these recorded S-waveform curves accompanying with loading process.

Consequently, the estimated arrival time of S-wave, named as the nominal time, can be determined from the specifically chosen point. We must state here again that the arrival time of S-wave is not the actual one, but an estimated one. Even if the arrival time of S-wave is not the exact one, but the evolution on the identified time for the S-wave can be able to correctly reflect, as well as some associated deduced parameters such as the dynamic Young's modulus and dynamic Poisson ratio presented below. The evolutions of both P- and S-wave velocities as a function of axial strain for the two oedometric tests are simultaneously presented in Figure 3.8.

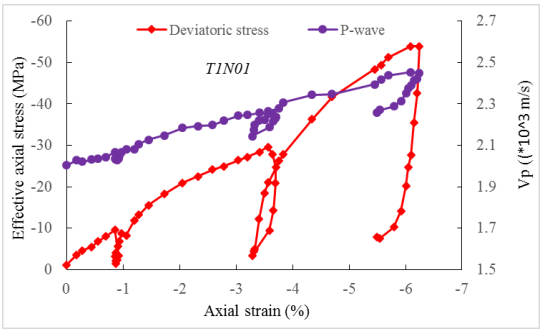

(1) Velocity of P-wave

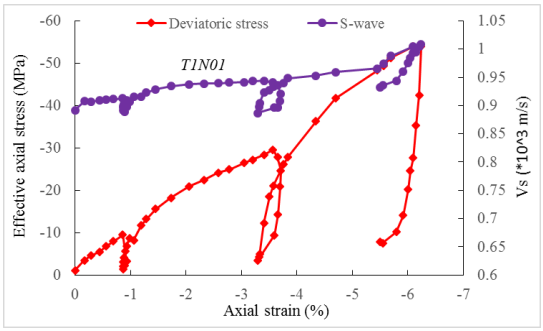

(2) Velocity of S-wave

(a) Experimental results obtained from the sample "T1N01" with strain rate of $5*10^{-6}$ 1/s

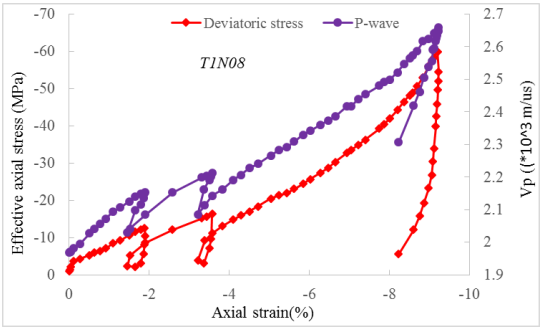

(1) Veolicity of P-wave

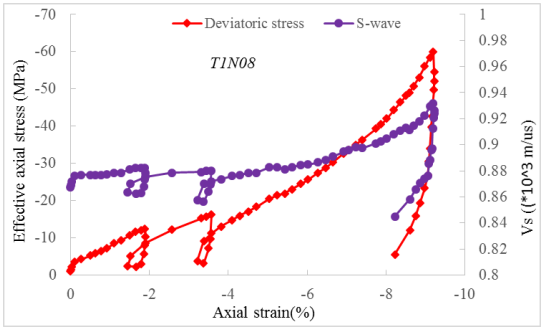

(2) Velocity of S-wave

(b) Experimental results obtained from the sample "T1N08" with strain rate of $5*10^{-7}$ 1/s

Figure 3.8 Evolution of velocity of both P- and S-wave with axial strain at axial direction of sample for the two oedometric tests

It can be seen in Figure 3.8 that the velocities of both P- and S-wave increase at loading but decrease at unloading. The discussion on the influence of loading rate on velocity of P-wave will be discussed later. However, as the arrival time of S-wave is not the exact one, it's very difficult to identify the same point on the S-waveform curves obtained from different tests and different samples. Therefore, it's unnecessary or impossible to discuss the influence of loading rate on velocity of S-wave.

The velocity of elastic wave can be commonly used to reflect the change of microstructure of material. The measured data on the velocities of both P- and S-wave, by means of the Eq. 3.1, can be used to obtain the dynamic elastic moduli of sample at the axial orientation.

$$E_d = \rho V_s^2 \frac{3V_p^2 - 4V_s^2}{V_p^2 - V_s^2};\ \nu_d = \frac{V_p^2 - 2V_s^2}{2(V_p^2 - V_s^2)} \tag{3.1}$$

in which ρ represents the mass per unit volume of material, and V_p and V_s represent the velocity of P-wave and S-wave, respectively. The ν_d is the dynamic Poisson ratio and E_d the dynamic Young's modulus of material. The alterative elastic parameters such as dynamic bulk modulus and dynamic shear modulus can be also calculated in terms of the relationships among those elastic modulus.

On account of the identification on the arrival time of S-wave, it is thus impossible to reflect the effect of loading rate on those elastic modulus. Consequently, we only focus on discussing the evolution of microstructure of synthetic clay during the loading process. Here, the dynamic Young's modulus E_d and the dynamic Poisson ratio ν_d are then chosen. Meanwhile, as the evolutions of velocity of P-wave (and S-wave) for the two oedometric tests are similar with each other, only the evolutions of E_d and ν_d as a function of axial strain obtained from the sample "*T1N08*" are shown in Figure 3.9. It can be seen that both the two elastic parameters increase at loading and decrease at unloading. When axial strain is more than 5.5% (at the fourth phase), an accelerated increase of E_d can be observed, but a progressive decreasing rate for the ν_d.

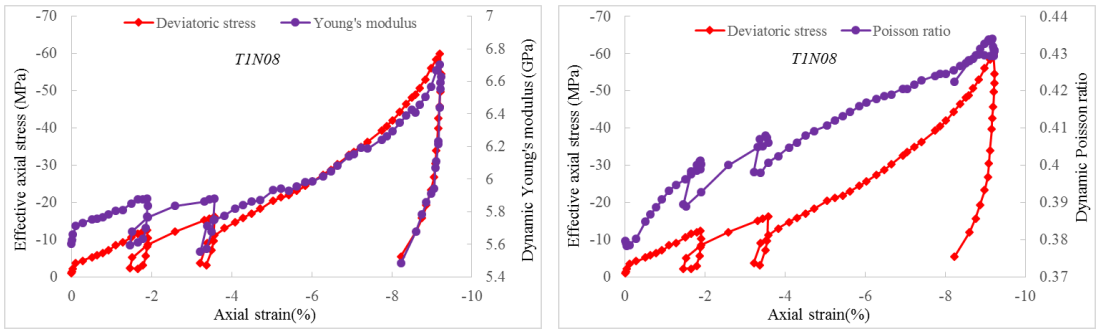

(a) Dynamic Young's modulus E_d (b) Dynamic Poisson ratio ν_d

Figure 3.9 Evolutions of dynamic modulus for the sample "*T1N08*" at the oedometric loading condition

3.4.2 Conventional triaxial compression

3.4.2.1 Experimental procedure

The conventional triaxial compression test is performed in order to obtain the basic mechanical behavior of the synthetic clay studied. The testing procedure for the conventional triaxial compression test is completely similar with that as mentioned into the section 2.3 in Chapter 2. Considering the influence of loading rate on mechanical behavior of synthetic clay, the flow-controlling loading mode with flow rate of injected oil of 0.005ml/min is adopted for application of deviatoric stress. The corresponding loading rate of axial strain of sample is about $5.0 \times 10^{-7}\ 1/s$. The multistage cycle loading-unloading is performed again due to the same reasons as those for the oedometric test. The schematic illustration of the loading path of the conventional triaxial compression test in stress meridian plane (p, q) is also shown in Figure 3.5.

3.4.2.2 Experimental results

In Figure 3.10, we present axial, radial strain as functions of deviatoric stress with different confining pressures. The mechanical behavior of synthetic clay strongly depends on confining pressure, such as the initial elastic modulus. From the loading-unloading cycle on the stress-strain curves, an obvious irreversible plastic deformation

can be observed. At confining pressure of 4MPa, a quasi-perfect plastic flow or a slight softening behavior after a nonlinear hardening phase can be observed. Instead of that, at confining pressure of 9MPa, the synthetic clay shows a continuous plastic hardening behavior with a declining growth rate. In view of the own-defined strength as mentioned in Chapter 2, the strength increases with increasing confining pressure.

There exists a clear transition from volumetric compressibility to dilatancy for the two confining pressures. The volumetric transition at the low confining pressure becomes more significant than the high one. That may be related to the over consolidation ratio and pore structure of synthetic clay. As we know, when the effective confining pressure is of 2MPa, the synthetic clay can be considered as an over-consolidated soil (the lateral pre-consolidation pressure of about 4.7MPa). Due to a relative high porosity for the synthetic clay, it is easier to take place the plastic pore collapse than the plastic friction shear slip. Accordingly, the compaction of volumetric deformation of sample becomes more significant. However, when the effective confining pressure of 7MPa, the synthetic clay can be considered as a normal consolidated soil. Although the synthetic clay has a relative high initial porosity, the porosity of synthetic clay after the application of effective confining pressure of 7MPa remarkably decreases, so that the plastic pore collapse becomes less important and may be identical to or less than the plastic friction slip. The compaction of volumetric deformation of sample at a relatively high confining pressure will become more and more insignificant.

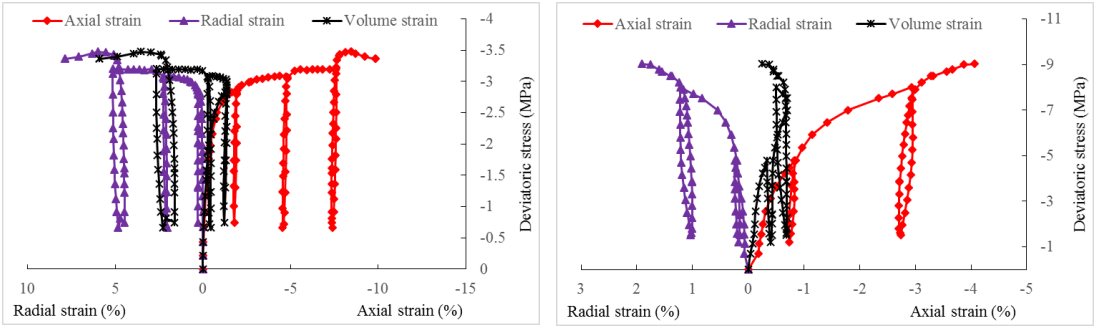

(a) Confining pressure of 4MPa *(b) Confining pressure of 9MPa*

Figure 3.10 Stress-strain curves of the conventional triaxial compression tests under different confining pressures, and pore pressure of 2MPa: (a) Confining pressure of 4MPa, (b) Confining pressure of 9MPa

During the loading process, the velocities of P- and S-wave in the axial direction of sample are also measured. The evolutions of velocities of both P- and S-wave versus the axial strain for the two tests are presented in Figure 3.11. The deviatoric stress-axial strain curves are also shown, in which only those measured points of elastic wave are displayed. The velocities of P-wave for the two tests with two different confining pressures increase at the beginning of deviatoric loading, after that, it almost keeps constant at low confining pressure but presents a continuous increase at high confining

pressure. On the contrary, the velocity of S-wave always decreases during the loading process of deviatoric stress, even at the beginning phase. We can also see that the velocity of P-wave decreases but the S-wave one increases during the unloading process of deviatoric stress. Compared the elastic wave velocities obtained from the triaxial compression test and the oedometric test (Figure 3.8 and Figure 3.11), the loading path has a significant influence on mechanical behavior and microstructure evolution of the synthetic clay studied.

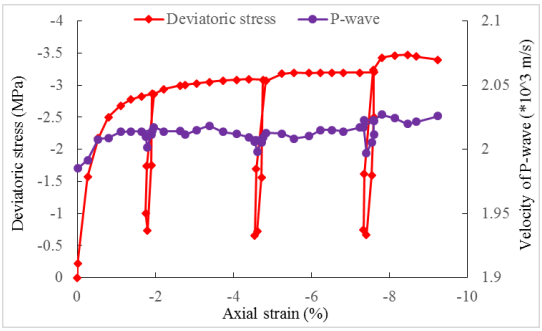

(1) Vp

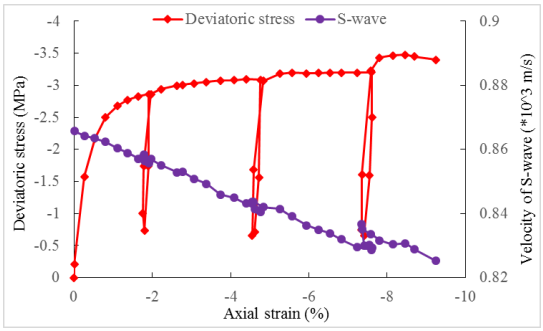

(2) Vs

(a) Sample "T1N07" with confining pressure of 4MPa

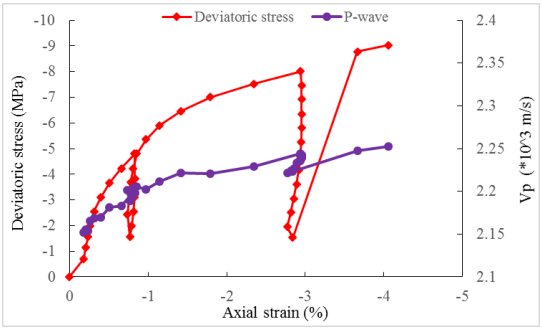

(1) Vp

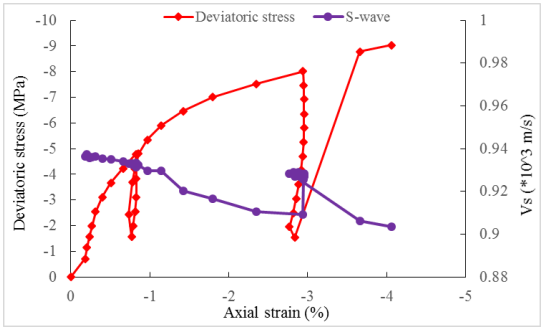

(2) Vs

(b) Sample "T1N03" with confining pressure of 9MPa

Figure 3.11 Evolutions of velocities of elastic wave for the triaxial compression tests under two different confining pressures

In terms of the results on velocities of elastic wave, the dynamic elastic modulus of synthetic clay during the process of deviatoric loading can be also obtained. In Figure 3.12, the E_d and ν_d versus axial strain obtained from the sample "*T1N07*" with confining pressure of 4MPa are shown. The E_d decreases with increase of deviatoric stress, whereas the ν_d presents an increasing characteristic. Accordingly, the elastic properties of the synthetic clay are degraded due to application of deviatoric loading. We can notice that both the decreasing rate of E_d and the increasing rate of ν_d seem to tend to a constant value. The evolutions for the two modulus differ with those at the oedometric test.

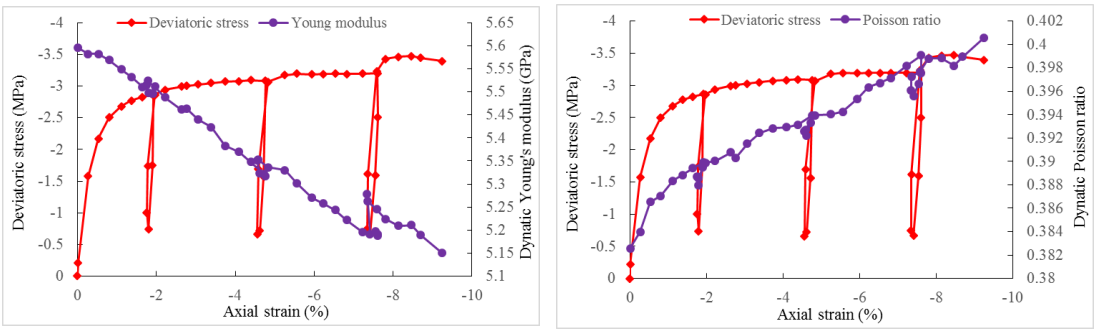

(a) E_d *(b)* ν_d

Figure 3.12 Evolutions of dynamic elasticity modulus for the sample "*T1N07*" obtained from the triaxial compression test with confining pressure of 4MPa

3.4.3 Conventional triaxial compression test after oedometric loading

3.4.3.1 Loading procedure

After the initial equilibrium state of sample has completed, the sample is then undergone the complete confined compression loading identical to the oedometric test with a flow rate of injected oil of 0.005ml/min for deviatoric loading, marked as the first loading stage. When the effective axial pressure imposed on sample is somewhat larger than but not much way above the pre-consolidation pressure, the deviatoric pressure keeps constant, whereas the confining pressure increases to the desired value through the flow-controlling loading mode with a flow rate of 0.05ml/min, marked as the second loading stage. Such stress state is kept until the deformation of sample remains stable. The purpose is to dissipate the excessive hydrostatic porous pressure in sample. Finally, the confining pressure keeps constant, and the deviatoric pressure continuously increases also through the flow-controlling loading mode with the flow rate of 0.005ml/min till the failure of sample or beyond the measuring range of the lateral deformation collar, marked as third loading stage.

One loading-unloading cyclic of deviatoric stress is performed in the last loading stage, in other words, in the conventional triaxial loading process. Meanwhile, the ultrasonic wave test is also performed. The schematic illustration of loading path for such triaxial compression test corresponding to a monotonic loading process in stress meridian plane is still shown into Figure 3.5. Two tests are performed. The first test conducted on the sample "*T1N04*" is consisted of oedometric loading till to the pre-consolidation pressure, triaxial test with confining pressure of 9MPa and pore pressure of 2MPa. The second test conducted on the sample "*T1N06*" is consisted of oedometric loading till to the pre-consolidation pressure; triaxial test with confining pressure of 11MPa and pore pressure of 2MPa.

3.4.3.2 Experimental results

The effective axial stress with strain curves for two tests with two different confining

pressure at the third loading stage are firstly presented in Figure 3.13. The differences between the two curves before the second stage are insignificant to be observed. At the first loading stage, i.e., the oedometric loading process, the curves of effective axial stress vs. axial strain for the two tests are almost similar with the one obtained from the oedometric test one. After that, the augmentations of confining pressure for the two test are set to be different. That leads to the separation of the two curves. At this stage, the volumetric strain of sample is compressive because of increase of confining pressure. At the third loading stage, the two curves present a nonlinear continuous plastic hardening characteristic, which is similar with the one obtained from the conventional triaxial compression test with a relatively high confining pressure. Meanwhile, a clear transition from volumetric compressibility to dilatancy for the two tests can be clearly observed (Figure 3.14).

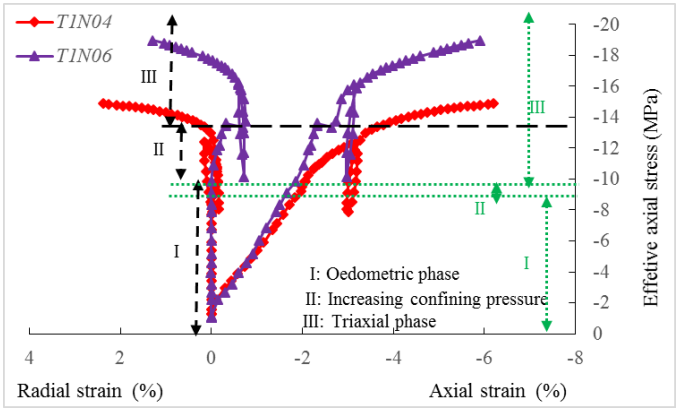

Figure 3.13 Effective axial stress-strain curves obtained from triaxial compression test after oedometric loading with different confining pressures at the third loading stage

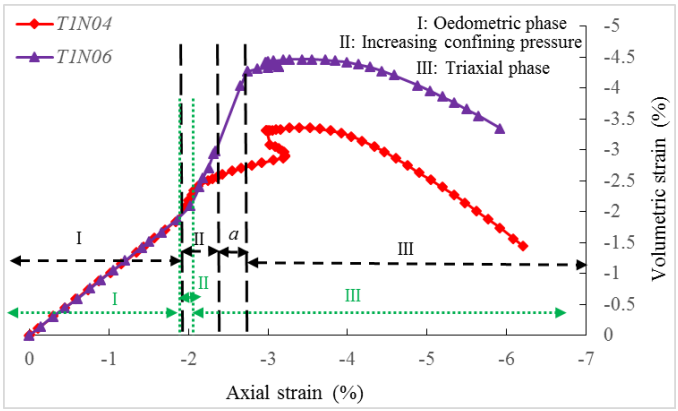

Figure 3.14 Evolutions of volumetric strain with axial strain for the two tests

From Figure 3.14, it states again that the differences of mechanical behavior between the two tests at the first loading stage are very small. It's very interesting to observe a

phenomenon that the transition points of volumetric compressibility to dilatancy for the two tests almost occurs at the same value of axial strain. After the transition point, the two curves (Figure 3.14) seem to parallel with each other, even if the confining pressures for the two tests at the third loading stage are different. In this figure, the symbol "*a*" represents the creep process existing in the second stage. We can see that the stage "*a*" with a large augmentation of confining pressure of 3MPa becomes more significant than that with a low one of 1MPa. Thus, the rheological behavior of synthetic clay is significant. We attribute it to the second stage, hereinafter.

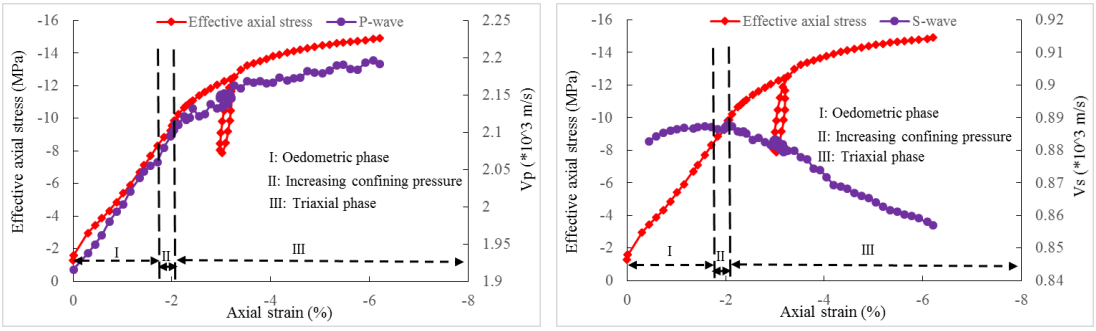

(1) Vp *(2) Vs*

(a) Sample "T1N04" with confining pressure at the third stage being of 9MPa

(1) Vp *(2) Vs*

(b) Sample "T1N06" with confining pressure at the third stage being of 11MPa

Figure 3.15 Evolutions of velocities of elastic wave obtained from the conventional triaxial compression test after oedometric loading with different confining pressure at the third stage

The evolutions of velocities of P- and S-wave versus axial strain for the two tests are shown in Figure 3.15. The velocity of P-wave for the two tests increases at the loading process. The velocity of S-wave for the two tests exist somewhat differences at the first loading stage. For instant, an increase of velocity of S-wave for the sample "*T1N04*" and a slight decrease for the sample "*T1N06*" can be observed. At the second and third loading stages, the evolutions of velocity of S-wave for the two tests are similar with each other. During the loading process of confining pressure, the velocity of S-wave increases; whereas at the process of deviatoric loading corresponding to the third loading stage, it presents a continuous decrease.

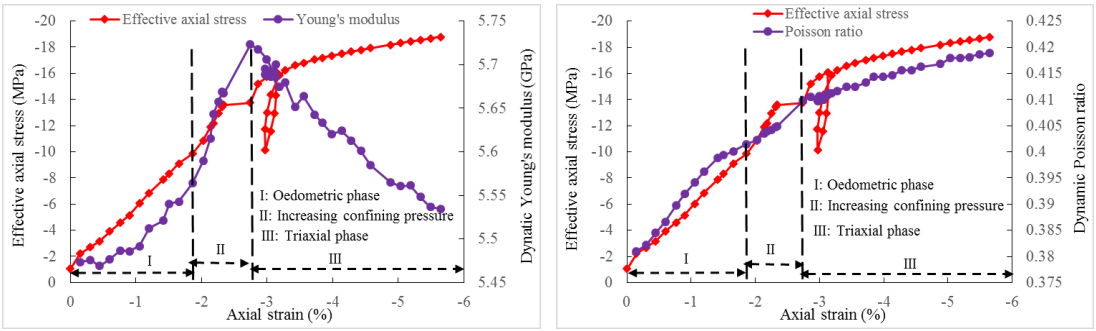

(a) Dynamic Young's modulus *(b) Dynamic Poisson ratio*

Figure 3.16 Evolutions of the two dynamic modulus of the sample T1N06 for the triaxial compression test after oedometric loading accompanying with effective confining pressure of 9MPa at the third loading stage

Comparing the experimental results on the velocities of P- and S-wave obtained from the three types of loading paths, the evolutions of velocity of both P- and S-wave for the third test can be predicted and deduced from the first two tests; in other words, the evolution of velocity of elastic wave of the synthetic clay is directly related to loading path. The evolutions of the dynamic Young's modulus and dynamic Poisson ratio of the sample T1N06 are shown in Figure 3.16. According to it, the mechanical properties of the synthetic clay is strengthened at the first two stage, but is degraded at the last stage.

3.4.4 Velocity of elastic wave

In this section, we mainly discuss the influences of loading rate and confining pressure on velocity of P- and S-wave. As it's difficult to identify the onset point of S-wave, the influence of loading rate on the velocity of S-wave is not discussed here. In order to display the influence of the two considered factors, the evolutions of velocities of P- and S-wave with axial strain respectively obtained from the oedometric test and the conventional triaxial test are shown into Figure 3.17.

From Figure 3.17a, the influence of confining pressure on velocities of P- and S-wave can be obviously observed. For the synthetic clay, both the velocities of P- and S-wave increase with augmentation of confining pressure. The evolution of velocity of P-wave is dependent on confining pressure. At a relatively low confining pressure, it almost keeps constant during the loading process of deviatoric stress, but at high one, it increases continuously. Whereas the evolution of velocity of S-wave for the two confining pressures both present a continuous decrease (Figure 3.17c).

From Figure 3.17b, when the axial strain is less than 2%, where the corresponding effective axial stress of about 19MPa has already been above the pre-consolidation pressure, the influence of loading rate on the velocity of P-wave is not obvious at this phase. After that, the evolutions between the two tests with different loading rates are similar with each other, but the velocity of P-wave for the sample "*T1N08*" with a low

loading rate is less than that of the sample "*T1N01*" with a high loading rate. The phenomenon may be associated with the excessive hydrostatic pore pressure, effective stress and another factors. The influences of those factors on the compressional velocity (P-wave) are very complex and are still an open issue, which have been studied by many authors (Biot, 1956b; Brandt, 1955; Banthia et al, 1965; Gardner et al 1965; Todd and Simmons, 1972).

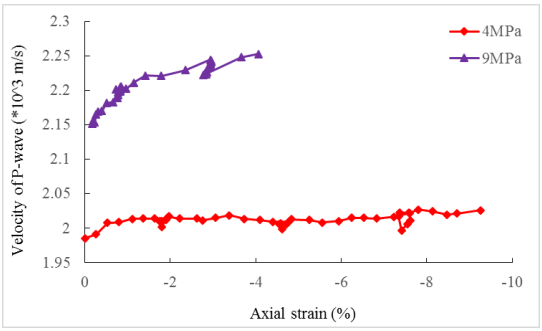

(a) Confining pressure effect on Vp

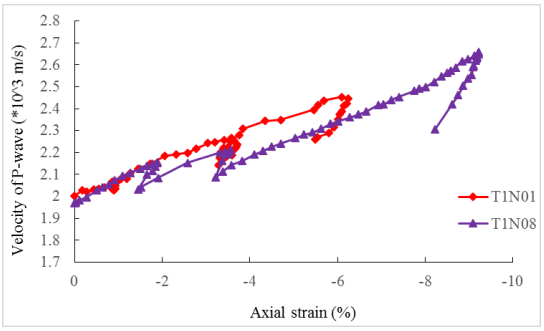

(b) Loading rate effect on Vp

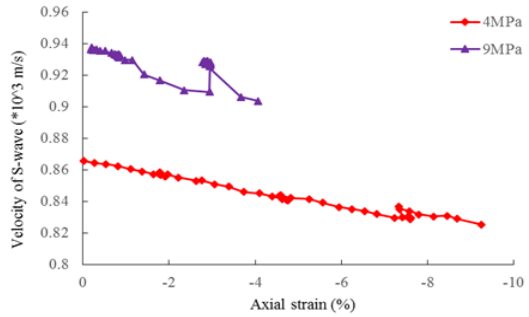

(c) Confining pressure effect on Vs

Figure 3.17 Influence of loading rate and confining pressure on velocities of P- and S-wave

3.5 Conclusion

In this chapter, we aim to investigate mechanical behavior and microstructure evolution of synthetic clay to try to provide a laboratory investigation for the argillite which is taken as the overburden rock-layer adjacent to the petroleum storage layer. For the synthetic clay, the mineral composition and mass proportion among them are set to be identical to the in-situ argillite. The saline water with concentration of sodium chloride of 3.5% is used as the mixture solution for preparation of the synthetic clay. A series of repeatable uniaxial consolidation tests have been conducted, where the imposed consolidation pressure is set to be identical to the effective vertical stress in situ of the argillite. Through the consolidation test, the consolidated synthetic clay can be obtained with porosity of about 0.33 and the dry density being about 1.8g/cm^3. The synthetic clay samples are then used to perform the three types of triaxial compression tests which are the conventional triaxial compression test, oedometric test, conventional triaxial

compression test after oedometric loading. The following main remarks can be issued:

(1) The porosity of sample at the each stage of consolidation decreases with increasing consolidation pressure. The reduction of porosity is mainly concentrated at the stage "*S2*" where the consolidation pressure increases from 0.71MPa to 2.48MPa. The time for completion of primary consolidation significantly increases with augmentation of consolidation pressure due to compaction of pore size, and reduction of permeability.

(2) Four phases can be identified from the effective axial stress versus axial strain curves obtained from the oedometric test. The synthetic clay presents a plastic strengthening behavior due to increase of contact surface between grains caused by pore collapse. The velocities of both P- and S-wave increase with augmentation of axial stress, as well as the dynamic Young's modulus and dynamic Poisson ratio. The mechanical behavior of synthetic clay is enhanced with increasing loading rate. The greater the loading rate, the higher resistance of synthetic clay.

(3) The mechanical behavior of synthetic clay strongly depends on confining pressure through the conventional triaxial compression test with two different confining pressures. At confining pressure of 4MPa, the stress-strain curves present a quasi-perfect plastic flow or softening behavior, but at confining pressure of 9MPa, a continuously plastic hardening behavior with a declining hardening rate can be observed. The volumetric deformation of synthetic clay is also dependent on confining pressure. With increasing confining pressure, the transition from volumetric compressibility to dilatancy becomes less obvious. The evolutions of velocities of P- and S-wave are associated with confining pressure. At a low confining pressure, during the process of deviatoric loading, the velocity of P-wave almost keeps constant after an increase at the beginning of loading, whereas it presents a continuous increase at a high confining pressure. For the two tests, the velocity of S-wave always decreases, as well as the dynamic Young's modulus, but the dynamic Poisson ratio increases during the process of deviatoric loading.

(4) Based on the experimental results obtained from the conventional triaxial compression test after oedometric loading, the initial difference among samples can be ignored. In view of the stress-strain responses at the third loading phase obtained from the two tests, the dependency of mechanical behavior on confining pressure can be confirmed again. The transition from volumetric compressibility to dilatancy at the third loading phase for the two tests with two different confining pressures (9 and 11MPa) seems to occur at the same axial strain, after that, a parallel evolution of volumetric strain between them can be observed.

(5) Accounting for the evolutions of velocities of P- and S-waves, as well as the dynamic elastic modulus obtained from the combined test, combined with the experimental results obtained from the oedometric test and the conventional triaxial compression test, it can be confirmed that the mechanical behavior and microstructure evolution of synthetic clay strongly depends on loading path and loading rate.

(6) Compared with the experimental results obtained from the drilled cored argillite sample (the experimental results on the argillite which have been reported for TOTAL are not presented here), the mechanical behavior of the argillite differs from the studied synthetic clay one. For instant, for the conventional triaxial compression test, the measured failure/peak strength and the velocities of P- and S-wave of the argillite are obviously higher than those of the synthetic clay, and the brittleness of the argillite is significant stronger than the synthetic clay one. The differences on mechanical behavior and ultrasonic wave property between the argillite and the synthetic clay may be related to pre-consolidation pressure, mineral composition, water content, temperature and physical-chemical reaction, porosity (argillite of 21%, synthetic clay of 33%) and degree of saturation (partial saturation for the natural argillite, complete saturation for the synthetic clay).

In the following chapter, a schematic illustration on the micromechanical-based macroscopic elastic-plastic criterion is firstly presented with the discussions on parameter identification and parameter sensitivity analyzation, from which the influences of porosity and mineral composition on mechanical behavior of material can be taken into account. After that, the above obtained experimental data are used to verify the suitability of the model for the synthetic clays studied.

Chapter 4 Modelling of poromechanical behaviors of synthetic clay

4.1 Introduction

As a kind of porous material with a relatively low permeability, a relatively high plasticity, a good self-recoverability and the absence of major fractures, synthetic clays such as the synthetic bentonite soils have been largely investigated in the context of feasibility study for geological storage of radioactive nuclear wastes, fossil resources and greenhouse gas, and exploitation of petroleum and are chosen as one of potential geological barriers. A number of experimental investigations have been performed on various porous synthetic clays (Wang et al, 2013; Wang, 2012; Martin et al, 2006; Turan et al, 2009; Domitrovic and Kovacevic Zelic, 2013; Loto and Adebayo 1990; Bianca, 2008; Yun et al, 2007; Brendan, 2014; Prashant, 2004, just to mention a few). Most experimental results have revealed that the mechanical behaviors of such porous synthetic clays exhibit some specific features such as strong pressure sensitivity, plastic pores collapse, and stronger dependency on both pore and mineral composition distributions.

Based on experimental evidences and in the framework of irreversible thermodynamics, numbers of macroscopic elastic-plastic-damage models have been developed with taking into account the effects of multi-physical coupling. The antecedent fundamental work for investigating the mechanical mechanism of deformation of porous materials at the macroscopic scale is firstly developed by Terzaghi (1925, 1943) and Biot (1941). In order to take into account the plastic pore collapse of porous material due to hydrostatic compression, the plastic yield criterions proposed should be the close-formed characteristic in the stress/strain space, i.e., a cap-formed yield surface. This is realized either through applying two distinct yield surfaces (Zhou et al, 2013; Xie and Shao, 2006, 2012; Homand and Shao, 2000, Issen, 2002) or a solely closed one (Shima ent Oyane, 1976; Lade and Kim, 1995; Lade, 1977; Hofstetter et al, 1993; Aubertin and Li, 2004).

However, both the yield criterion and the plastic potential for majority of macroscopic phenomenal models do not explicitly depend on porosity and mineral composition. Accordingly, they may be unable to take into consideration the main features at microscopic scale, such as pore, mineral composition, micro-crack, and so on. In order to overcome the above mentioned shortcoming of the macroscopic model and to interpret in essence the effects of porosity, mineral compositions and microstructure on hydro-mechanical behaviors of material, inspired by the reference work proposed by Gurson (1977) for the porous metal materials, with the help of various linear or

nonlinear homogenization techniques, many micro-macro upscaling models have been proposed for porous geomaterials (Guo et al, 2008; Lin et al, 2011; Maghous et al, 2009; Barthelemy and Dormieux, 2003; Shen et Shao, 2016; Lin et al, 2012; Shen et al, 2012 and 2013; Bikong et al., 2015; Huang et al., 2014; Jiang et al., 2015; just to mention a few). The influences of both porosity and mineral composition on mechanical behaviors of material can be taken into account through the micromechanical model which can give a more reasonable interpretation on both mechanical mechanism and microstructure evolution of material compared to the classically macroscopic model.

In view of this and based on experimental investigations on the synthetic clays studied, we thus adopt the micromechanical-based macroscopic model proposed by Shen et al. (2013) to account for the effects of both porosity and volumetric fraction of sand grain (named as inclusion for the authors). A detailed introduction on the model is firstly presented, accompanying with the parameter identification on the model. After that, the parameter sensitivity analyzation are also performed in order to obtain an in-depth knowledge on the model. Afterwards, comparisons between the model predictions and experimental results of the previous synthetic clays obtained from different triaxial compression tests are given to illustrate the suitability of the model for the synthetic clays studied. Finally, some discussions to improve the performance of the model are then illustrated.

4.2 Micromechanical-based macroscopic model

Based on the previous experimental data obtained from the synthetic clays studied, the micromechanical-based macroscopic model proposed by Shen et al. (2013) is firstly used to illustrate the adaptability of the model for the synthetic clays, through which the influences of both porosity and mineral composition on mechanical behavior of material can be reflected.

Based on the work performed by Shen et al. (2013), a two-steps homogenization procedures is applied in order to obtain the explicit form of the macroscopic plastic criterion and plastic potential for the clayey rock. For this, a representative volume (RVE) of a clayey rock at three scales is considered. The three scales are the macroscopic scale, mesoscopic scale, and microscopic scale, respectively. At macroscopic scale, the clay rock can be considered as an equivalent homogeneous medium. At mesoscopic scale, the clayey rock is taken as a heterogeneous material composed of a clay matrix (homogeneous) and mineral inclusions such as grains of quartz and calcite. At microscopic scale, the clay matrix is considered as a porous plastic compressible medium having a plastic solid phase and pores. Accordingly, the porosity is entirely included in the clay matrix.

For the sake of simplicity, the inclusions such as quartz and calcite are replaced by an effective inclusion by comparing the elastic properties of the clay matrix and of the

grains, and are considered to be randomly embedded in the porous clay matrix. The effective inclusion is characterized by a linear isotropic elastic model due to the significant difference of stiffness between sand and solid phase of clay matrix, and an isotropic elastoplastic criterion such as the Drucker-Prager criterion is used to describe the mechanical behavior of the solid phase in the clay matrix, and the pores are assumed spherical.

The so-called modified secant moduli method (Suquet, 1995) is used to determine the mesoscopic criterion of the clay porous matrix, which is recently demonstrated to be particularly efficient in the context of a non-associated flow rule (Maghous et al., 2009). The method is also used in the second step of homogenization to determine the macroscopic criterion of clayey rock. Both the compressibility of the solid phase in the clay matrix and the influence of porosity on mechanical behaviors of clayey rock can be explicitly taken into account from the macroscopic proposed model (Shen et al., 2013), as well as the rigid inclusion. In what follows, a schematic illustration on the model is presented.

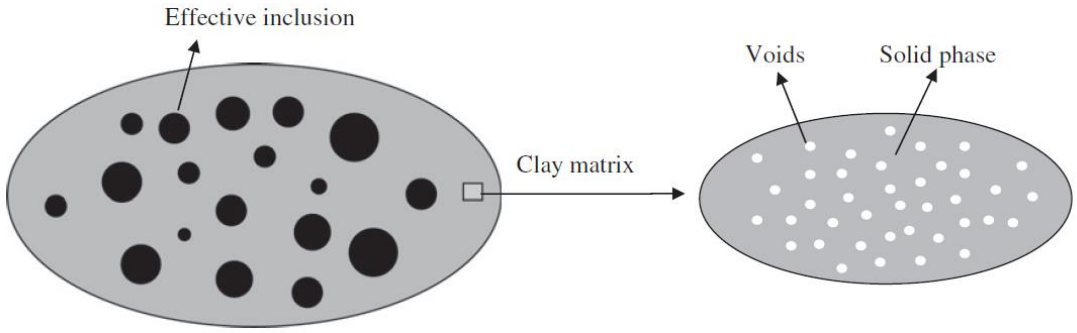

Figure 4.1 Representative volume element of clayey material (Shen et al, 2013)

The representative volume element of clayey rock at mesoscale is schematized through Figure 4.1. The clayey rock is considered as a three-phase composite constituted of clay mineral, pore and effective inclusion. Let us denote total volume of the REV as Ω, the volumes of pore, effective inclusion and solid phase in the clay matrix are represented as Ω_p, Ω_i and Ω_m, respectively. The porosity of the porous clay matrix f, which will be needed in the modeling and the volumetric fraction of the effective inclusion ρ are:

$$f = \frac{\Omega_p}{\Omega_p+\Omega_m}, \quad \rho = \frac{\Omega_i}{\Omega_i+\Omega_m+\Omega_p}, \quad \Omega_i + \Omega_m + \Omega_p = \Omega \tag{4.1}$$

The definition on the volumetric fraction of effective inclusion is similar as the commonly classical definition on the volume percentage of phase. We should stress that the porosity f is defined as the clay matrix porosity but not the macroscopic porosity $f_{ma} = \Omega_p/\Omega$ of clayey material.

As we have mentioned above, the solid phase in the clay matrix is assumed to obey the Drucker-Prager criterion which can be expressed as:

$$\phi^m(\tilde{\boldsymbol{\sigma}}) = \tilde{\sigma}_d + T(\tilde{\sigma}_m - h) \leq 0 \qquad (4.2)$$

in which the term $\tilde{\sigma}$ denotes the local stress tensor in solid phase at microscale, and $\tilde{\sigma}_d = tr(\tilde{\boldsymbol{\sigma}})/3$ and $\tilde{\sigma}_m = \sqrt{\tilde{\boldsymbol{\sigma}}' : \tilde{\boldsymbol{\sigma}}'}$ (with $\tilde{\boldsymbol{\sigma}}' = \tilde{\boldsymbol{\sigma}} - \tilde{\sigma}_m \boldsymbol{I}$) are the equivalent stress and mean stress of the local stress tensor $\tilde{\sigma}$, respectively. The $\boldsymbol{I}$ is the second order identity tensor. The parameter h represent the hydrostatic tensile strength while T denotes the friction coefficient of solid phase in the clay matrix, respectively.

For the first step homogenization, the results obtained by Maghous et al. (2009) is directly adopted to describe the plastic behavior of the porous medium at mesoscopic scale. The criterion is expressed as:

$$F^{mp}(\boldsymbol{\sigma}, f, T) = \frac{1+2f/3}{T^2}\sigma_d^2 + \left(\frac{3f}{2T^2} - 1\right)\sigma_m^2 + 2(1-f)h\sigma_m - (1-f)^2h^2 \leq 0 \qquad (4.3)$$

where $\boldsymbol{\sigma}$ represents the stress tensor at mesoscopic scale, which is identical to the scale of REV, and $\sigma_m = tr(\boldsymbol{\sigma})$ and $\sigma_d = \sqrt{\boldsymbol{\sigma}' : \boldsymbol{\sigma}'}$ with $\boldsymbol{\sigma}' = \boldsymbol{\sigma} - \sigma_m \boldsymbol{I}$ represent the mean stress and the equivalent stress, respectively. It's noted that some previous works show that the elliptic criterion given in Eq.4.3 is quite inaccurate to describe the effective yield stress of the porous material with a Drucker-Prager type solid matrix. It's particularly observed that the yield criterion is in disagreement with experimental data and computational results for porous Drucker-Prager geological material due to the symmetry of the yield criterion with respect to its middle vertical axis. Although some more accurate criteria have been proposed, it's commonly difficult to obtain an explicit form of the support function for a porous matrix based on those more accurate criteria. Accordingly, in order to obtain a closed-form macroscopic criterion for the effective plastic behavior of clayey rock, the simple elliptic criterion given in Eq.4.3 is adopted.

In terms of Eq.4.3 and applied the normality rule (the associated plastic flow rule is firstly taken into account in here, whereas the non-associated plastic flow rule is proposed inspired by the work of Maghous et al. (2009)), the mesoscopic strain rate of the porous clay matrix can be expressed as:

$$\boldsymbol{d} = \frac{T^2}{1+2f/3}\frac{d_d}{2\sigma_d}\left[\frac{1+2f/3}{T^2}2\boldsymbol{\sigma}' + \left(\frac{3f}{2T^2} - 1\right)\frac{2\sigma_m}{3}\boldsymbol{I} + \frac{2(1-f)h}{3}\boldsymbol{I}\right] \qquad (4.4)$$

in which $d_d = \sqrt{\boldsymbol{d}' : \boldsymbol{d}'}$, and $\boldsymbol{d}' = \boldsymbol{d} - d_m \boldsymbol{I}$ represents the deviator part of $\boldsymbol{d}$, and $d_m = tr(\boldsymbol{d})/3$ is the mean strain rate.

Accounting for the absolute convexity and closure characteristic of the yield function $F^{mp}(\sigma, f, T)$ in the stress space, and with the help of Eq.4.3 and Eq.4.4, the support function π^{mp} can be readily expressed as function of both volumetric strain rate and equivalent deformation rate of the porous clay matrix (Shen et al., 2013):

$$\pi^{mp} = (1-f)h\sqrt{\frac{3f}{3f-2T^2}\frac{T^2}{1+2f/3}} \times \sqrt{d_d^2 + \frac{1+2f/3}{3f/2-T^2}d_v^2} - (1-f)h\frac{2T^2}{3f-2T^2}d_v \quad (4.5)$$

where $d_v = tr(\boldsymbol{d})$ is the volumetric strain rate of the porous clay matrix.

The stress-strain relationship derived from the support function π^{mp} can be obtained. With the help of application of the second-step homogenization and a series of operators, the overall potential of composite material is obtained and reads:

$$W = \frac{1}{2}\boldsymbol{D}:\mathbb{C}^{hom}:\boldsymbol{D} + \sigma_{eq}^{p} tr(\boldsymbol{D}) \quad (4.6)$$

where $\boldsymbol{D}$ is the macroscopic strain rate, σ_{eq}^{p} denotes the isotropic pre-stress.

Finally, the macroscopic criterion of the composite constituted of the porous matrix reinforced by rigid inclusions can be delivered as the following form (Shen et al., 2013):

$$\Phi(\Sigma, f, T) = \Theta\Sigma_d^2 + \left(\frac{3f}{2T^2} - 1\right)\Sigma_m^2 + 2(1-f)h\Sigma_m - \frac{3+2f+3f\rho}{3+2f}(1-f)^2h^2 \leq 0 \quad (4.7)$$

in which $\Theta = \frac{\frac{1+2f/3}{T^2} + \frac{2}{3}\rho\left(\frac{3f}{2T^2}-1\right)}{\frac{4T^2-12f-9}{6T^2-13f-6}\rho+1}$.

The friction coefficient T is taken as a function of the locale equivalent plastic strain of solid phase in the clay matrix ε^p in order to take into account the plastic hardening of the solid matrix. The exponential functional form is adopted to describe the hardening law of the friction coefficient T:

$$T = T_m - (T_m - T_0)e^{-b_1\varepsilon^p} \quad (4.8)$$

in which T_0 is the initial value of the friction coefficient of solid phase in the clay matrix and decides the initial yield surface of the solid phase, and T_m is the asymptotic/ultimate value of the frictional coefficient. The parameter b_1 controls the kinetics of plastic hardening of the friction coefficient due to plastic deformation.

The following macroscopic plastic potential for the porous clayey material is proposed by Shen et al. (2013), which can be read as:

$$G(\Sigma, f, T, t) = \vartheta\Sigma_d^2 + \left(\frac{3f}{2Tt} - 1\right)\Sigma_m^2 + 2(1-f)h\Sigma_m - \frac{3+2f+3f\rho}{3+2f}(1-f)^2h^2 \quad (4.9)$$

in which $\vartheta = \frac{\frac{1+2f/3}{Tt} + \frac{2}{3}\rho\left(\frac{3f}{2Tt}-1\right)}{\frac{4Tt-12f-9}{6Tt-13f-6}\rho+1}$. The parameter t is the dilatancy coefficient, controlling the transition from volumetric compressibility to dilatancy, which is generally related to the plastic deformation history. In view of this, The exponential

functional form is again adopted to describe the evolution of the dilatancy coefficient t:

$$t = t_m - (t_m - t_0)e^{-b_2\varepsilon^p} \tag{4.10}$$

Based on the flow rule, the macroscopic plastic strain rate of the heterogeneous composite material can thus be given as follows:

$$D^p = \dot{\lambda}\frac{\partial \mathrm{G}(\Sigma, f, T, t)}{\partial \Sigma} \tag{4.11}$$

where $\dot{\lambda}$ is the plastic multiplier and satisfies the following loading-unloading condition:

$$\begin{cases} \dot{\lambda} = 0, \ if\ \Phi < 0;\ or\ \Phi = 0 \text{ and } \dot{\Phi} \leq 0 \\ \dot{\lambda} \geq 0, \ if\ \Phi = 0 \text{ and } \dot{\Phi} > 0 \end{cases} \tag{4.12}$$

The variation of porosity and volumetric fraction of inclusion can be determined from the kinematical compatibility, and then they are expressed as follows:

$$f = \frac{1-f}{1-\rho}tr(\boldsymbol{D}^p) - (1-f)T\dot{\varepsilon}^p;\ \dot{\rho} = -\rho tr(\boldsymbol{D}^p) \tag{4.13}$$

It is obvious to observe that the macroscopic yield criterion explicitly allows for taking into account the influence of the microstructure parameters such as porosity and volumetric fraction of mineral phase.

4.3 Identification of model parameters

There exist ten or thirteen model parameters respective for the associated plastic flow and the non-associated one, among of which the two physical parameters are the porosity f and the volumetric fraction of effective inclusion ρ, two sets of elastic parameters which are the Young's modulus and the Poisson ratio respective for the effective inclusion and the solid phase in the clay matrix, i.e., E_i, υ_i for the sand phase and E_s, υ_s for the illite phase considering the synthetic clays studied, and four plastic parameters (T_0, T_m, b_1 and h) for the associated model but seven plastic parameters (T_0, T_m, b_1, t_0, t_m, b_2 and h) for the non-associated model. For the reason of simplicity, the identification on the model parameter for the associated model is firstly illustrated below. For the non-associated one, the procedure for the identification of model parameter is almost similar with the former one. That will be briefly illustrated in later.

First all, It's very easy to determine the two physical parameters f and ρ based on the model definition, which will be firstly interpreted at the following parts. The determination on the four elastic parameters respective for the effective inclusion (sand) and the solid phase in the clay matrix (illite) (E_s, υ_s, E_i and υ_i) are subsequently

presented. Finally, the identification on the four plastic parameters (T_0, T_m, b_1 and h) for the solid phase in the clay matrix are illustrated. We here focus on how to identify the values of the model parameters for the five different synthetic clays with pre-consolidation pressure of 34.8MPa, which are thereinafter marked as the alphabet symbol "*Gx*". The synthetic clays with the pre-consolidation pressure of 7.8MPa are hereinafter represented by the alphabet symbol "*Tx*".

4.3.1 Physical parameters

The porosity f and volumetric fraction of inclusion ρ, as we have mentioned in previous chapter, are both determined based on the dimension of sample after consolidation test, density of each type of mineral composition and the corresponding drying mass, and the incompressible assumption for mineral particle. Porosity and volumetric fraction of inclusion (sand) respective for the five different synthetic clays "*Gx*" are all listed into Table 4.3.

4.3.2 Elastic parameters

The four elastic parameters for the studied synthetic clays are E_s, υ_s for the illite phase and E_i, υ_i for the sand phase. Based on the existing data found in literature (Panet and Fourmaintraux, 2004; Lide, 2004) as well as the mineralogical composition contained into the sand GA39, the two elastic modulus for the sand (quartz) are $E_i = 95GPa, \upsilon_i = 0.12$.

However, the elastic properties of the clay matrix are not precisely known and there is no direct measurement available. Inspired by the work proposed by Guery (2007), the elastic properties of the clay matrix can be determined through an iterative inversed procedure. Starting from experimental values of elastic properties measured on anyone type of the five synthetic clays and those of the quartz, the elastic properties of the clay matrix can be obtained by using the linear homogenization scheme (Mori-Tanaka).

The elastic properties of the clay matrix are related to those of its solid phase and porosity. Accordingly, a Mori and Tanaka (1973) homogenization scheme is used to obtain the elastic properties of the clay matrix and is expressed as:

$$k_0^{hom} = \frac{4(1-f)k_s\mu_s}{4\mu_s+3fk_s};\ \ \mu_0^{hom} = \frac{(1-f)\mu_s}{1+6f(k_s+2\mu_s)/(9k_s+8\mu_s)} \qquad (4.14)$$

in which k_s and μ_s represent the bulk modulus and shear modulus of the solid phase in the clay matrix, respectively; k_0^{hom} and μ_0^{hom} represent the homogenized bulk modulus and the homogenized shear one of the clay matrix. Therefore, knowing the value of k_0^{hom}, μ_0^{hom} and the porosity of the clay matrix, it allows us to determine k_s and μ_s using Eq. 4.14.

Consequently, on obtains the following typical values for the solid phase in the clay matrix for the five synthetic clays studied: $E_s = 5GPa$ and $\upsilon_s = 0.33$. We assume

that the values of the elastic properties of the solid phase in the clay matrix for the synthetic clay "*Tx*" are identical to those of the synthetic clay "*Gx*".

4.3.3 Plastic parameters

In regard of the associated model, there are only four plastic parameters which are the three plastic hardening parameters (T_0, T_m, b_1) and the hydrostatic tensile strength parameter (h). Since, in the case of the normality rule, the three pairs of paramters: $T_0 = t_0$, $T_m = t_m$ and $b_1 = b_2$, are set to be identical with each other. The following procedures for identification of the plastic parameters are performed. Numerical fitting of triaxial compression tests with different confining pressures performed on anyone of the five synthetic clays with a given mineralogical composition is firstly carried out to identify the values of the plastic parameters. The identified parameters are then validated through the other tests performed on different mineralogical compositions and porosity. In the present work, the stress-strain curves the synthetic clay G2 obtained from the conventional triaxial compression tests with two different values of confining pressures, are chosen to identify the plastic parameters. The following typical values are also listed into Table 4.3.

The four plastic parameters for the synthetic clay "*Tx*" are identified from the experimental results based on the conventional triaxial compression tests with two different confining pressures, which are listed into Table 4.5.

Before the comparisons between the model predictions and experimental results with consideration on confining pressure effect, mineralogical composition influence and loading path effect are performed, the parameter sensitive analyzation associated to the model are first carried out in order to obtain a comprehensive knowledge on the mechanical response of the model.

4.4 Parameter sensitivity analyzation

In this section, the main purpose is to analyze the influence of model parameter on the mechanical responses of the model.

4.4.1 Macroscopic yield criterion

The values of the model parameters identified from the experimental data of the synthetic clay G2 are taken as the reference values as listed into Table 4.1. We want to illustrate the influence of the porosity f, volumetric fraction of inclusion ρ, frictional angle on the surface of plasticity in the stress plane. It should be stated that we make the others model parameters be its reference value as listed in Table 4.1, when one parameter such as porosity is taken as a changeable variable. The discussion on the parameter sensitive analyzation are in-detail illustrated in following three parts.

Table 4.1 Representative values for parameter sensitivity analyzation

Model Parameters	Phase-illite	Phase-sand
Elastic parameters	$E_s = 5\ GPa$	$E_i = 95\ GPa$
	$\nu_s = 0.33$	$\nu_i = 0.12$
Plastic parameters	$T_0 = 0.3$	
	$T_m = 0.58$	
	$b_1 = 15$	
	$h = 1.8\ MPa$	
Physical parameters	$f = 0.2$	$\rho = 0.25$

4.4.1.1 Porosity

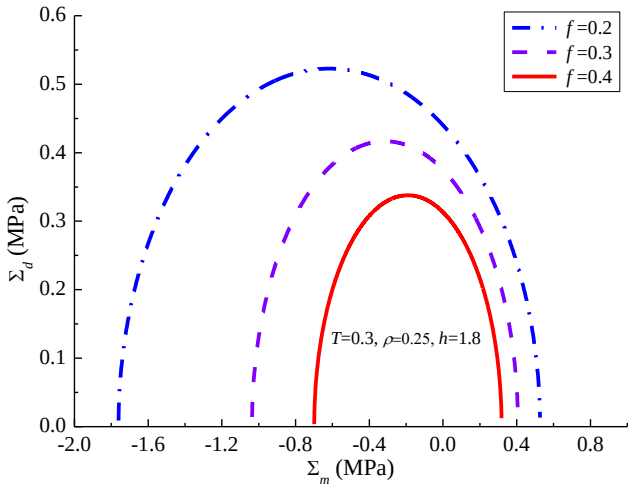

Figure 4.2 Influence of porosity on the macroscopic yield criterion in stress meridian plane $(\boldsymbol{\Sigma_m}, \boldsymbol{\Sigma_d})$

It can be seen in Figure 4.2 that the (initial) macroscopic yield surface presents a remarkable expansion with decrease of porosity. Meanwhile, the expansion effect in the compaction region where the macroscopic mean stress is negative is stronger than the tensile region with a positive macroscopic mean stress. One can notice that the symmetric axis of the yield surface progressively move towards the compaction region with decrease of porosity. The evolution mode of the yield surface due to the variation of porosity is analogous to the characteristic of the mixing hardening. Considering a fixing loading path such as the conventional triaxial compression/tension one, the dilatancy/compaction of the plastic volumetric strain predicted through the model will become more significant with increasing porosity.

4.4.1.2 Volumetric fraction of sand

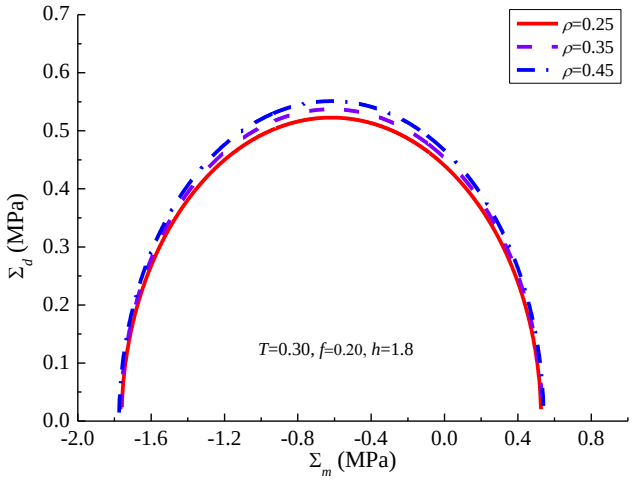

Figure 4.3 Influence of volumetric fraction of inclusion on the macroscopic yield criterion in stress meridian plane (Σ_m, Σ_d)

In Figure 4.3, the influence of volumetric fraction of inclusion on mechanical response of the model under hydrostatic stress loading condition is not obvious to be observed. From the mathematic point of view, the eccentricity of the yield curve increases with augmentation of volumetric fraction of inclusion. Meanwhile, the symmetric axis of the yield surface in stress meridian plane keeps fixing for any value of volumetric fraction of inclusion. The evolution of the yield surface due to variation of the volumetric fraction of inclusion is analogous to the characteristic of the isotropic hardening. The smaller the included angle between the line of loading path and the coordinate axis of Σ_d (equivalent shear stress) is, the greater the limit of elastic stress has. Compared with Figure 4.2, it is particularly observed that the plasticity criterion is more sensitive to porosity than the volumetric fraction of inclusion.

4.4.1.3 Cohesion of solid phase

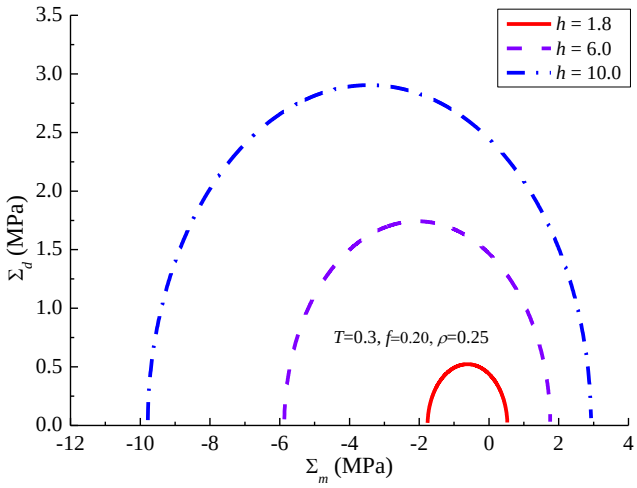

Figure 4.4 Influence of cohesion on the macroscopic yield criterion in stress plane $(\boldsymbol{\Sigma_m}, \boldsymbol{\Sigma_d})$

In Figure 4.4, the yield surface obviously expands with increasing cohesion. The symmetric axial of the yield surface progressively moves towards the negative direction of coordinate axial of the means stress Σ_m with increase of cohesion. That's very easy to understand from the yield criterion as expressed in Eq.4.7, from which the cohesion h is contained into the coefficient of the first order term Σ_m. The difference between the hydrostatic compression strength and the hydrostatic tension one becomes bigger and bigger with increasing cohesion, the asymmetry on mechanical properties on compression and tension region described through the criterion is consistent with those of geo-materials.

4.4.1.4 Friction coefficient of solid phase

The elastic region decided by the plasticity criterion in stress plane is controlled through the value of the parameter T. The greater the value of the T, the higher the elastic yield stress. In the stress plane, the evolution of the yield surface (Figure 4.5) presents a similar feature as the porosity one (Figure 4.2), whereas the expansion effect in the compaction region is obviously stronger than the tensile one and it becomes stronger than the porosity one.

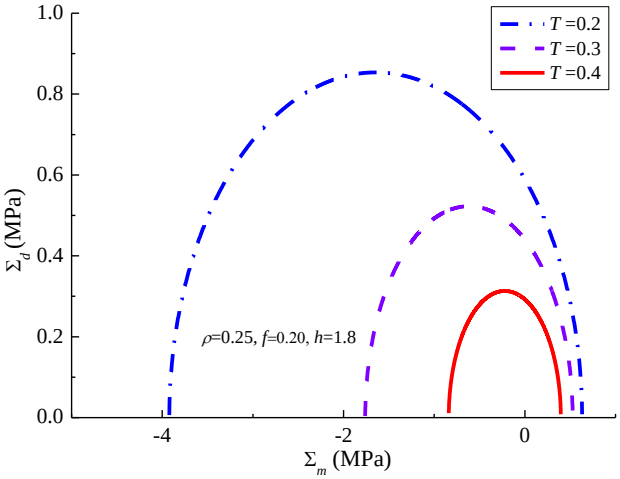

Figure 4.5 Influence of friction coefficient on the macroscopic yield criterion on stress plane $(\boldsymbol{\Sigma_m}, \boldsymbol{\Sigma_d})$

4.4.2 Stress-strain responses and strength properties

We here aim to investigate the influences of porosity ρ and volumetric fraction of inclusion f on the macroscopic stress-strain responses of the model with an associated plastic flow, and on the macroscopic strength parameters which are the macroscopic internal friction angle and cohesion based on the Mohr-Coulomb strength criterion. Before discussing that, the values of the model parameters as listed into Table 4.1 are chosen as the reference values.

4.4.2.1 Stress-strain responses

In Figure 4.6, the stress-strain response described through the associated plastic flow model depends on both porosity and volumetric fraction of inclusion. One can see that the deviatoric stress decreases with increase of porosity, but increases with increasing volumetric fraction of inclusion. From the left figure, it's obvious to observe that the initial yield stress decrease with increase of porosity as well as the lateral strain. Instead of this, one can see from the right figure that with increase of volumetric fraction of inclusion, the initial yield stress slightly increases and the lateral strain presents an increasing tendency in contrast with the porosity one.

Accordingly, the volumetric strain increases with augmentation of the volumetric fraction of inclusion, but decreases with the increasing porosity. The stress-strain response characteristics are generally coincided with the above discussions on the yield criterion. However, it's not easy to distinguish whether the influence degree of porosity on the modelling mechanical response is stronger than the volumetric fraction of inclusion one only through the stress-strain curves for different values of porosity and volumetric fractions of inclusion.

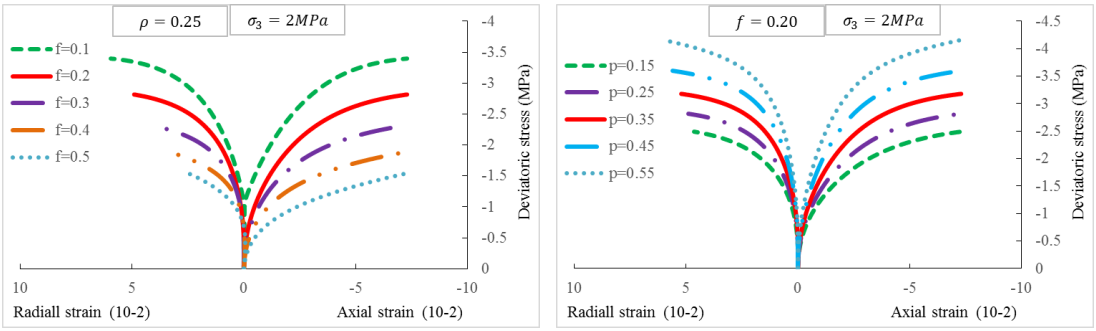

(a) Porosity *(b) Volumetric fraction of sand*

Figure 4.6 Influences of the physical parameters on the stress-strain responses of the associated model with effective confining pressure equal to 2MPa: (a) porosity f; (b) volumetric fraction of inclusion ρ

Consequently, in the next section, by means of the mathematical form of the macroscopic yield criterion and a given set of parameters values, with the help of the M-C strength criterion, the strength or peak stress corresponding to the conventional triaxial compression test at different confining pressures can be determined, and are used to illustrate the dependency of strength parameters on porosity, as well as volumetric fraction of inclusion.

4.4.2.2 Strength parameters based on Mohr-Coulomb criterion

In terms of the M-C strength criterion and the a given set of values of the model parameters as listed in Table 4.2, the two strength parameters (cohesion and internal friction angle) can then be determined.

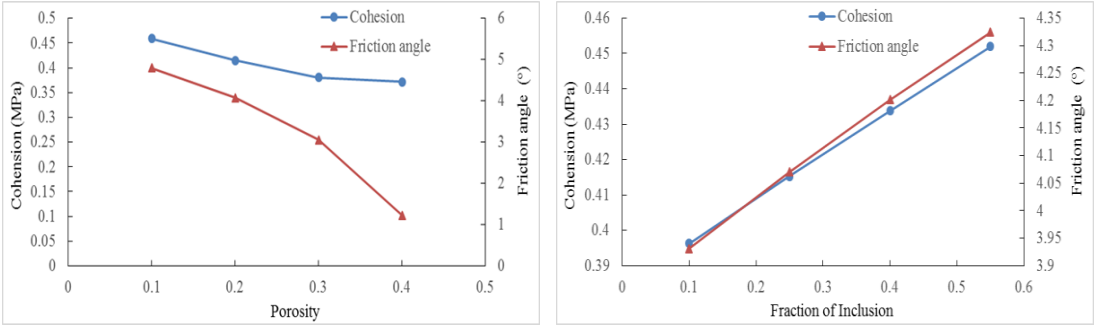

(a) Evolutions of both cohesion and internal friction angle with porosity *(b) Evolutions of both cohesion and internal friction angle with fraction of inclusion*

Figure 4.7 Correlation between strength parameters based on the M-C criterion and physical parameters: (a) Evolutions of both cohesion and internal friction angle with porosity; (b) Evolutions of both cohesion and internal friction angle with fraction of inclusion

We will briefly introduce the procedure related to obtaining the two strength parameters. Taking porosity as an example, the volumetric fraction of inclusion is set to be 0.25 and the friction coefficient T has reached to the asymptotic/ultimate value $T_m = 0.58$, the

strengths σ_1 for an invariable porosity ($f = 0.1, 0.2, 0.3$ and 0.4) and volumetric fraction of inclusion ($\rho = 0.25$) corresponding to the confining pressure $\sigma_3 = 0, 2, 4, 6, 8MPa$ can be easily obtained through the macroscopic yield criterion. After that, based on these obtained stress (σ_3, σ_1), the internal friction angle and cohesion can be calculated through the slope of the fitting straight line and its intercept with coordinate axial of σ_1. In Figure 4.7, the porosity as a function of cohesion and internal friction angle are both presented, as well as the volumetric fraction of inclusion.

One can see in Figure 4.7 that both the cohesion and internal friction angle decrease with increase of porosity. On the contrary, they both increase with increase of volumetric fraction of inclusion. Meanwhile, the influence of porosity on cohesion is slightly stronger than the one of the volumetric fraction of inclusion, whereas the influence of the volumetric fraction of inclusion on the internal friction angle is significantly weaker than the porosity one. For instant, when the porosity increases from 0.1 to 0.4, the cohesion and internal friction angle vary from 0.46 to 0.37 and 4.8 to 1.2, respectively. Nevertheless, when the volumetric fraction of inclusion also increases from 0.1 to 0.4, the cohesion and internal friction angle respectively vary from 0.39 to 0.43 and 3.9 to 4.2.

Table 4.2 Parameters values for analyzation on strength parameters based on M-C criterion

Model Parameters		Phase-illite matrix	Phase-inclusion of sand
Elastic parameters		$E_s = 5\ GPa$	$E_i = 95\ GPa$
		$\nu_s = 0.33$	$\nu_i = 0.12$
Plastic parameters		$T_0 = 0.3$	
		$T_m = 0.58$	
		$B = 15$	
		$h = 1.8\ MPa$	
Physical parameters	1	$f = 0.1, 0.2, 0.3, 0.4$	$\rho = 0.25$
	2	$f = 0.2$	$\rho = 0.1, 0.25, 0.4, 0.55$

4.5 Experimental validation

After the identification and sensitivity analyzation on model parameter have performed, in this section, we will use the above micromechanical-based macroscopic model to reproduce the macroscopic mechanical behavior of the synthetic clays, considering the influences of porosity and volumetric fraction of mineral phase (sand). As the pre-consolidation pressures imposed on the two series of synthetic clays "*Gx*" and "*Tx*" are different with each other, and the mineralogical composition and diameter of illite used to prepare the two series of synthetic clays "*Gx*" and "*Tx*" are different, the discussions on the verification of the micro-macro model respective for the two series of synthetic

clays "*Gx*" and "*Tx*" are separately illustrated through the following two parts.

4.5.1 Synthetic clays--"*Gx"*

The five different synthetic clays are used to systematically investigate the influence of porosity and mineralogical composition on the macroscopic mechanical behavior of the synthetic clays. As the experimental results of the synthetic clay "*G2*" obtained from the conventional triaxial compression tests have been used as the calibration of the model parameters, the comparisons between the model reproduction and the experimental results of the synthetic clay "*G2*" are used as a direct validation of the model capability.

With these parameters as listed in Table 4.3, in Figure 4.8 we show the comparisons between numerical results by the micro-macro model and experimental data for the remaining four different synthetic clays for the conventional triaxial compression tests with confining pressure of 4 and 9MPa, and pore pressure of 2MPa. The model predictions are in good agreement with the experimental data for the synthetic clays G1, based on which the influence of mineralogical composition on the macroscopic mechanical behavior of the synthetic clay "*G1*" as well as the porosity one can be well reflected. However, the model predictions seem to be unsuitable to correctly reproduce the main features of mechanical behavior of the three different synthetic clays ("*G3*", "*G4*" and "*G5*") with a relatively high content of sand. And with increase of such as from the synthetic clay "*G3*" to the "*G5*" one, the differences between the model predictions and the experimental results become more and more significant.

Table 4.3 Parameters values with associated plastic flow with a different value of porosity for the synthetic clays "*Gx*"

Typical value of model parameters			
Synthetic clay		Phase-illite	Phase-sand
Elastic parameters		$E_s = 5GPa$	$E_i = 95GPa$
		$\mu_s = 0.33$	$\mu_i = 0.12$
Plastic parameters		$T_0 = 0.30$	
		$T_m = 0.58$	
		$b_1 = 15$	
		$h = 1.8MPa$	
Physical parameters		$f =$	$\rho =$
	G1	0.23	0.12
	G2	0.20	0.25
	G3	0.28	0.37
	G4	0.39	0.48
	G5	0.62	0.53

Based on the model assumption on porosity, all pores are considered to only exist into the clay matrix, and the cementation between the solid phase in the clay matrix and the sand phase is considered to be completely bonded without destruction. Meanwhile, the sand particles are considered to be separated from each other and assumed to be embedded into the clay matrix. Practically, the assumption on porosity is in disagreement with the experimental observations through both the X-Ray Computed Tomography Scan (CT scan) and the Scanning Electron Microscope means (SEM) as shown in Appendix Figure.A.3 and Figure.A.4.

It can be observed from the two figures that there may exist at least two types of pores for the studied synthetic clays at two different scales, i.e., micro-pore and the meso-pore. The porosities corresponding to the two types of pores are respectively named as the microscopic porosity f_{mi} and the mesoscopic porosity f_{me}. Accordingly, let us denote the porosity existed in the porous clay matrix as the matrix microscopic porosity, i.e., $f = f_{mmi}$, hereinafter. The diameter of the micro-pore corresponding to the microscopic porosity f_{mi}, which is identical to that of the clay matrix pore, is assumed to be remarkably less than the mineralogical particle/aggregation one. Whereas the diameter of the meso-pore corresponding to the mesoscopic porosity f_{me} is assumed to have the same order of magnitude as the mineralogical particle/aggregation one. We should stress that the matrix microscopic porosity f_{mmi} is not equal to the microscopic porosity f_{mi}, i.e., $f_{mmi} \neq f_{mi}$, which will be illustrated below.

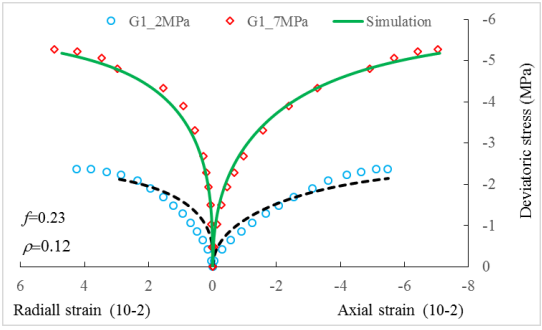

(a) Sythetic clays G1 (sand 15%)

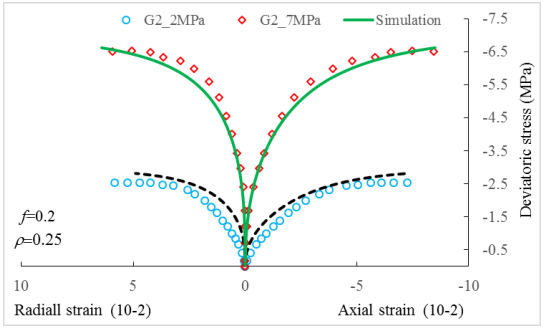

(b) Sythetic clays G2 (sand 30%)

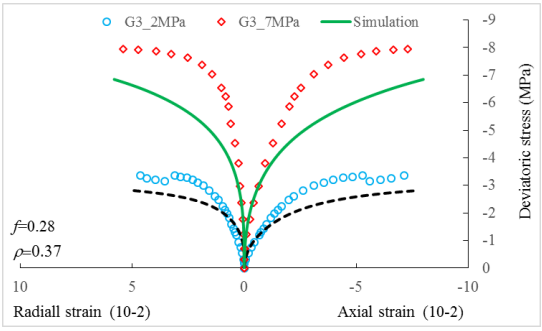

(c) Sythetic clays G3 (sand 45%)

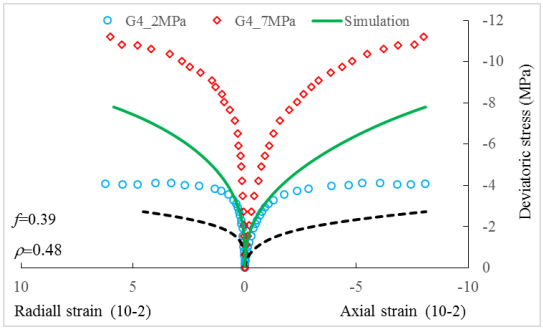

(d) Sythetic clays G4 (sand 60%)

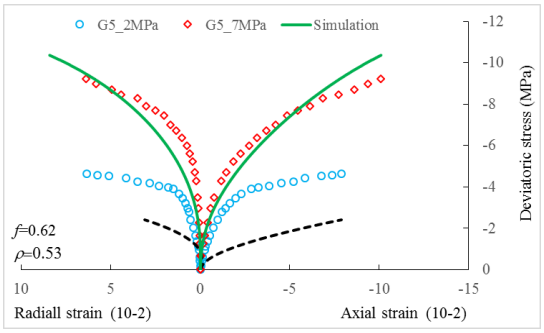

(e) Sythetic clays G5 (sand 75%)

Figure 4.8 Comparisons between numerical simulations and experimental data for the five synthetic clays obtained from the triaxial compression test with two different effective confining pressures of 2 and 7MPa, and pre-consolidation pressure of 34.8MPa

Considering some natural/synthetic geomaterials, there could exist the pore which can be directly seen through eyes such as macro-crack, cavity. This type of pore is often called as the macroscopic pore and the corresponding porosity is named as the macroscopic porosity f_{ma}. Based on the observation on the surface of all synthetic clays samples studied, there are not the macroscopic pore. Consequently, the interpretation on the macroscopic pore are not discussed in what follows.

In order to clearly understand the three types of porosities very well, the definitions on each of them are then schematically illustrated below. Taking into account the REV as shown in Figure 4.9, the total volume occupied by the RVE in space is considered to be V. We assume that the volume occupied by the micro-pore, meso-pore, sand and the solid phase (Illite) in the clay matrix are represented as V_{pmi}, V_{pme}, V_i and V_s, respectively. The total volume V of the REV and the total volume of pore V_p can be expressed as:

$$V = V_s + V_i + V_{pmi} + V_{pme};\quad V_p = V_{pmi} + V_{pme} \tag{4.15}$$

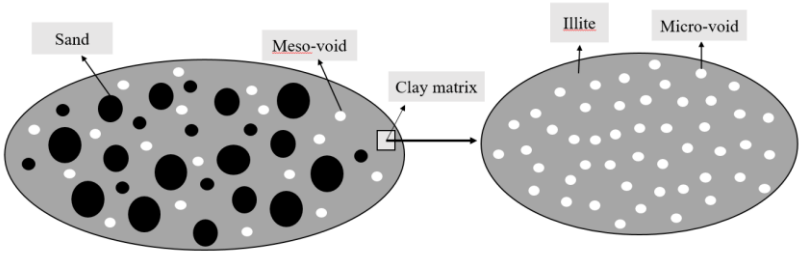

Figure 4.9 Representation of synthetic clay with mineral inclusion at mesoscopic scale, and pores at both microscopic and mesoscopic scale

Let us denote the volume of the clay matrix as V_{ms}. In the context of the signification on the clay matrix defined by the model, it can be read as:

$$V_{ms} = V_s + V_{pmi} \tag{4.16}$$

According to that, the definitions for the three types of porosity: f_{mi}, f_{me}, f_{ma}, and volumetric fraction of inclusion can be easily determined by us based on the following expressions.

$$f_{mi} = \frac{V_{pmi}}{V};\ f_{me} = \frac{V_{pme}}{\mathrm{V}};\ f_{ma} = \frac{V_p}{\mathrm{V}};\ \rho = \frac{V_i}{V} \tag{4.17}$$

Finally, the matrix microscopic porosity which is needed for the modelling takes the following form:

$$f_{mmi} = \frac{V_{pmi}}{V_{ms}} = \frac{\mathrm{V}-V_i-V_{pme}-V_s}{\mathrm{V}-V_i-V_{pme}} \neq \frac{\mathrm{V}-V_i-V_s}{V-V_i} \tag{4.18}$$

Accounting for the above mentions, it's necessary for us to determine the matrix microscopic porosity f_{mmi} due to reason that it is needed for the modelling of the model. However, on the one hand, due to the existence of meso-pore seen from Eq.4.18, the assumption on porosity adopted by the model can make the predicted mechanical behavior obtained through the model will degrade compared with those of the synthetic clay with a relatively low value of the microscopic matrix porosity. Meanwhile, for the reason of the existence of meso-pore and some potentially unavoidable errors on the back-calculated porosity, the porosity used for the modelling of the model as listed in Table 4.3 is not the real one for the five types of synthetic clays. On the other hand, the pre-consolidation pressures imposed on the five different synthetic clays ("*G1"*~ "*G5"*) are the same almost with the identical loading procedures among them. Moreover, the mineralogical components among the five synthetic clays are completely identical with each other, but with different mineral proportions.

Accordingly, in the context of the absence on the reliable experimental data on pore size and their distribution measured through the mercury intrusion test combined with some microscopic scanning technologies, it seems to be reasonable to assume that the matrix microscopic porosity for the five different synthetic clays can be considered to be identical.

Based on the above discussions, the matrix microscopic porosity with value of $f = f_{mmi} = 0.2$ for the five synthetic clays is adopted as listed in Table 4.4 in order to observe the model predictions and compare the model prediction with the experimental results again. First of all, we should point out that the influence of the meso-pore on mechanical behavior of synthetic clay is ignored. Secondly, for the reason of simplicity, the values for the other model parameters such as elastic parameters, plastic parameters and volumetric fraction of inclusion are also considered to be identical to those as listed into Table 4.3.

Table 4.4 Parameter values with associated flow rule, in the context of an identical value of porosity for the synthetic clays "*Gx*"

Typical value of model parameters			
Synthetic clay		Phase-illite	Phase-sand
Elastic parameters		$E_s = 5GPa$	$E_i = 95GPa$
		$\mu_s = 0.33$	$\mu_i = 0.12$
Plastic parameters		$T_0 = 0.30$	
		$T_m = 0.58$	
		$b_1 = 15$	
		$h = 1.8MPa$	
Physical parameters		$f =$	$\rho =$
	G1	0.20	0.12
	G2	0.20	0.25
	G3	0.20	0.37
	G4	0.20	0.48
	G5	0.20	0.53

With these parameters, the comparisons between the model predictions and the experimental results for the five synthetic clays are shown in Figure 4.10. One can see that, compared with the previous comparisons between the model predictions and the experimental results as shown in Figure 4.8, in a general way, the model can correctly reproduce the main features of mechanical behavior of the five synthetic clays with different mineral compositions, different macroscopic porosities with an identical matrix microscopic porosities.

It is noted that although the numerical simulations for the five synthetic clays at the effective confining pressure of 2MPa can be well consistent with the experimental data, the differences between the model predictions and experimental results with effective confining pressure of 7MPa becomes more and more inconsistent with increase of . That can be related to the following reasons, with the help of the microscopic scanning photos as shown in Figure.A.3 and Figure.A.4: (1) existence of mesoscopic pores; (2) meso-cracks existing at the contact interface between illite and sand; (3) skeleton structure transition of synthetic clay from that constructed through clay to that of sand with increase of .

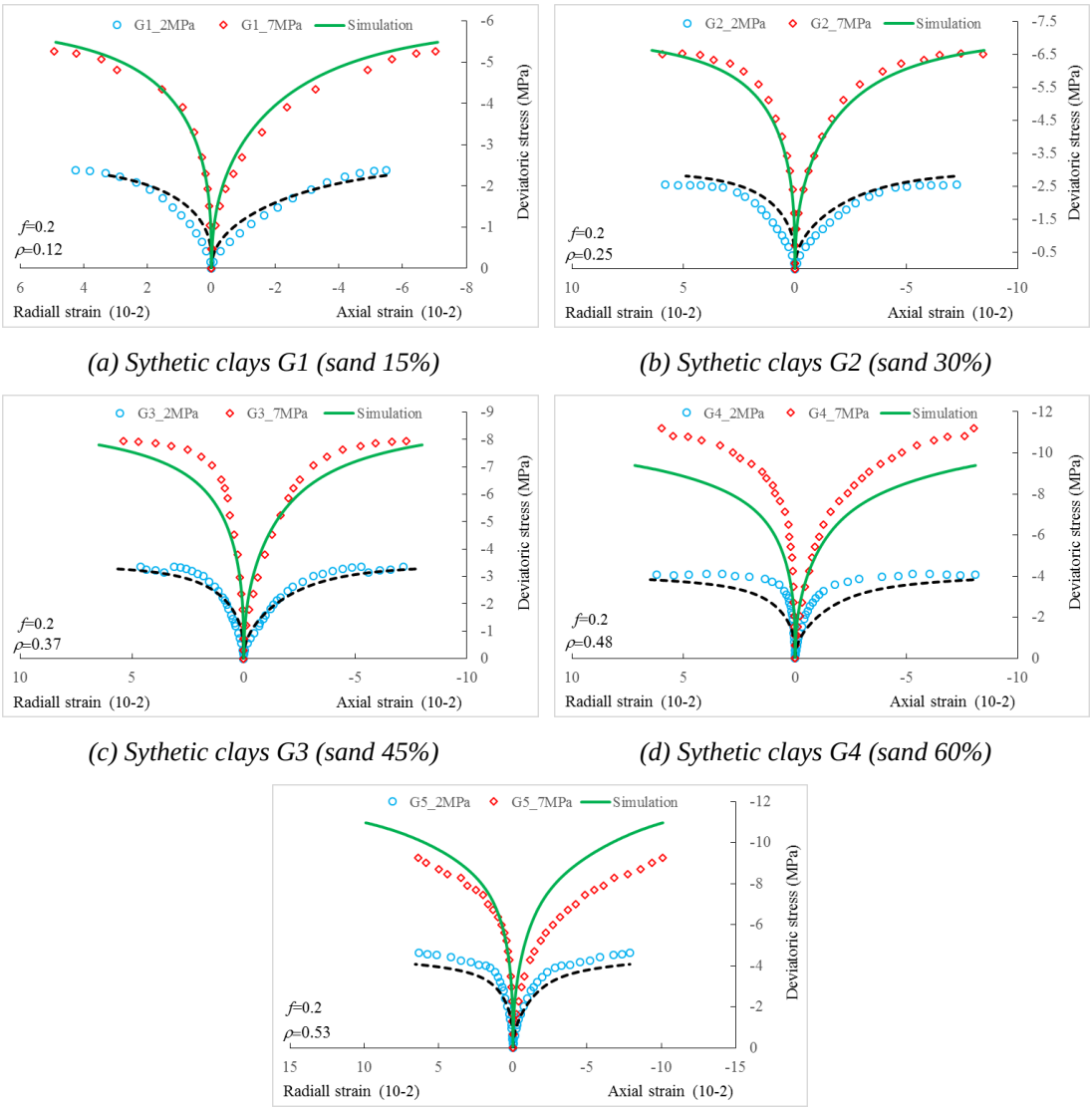

(a) Sythetic clays G1 (sand 15%)

(b) Sythetic clays G2 (sand 30%)

(c) Sythetic clays G3 (sand 45%)

(d) Sythetic clays G4 (sand 60%)

(e) Sythetic clays G5 (sand 75%)

Figure 4.10 Comparisons between numerical simulations and experimental data for the five synthetic clays obtained from the triaxial compression test with two different effective confining pressures of 2 and 7MPa, and the pre-consolidation pressure of 34.8MPa

4.5.2 Synthetic clays--"*Tx*"

For the synthetic clay "*Tx*", three different types of triaxial compression tests have been conducted, which are the conventional triaxial compression test, oedometric test and conventional triaxial test after oedometric loading, respectively. The loading paths corresponding to the third type of triaxial compression test can be easily obtained through a simple combination of the first two types of tests. Therefore, the work on the comparisons between the model predictions and the experimental results obtained from the conventional triaxial compression test after oedometric loading is not thus performed hereinafter.

Table 4.5 Parameters values of associated plastic flow model for the synthetic clays "*Tx*", identified through the experimental results obtained from the conventional triaxial compression test

Typical value of model parameters		
Synthetic clay	Phase-illite	Phase-sand
Elastic parameters	$E_s = 5GPa$	$E_i = 95GPa$
	$\mu_s = 0.33$	$\mu_i = 0.12$
Plastic parameters	$T_0 = 0.01$	
	$T_m = 1.0$	
	$b_1 = 50$	
	$h = 0.7MPa$	
Physical parameters	$f =$	$\rho =$
	0.41	0.20

Meanwhile, the influence of loading rate on mechanical behavior of material can't be taken into consideration through the model. The values of the model parameters for the synthetic clays "*Tx*" are identified based on the experimental results obtained from the conventional triaxial compression tests as listed in Table 4.5.

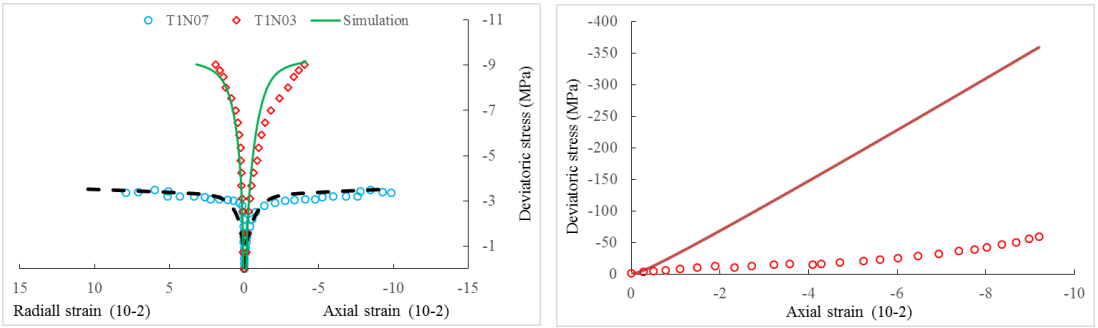

(a) Conventional triaxial compression test *(b) Oedometric test*

Figure 4.11 Comparisons between numerical simulations and experimental data of the synthetic clays with pre-consolidation pressure of 7.8MPa for: (a) conventional triaxial compression test; (b) oedometric test

With these parameters, the comparisons between the model predictions and experimental results obtained from the conventional triaxial compression tests with two different confining pressures and the oedometric test are simultaneously shown in Figure 4.11.

As we can see in Figure 4.11(a) that a relatively good consistence between the model predictions and experimental data obtained from the conventional triaxial compression tests can be observed. However, such consistence can be solely considered as the experimental calibration on the model performance. As the experimental data obtained from the conventional triaxial compression tests have been used for the identification on the model parameters.

One can see from Figure 4.11(b) that the model is unsuitable to reproduce the mechanical behavior of the synthetic clay for the oedometric loading path. It's obvious to observe that the effective axial stress is considerably overestimated by the model, compared with the experimental results of the oedometric test. That can be understood that the elastic region determined based on the experimental results of the conventional tiraxial compression test is overestimated for the oedometric loading path. As we know, once the model parameters are identified by means of the experimental data obtained from anyone type of triaxial compression tests such as the conventional triaxial compression test, the surface of the plasticity criterion in the stress space can be then completely confirmed, as well as the plastic potential surface. In order to give an intrinsic illustration on the over-estimated effective axial stress for the oedometric loading path, the associated plastic flow model is then used and discussed below.

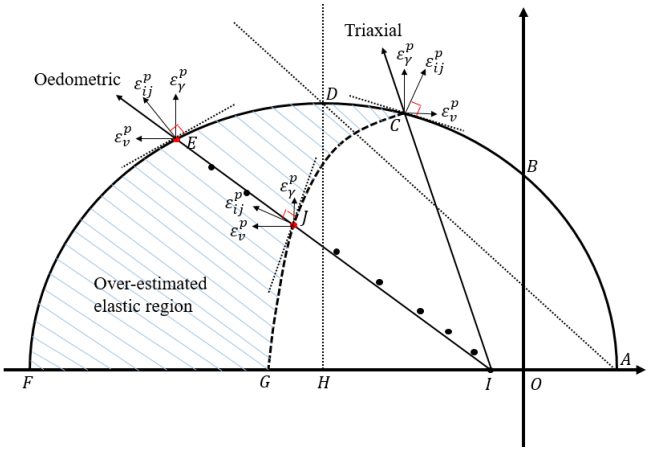

Figure 4.12 Schematic illustration on the macroscopic yield surface and the loading paths respective for the oedometric test and conventional triaxial compression test in the stress meridian plane $(\boldsymbol{\Sigma_m}, \boldsymbol{\Sigma_d})$

The loading paths respective for the two types of triaxial compression tests and the surface of plasticity criterion (the elliptic curve with solid line described through "ABCDEF") in stress meridian plane are schematically shown in Figure 4.12, where we assume that the plasticity criterion is confirmed based on the experimental results of the conventional triaxial compression test. With the help of the Figure 4.12, the over-estimated axial stress can be interpreted through the following main remarks. First all, we assume that the practical surface of plasticity for the synthetic clays studied in the

stress plane can be described through the curve “ABCJH” instead of the “ABCDEF”. Accordingly, it is particularly observed that there exists an over-estimated elastic region for the oedometric loading path, which will lead to an excessively high elastic yield stress. Meanwhile, the volume of plastic strain at the point “E” corresponding to the loading path of the oedometric test, which is completely determined by the orientation of the differential derivative of the yield function versus stress tensors perpendicular to the yield surface towards to the outside, is remarkably lower than . In order to make the lateral deformation of sample keep constant, the lateral stress or confining pressure needs to increase faster than that with the same deviatoric stress or axial strain.

We can notice once again that the mathematical form of the yield criterion in the stress meridian plane has the elliptic feature. Nevertheless, the failure surface in stress space for most geomaterials determined through experiments at laboratory with various loading paths commonly presents an irregular surface profile. The mathematical form has some shortcomings to suitably account for the mechanical behavior of our synthetic clays studied under various loading paths. Although the quality of the numerical predictions relates to the accuracy of the yield criterion, more accurate yield criteria are not able to guarantee the validity of an associated flow rule, which has been studied and illustrated by Shen (2011).

In view of this, in the next work, we propose to employ the following two means to improve the accuracy of the model on the overestimated deviatoric stress only for experimental results of the oedometric test, respectively.

4.5.2.1 Associated plastic flow for oedometric test

Table 4.6 Typical values of parameters for the associated model for the synthetic clays “Tx”

Typical value of model parameters		
Synthetic clay	Phase-illite	Phase-sand
Elastic parameters	$E_s = 5GPa$	$E_i = 95GPa$
	$\mu_s = 0.33$	$\mu_i = 0.12$
Plastic parameters	$T_0 = 0.01$	
	$T_m = 0.46$	
	$b_1 = 50$	
	$h = 12.5MPa$	
Physical parameters	$f =$	$\rho =$
	0.41	0.20

For the first method, the associated plastic flow rule are still adopted to predict the mechanical behavior of the synthetic clay, but the values of the plastic parameters which differ from these presented into Table 4.5 are listed into Table 4.6. The purpose of that

is to change the profile of the yield criterion in order to make the slope of the direction of the differential derivative of the yield surface with the stress tensor corresponding to the loading path of the oedometric test become greater.

Using the values given in Table 4.6, we show the numerical prediction of the associated model and compare it with the experimental data in Figure 4.13. A good agreement between them can be observed.

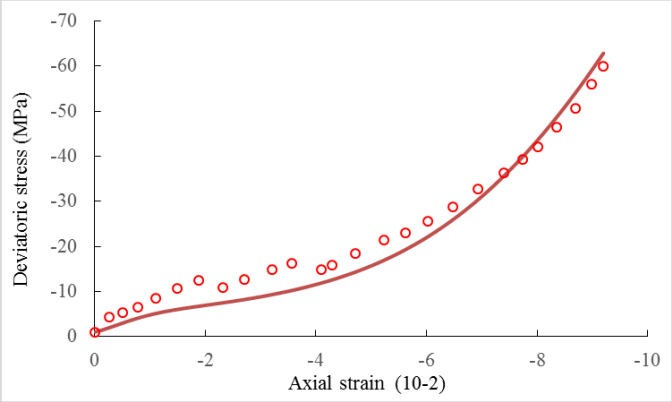

Figure 4.13 Comparison between numerical prediction by applying the associated plastic flow rule and experimental data for the oedometric test

4.5.2.2 Non-associated plastic flow for oedometric test

The values of the model parameters identified from the experimental data of the conventional triaxial compression tests lead to a remarkably overestimated axial stress. Apart from the first method, the non-associated plastic flow rule can be also used to improve the overestimated axial stress. In view of this and based on the sensitive analyzation of model parameters performed in previous section, we choose the following values of the model parameters for the prediction of the non-associated model as listed into Table 4.7.

In Figure 4.14, we show comparisons between experimental data and numerical predictions with a good agreement between them. The non-associated model can also significantly improve the prediction as well as the associated one (Figure 4.13).

But we should stress that if the values of the model parameters as listed into either Table 4.6 or Table 4.7 respectively corresponding to the associated and non-associated models are used to predict the mechanical behavior of the synthetic clay in the conventional compression tests, a less accurate for the two tests can also be observed through the comparison between experimental data and numerical simulations. The comparison is here not presented and discussed.

In a word, by means of the homogenization method, the influences of mesoscopic pore, pore collapse destruction should be taken into account for formula of macroscopic

criterion by means of the multiscale approaches in order to improve the model performance with more reasonable considerations.

Table 4.7 Typical values of parameters for the non-associated model for the synthetic clays "*Tx*"

Typical value of model parameters		
Synthetic clay	Phase-illite	Phase-sand
Elastic parameters	$E_s = 5GPa$	$E_i = 95GPa$
	$\mu_s = 0.33$	$\mu_i = 0.12$
Plastic parameters	$T_0 = 0.01$	
	$T_m = 0.77$	
	$b_1 = 150$	
	$t_0 = 0.01$	
	$t_m = 0.20$	
	$b_2 = 150$	
	$h = 0.7MPa$	
Physical parameters	$f =$	$\rho =$
	0.41	0.20

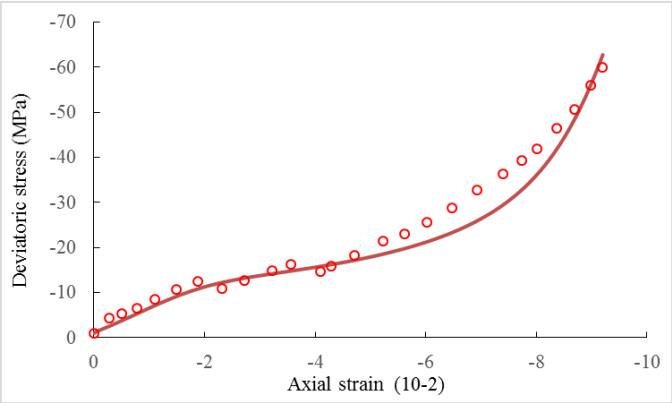

Figure 4.14 Comparison between numerical simulations by applying the non-associated plastic flow rule and experimental data for the oedometric test

4.6 Conclusion

A micromechanical-based macroscopic elastoplastic model is adopted to describe the mechanical behavior of synthetic clay. The effects of both mineral compositions and

porosity can be explicitly taken into account through the macroscopic criterion. Two types of macroscopic plastic flow rule (associated and non-associated) are considered. The adopted model is implemented in a conventional finite element method computation code. The following main remarks can be issued.

(1) Sensitive analyzations of model parameter on the model properties are presented where the dependencies of the macroscopic yield surface on porosity, volumetric fraction of sand, internal friction angle are presented respectively. By means of the M-C strength criterion and the expression form of the macroscopic yield criterion, the two strength parameters (cohesion and internal friction angle) are obtained. The cohesion of macroscopic material increase with increasing volumetric fraction of sand, but decreases with increase of porosity, as well as the internal friction angle. The influence of porosity on mechanical properties of the model is obviously stronger than the volumetric fraction of sand.

(2) The parameters of model are identified from triaxial compression test for a given mineral composition and then used to simulate triaxial compression tests for other synthetic clays with different mineral compositions, different macroscopic porosity and different loading paths. For the five different synthetic clays "*Gx*", if all pores exist solely inside the clay matrix, there is bad agreement between numerical prediction and experimental data regarding with increase of mass content of sand; whereas if the matrix microscopic porosities for the five different synthetic clays are set to be identical, a good agreement between numerical results and experimental data can be obesered.

(3) For the synthetic clay "*Tx*", an overestimated axial stress obtained from the model prediction can be observed for the loading path corresponding to the oedometric test. That's due to that once the model parameters are identified from the experimental data obtained from a specific loading path, the form of the macroscopic yield criterion in stress plane can be uniquely defined. The elliptic feature of the macroscopic criterion is not accordant with the practical geomaterials determined from experimental tests. Two methods are proposed to try to improve the performance of the model, the associated and non-associated plastic flow rule with alternative values of parameters solely identified from the oedometric test.

Chapter 5 Conclusions and Perspectives

5.1 General conclusions

The main objective of the work presented consists in a systematic experimental investigation on both consolidation properties and mechanical behavior of porous synthetic clay, also contains a numerical investigation on mechanical behavior of synthetic clay. The work can be divided into the following parts: (1) experimental studies on consolidation property, mechanical behavior and permeability of five different synthetic clays among which the mass proportion between illite and sand is set to be different; (2) experimental investigations on consolidation property and mechanical behavior of synthesis clay to provide a laboratory investigation for the offshore marine petroleum engineering; (3) calibration and verification for micromechanical model. Some details are addressed as follows:

After a general introductive review on experimental investigations and numerical simulations on consolidation property and mechanical behavior of synthetic clay, we have experimentally investigated in Chapter 1 the compaction behavior, porosity, compaction modulus, consolidation coefficient and permeability of the five different synthetic clays. First of all, considering the condition of large deformation of the synthetic clay in slurry, two self-designed consolidation oedometers have been developed by Laboratory of Mechanics of Lille (*LML*, Lille, France) in order to keep the applied pressure stability at a large range of pressure for the consolidation test. The consolidation test with consolidation pressure of about 35MPa have been performed step by step. The compaction time for each stage of consolidation is mainly based on the time for completion of primary consolidation. With increase of consolidation pressure, the compaction of synthetic clay become more and more difficult. Both permeability and porosity of synthetic clay decrease with augmentation of consolidation pressure, in contrary, compaction modulus presents an increasing trend. The consolidation coefficient is strongly dependent on mineral composition, and the optimal porosity of synthetic clay depends on both mineral composition and consolidation pressure. The influence of mineral composition on permeability of synthetic clay is significant. The difference of permeability among the five synthetic clays can arrive at two orders of magnitude.

In Chapter 2, we have experimentally investigated the mechanical behavior and permeability of the five synthetic clays obtained through the consolidation test carried out in Chapter 1. The triaxial compression tests with two different confining pressures have been conducted. The mechanical properties of synthetic clay such as initial elastic modulus and strength strongly depends on confining pressure and mineral composition. Both the initial elastic modulus and the strength increase with increasing confining

pressure as well as sand content. At a relatively low confining pressure, the initial nonlinear characteristic on the stress-strain curves becomes more significant and a quasi-perfect plastic flow or softening behavior can be observed rather than a continuous plastic hardening behavior at a relatively high confining pressure. Meanwhile, the characteristic of either plastic flow or plastic hardening of synthetic clay is also related to mineral composition. With increase of sand content, it is easy to occur a continuous plastic hardening behavior for the synthetic clay. The permeability of synthetic clay decreases with increase of confining pressure, and the influence of confining pressure on permeability is progressively weakened with increase of sand content. However, the influence of accumulated irreversible deformation on permeability during the process of deviatoric loading is not significant based on those chosen measured points. The transition from volumetric compressibility to dilatancy occurs much earlier and the volumetric dilatancy is more important under low confining pressure than high one. With the help of two plastic mechanical mechanisms, the correlations among volumetric strain, confining pressure and porosity/mineralogical composition for the synthetic clays have been interpreted as well as permeability.

In Chapter 3, in context of the exploitation of the offshore marine petroleum, consolidation test, with consolidation pressure identical to the current effective vertical pressure of the argillite in situ, have been performed on a specific chosen synthetic clay. The mineral proportion of the synthetic clay is set to be equal to the argillite one. The porosity of sample during consolidation is determined and briefly analyzed. Three types of triaxial compression tests have been conducted to investigate the influence of loading path and loading rate on mechanical behavior and microstructure evolution of synthetic clay, which are the oedometric test, conventional triaxial compression test, and conventional triaxial compression test after oedometric loading. The mechanical behavior of synthetic clay depends on confining pressure, loading rate and loading path. The higher the loading rate of axial strain, the greater the ratio of effective radial/lateral stress to effective axial stress. The volumetric strain and the transition from volumetric compressibility from dilatancy are obviously associated with confining pressure. On the other hand, the ultrasonic wave test have been simultaneously performed for all compression tests. The evolutions of velocities of both P- and S-waves at axial direction of sample depend on loading path and confining pressure. The velocity of P-wave increases with increase of confining pressure. The velocities of the two waves increase for the oedometric loading path. However, for the conventional triaxial compression loading path, the velocity of P-wave almost keeps constant or slightly increases, whereas the S-wave one always decreases at the process of deviatoric loading. The influence of loading rate on velocity of P-wave is insignificant. The variation of velocity of ultrasonic waves can be directly related to the microstructure evolution or elastic property of material. Accordingly, in terms of the correlation between the velocity of elastic wave and the dynamic elastic modulus, the evolutions of both the dynamic Young’s modulus and dynamic Poisson ratio of synthetic clay for the three

types of loading paths are also analyzed and discussed.

In the last part, the experimental results obtained from the synthetic clays ("*Gx*" and "*Tx*") is used to verify the suitability of the micromechanical-based macroscopic elastoplastic model proposed by Shen et al. (2013) for these synthetic clays. Based on the model, the clay matrix of synthetic clay is considered to be constructed by illite phase obeying to the Drucker and Prager type yield criterion, the sand is considered as the inclusion phase with a linear elasticity, and all pores only exist inside the clay matrix. The basic performance of the model is discussed through parameter sensitivity analysis such as porosity, fraction of inclusion, cohesion and internal friction angle of solid phase in the clay matrix. In particular, the influence of porosity and volumetric fraction of inclusion on mechanical behavior of material can be well reflected by the model. The values of model parameters are identified by means of the experimental results of the synthetic clay "*G2*", It can be shown through the comparisons between the numerical predictions and experimental data for the synthetic clays "*GxNx*" that the model may be not suitable to describe the mechanical behavior of synthetic clay, if all pores are considered to only exist inside the clay matrix. The porosity based on the model is defined as the micro-porosity. Nevertheless, based on the microphotograph observation of the two synthetic clays "*G1*" and "*G4*" obtained from the SEM, there are two types of pores: micro-pore and meso-pore. Thus, we assume that the microscopic porosity for the five synthetic clays can be considered to be identical due to same pre-consolidation pressure and mineral components in the five synthetic clays. Without consideration on meso-pore effect, a good agreement between modelling prediction and experimental data can be obtained. For the synthetic clays "*Tx*", the values of model parameters are identified through the experimental data obtained from the conventional triaxial compression tests. However, the model can't reproduce the mechanical behavior of the synthetic clay with different loading paths. Some interpretations on the significant difference between model prediction and experimental data have been discussed. Two different ways are proposed to improve the overestimated axial stress.

5.2 Perspectives

From a careful examination of the body of research, it is possible to suggest a number of perspectives for further experimental, theoretical researches and developments, accompanying with the help of measurement technique at microscopic scale, along this line.

- For the uniaxial consolidation test, it's interesting to investigate the evolution of lateral pressure during the consolidation process. The ratio between effective lateral stress and effective axial stress, K_0, is a critical parameter to know the mechanical property of material related to sedimentation, and the coefficient K_0 is very important for engineering design. Moreover, it's very interesting to

directly obtain the permeability of material during the consolidation process, an improvement on oedometer will be thus done.

- Considerations of different clay minerals such as smectite and kaolinite, different chemical solutions with different concentrations, temperature for consolidation property and mechanical behavior of synthetic clay are worthy of the further investigations

- In our study, the mineral composition of synthetic clays are known, but the pore size and distribution are unknown at present. Accordingly, it's very necessary to investigate the pore size and distribution by means of mercury intrusion test combined with microscopic scanning technologies such as X-Ray diffusion. When a comprehensive knowledge on microstructure and mineral composition of synthetic clay is obtained, a more suitable model can be proposed to give a more reasonable interpretation on the evolutions of mechanical behavior of synthetic clay with various loading paths. A micromechanical model taking into consideration of geometric nonlinearity will be performed in the next work, as well as consideration on geometric nonlinearity.

Appendix 1: Representative consolidation curves for the synthetic clays "*GxNx*"

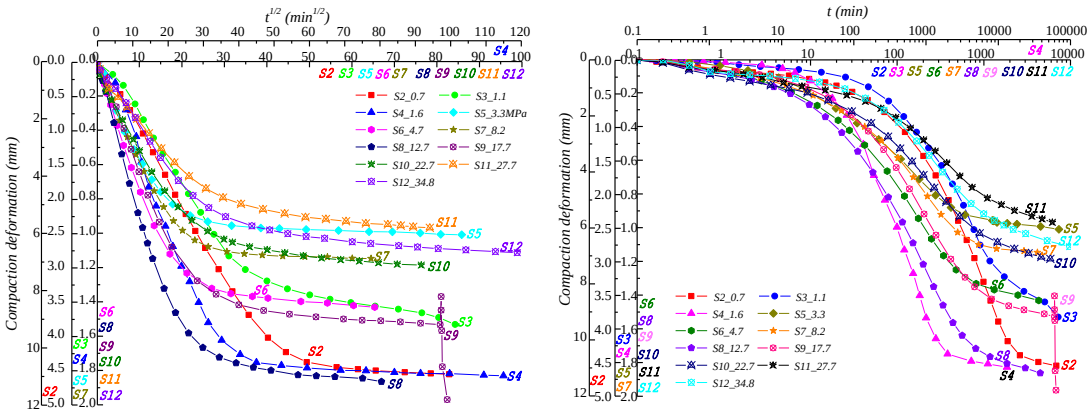

(a) G1N02 with FS:IC=15: 85

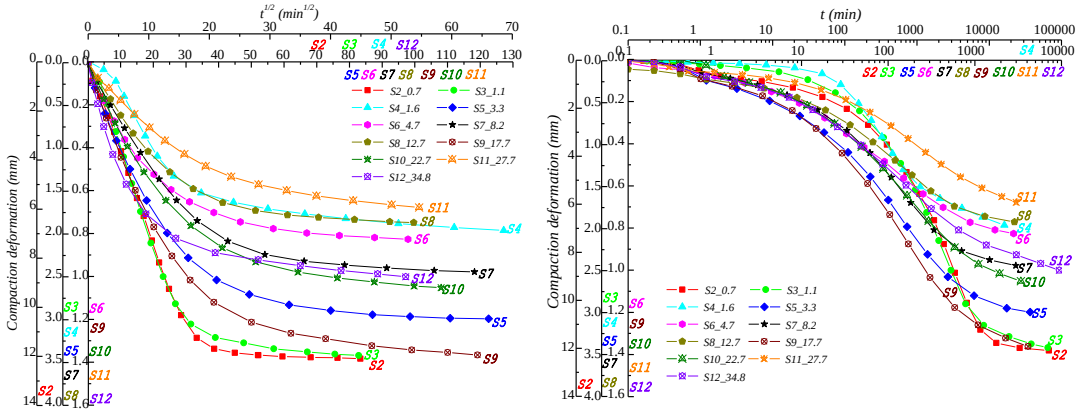

(b) G2N01 with FS:IC=30: 70

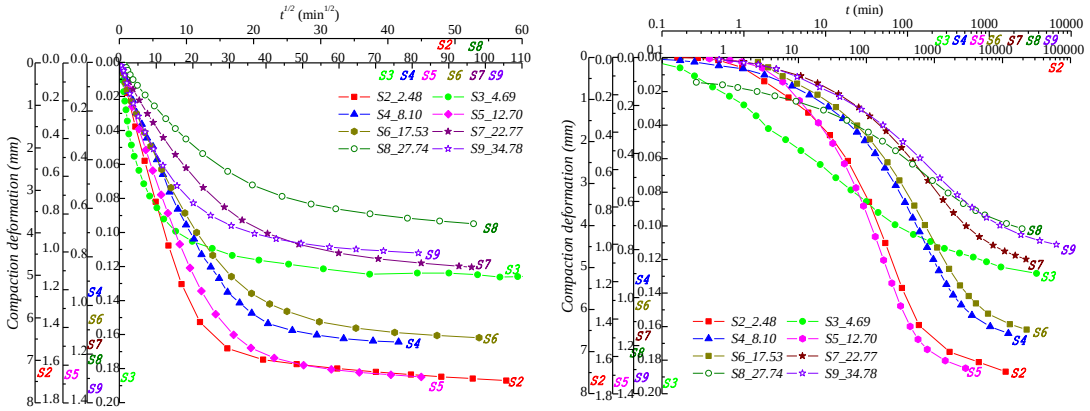

(c) G3N02 with FS:IC=45: 55

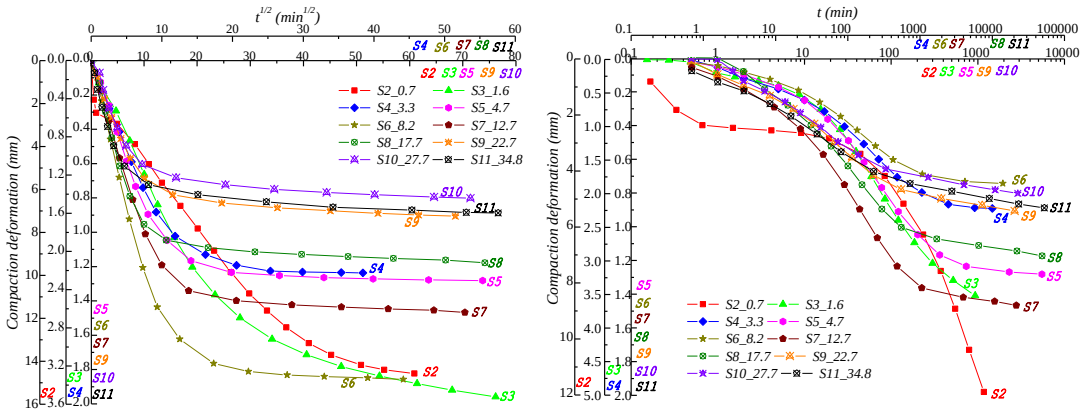

(d) G4N02 with FS:IC=45: 55

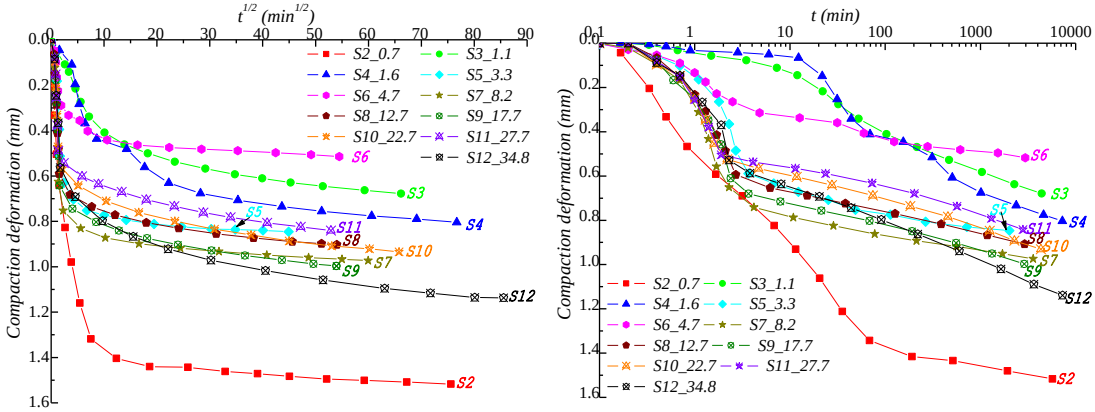

(e) G5N02 with FS:IC=45: 55

(1) Typical δ_{sc} versus $\sqrt{t}$ curves *(2) Typical δ_{sc} versus $lg(t)$ curves*

Figure.A. 1 Compaction deformation-time curves of the synthetic clays "GxNx" for each stage of consolidation pressure: (1) Typical $\delta_{sc} - \sqrt{t}$ curves; (2) Typical $\delta_{sc} - lg(t)$ curves

Appendix 2: Consolidation coefficient for synthetic clays "*GxNx*"

Table.A. 1 Consolidation coefficient of sample for each stage of consolidation pressure by applying the Taylor's method

Sample	Coefficient of consolidation at each level of consolidation pressure C_v(*10^{-8} m^2/s)										
	S2	S3	S4	S5	S6	S7	S8	S9	S10	S11	S12
G1N01	1.31	0.64	0.98	2.71	2.06	2.05	2.06	1.73	2.21	1.41	1.34
G1N02	1.18	1.17	1.09	4.83	3.44	2.43	2.40	1.91	1.59	1.05	1.07
G2N02	1.95	2.07	2.03	4.10	5.53	3.36	3.64	3.18	2.76	1.91	2.15
G2N02	0.87	0.77	0.58	2.17	1.94	2.30	2.04	1.88	1.93		2.81
G3N01	2.23	19.21	6.13	5.03	5.20	4.83	4.95	4.77			
G3N02	3.34	55.34	3.19	2.72	2.81	3.17	3.25	4.01			
G4N02	1.93	4.88	18.74	12.64	18.67	21.61	22.99	32.50	44.41	38.26	
G4N03	2.25	3.89	23.54	13.81	21.33	21.94	24.77	37.55	42.26	35.14	
G5N01	89.98	13.11	26.37	273.4	269.6	461.9	611.3	518.5	345.4	728.6	478.3
G5N02	68.74	20.68	27.77	347.8	249.2	477.9	393.3	536.3	314.5	553.7	462.1

Appendix 3: Representative photos for the synthetic clays "*GxNx*" after consolidation test

Figure.A. 2 Representative photos of sample for each type of the five synthetic clays "GxNx": (a) After consolidation tests but before triaxial compression test; (b) After triaxial compression test

Appendix 4: Photos of the synthetic clay "*Gx*" through *SEM*

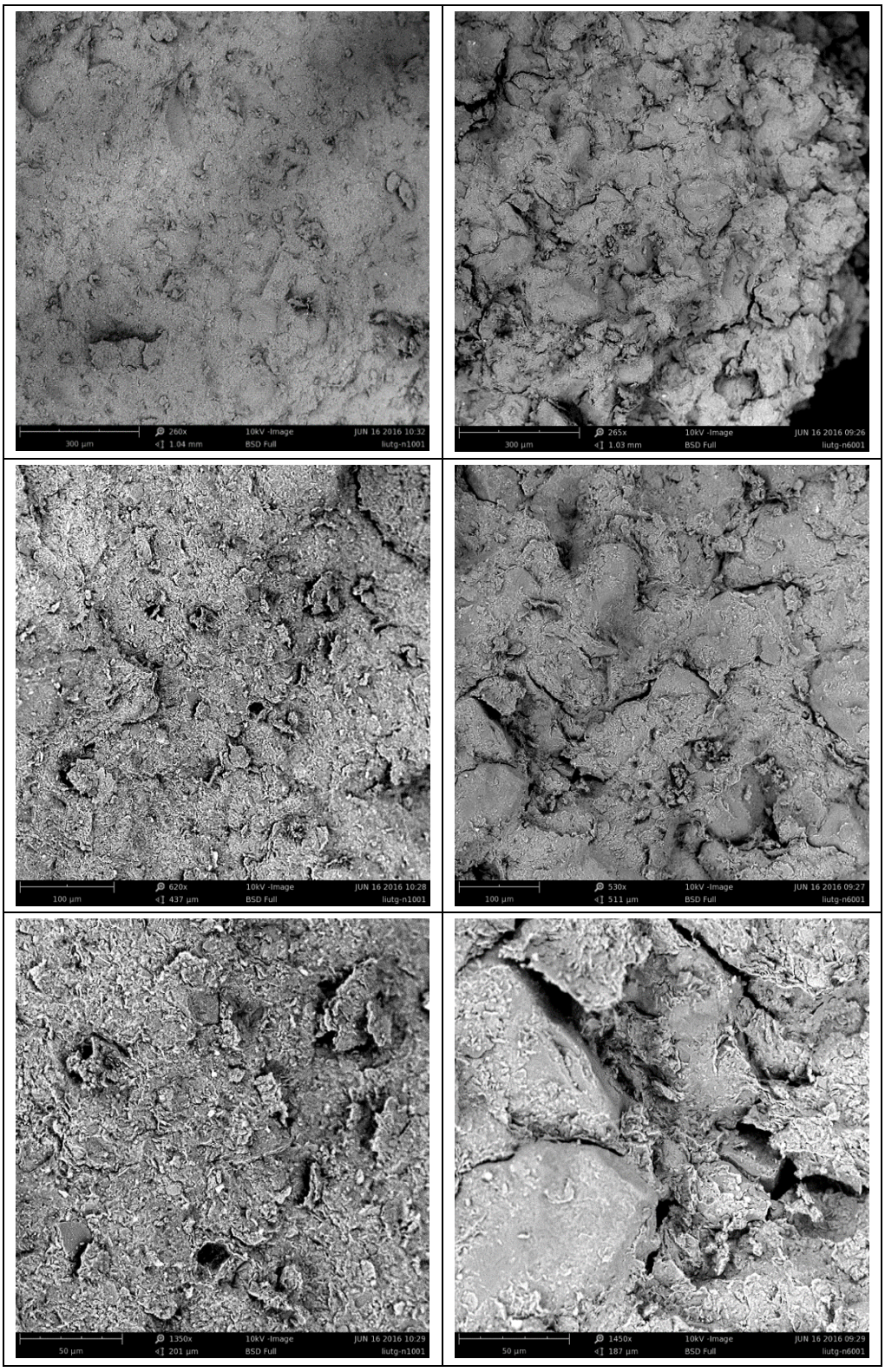

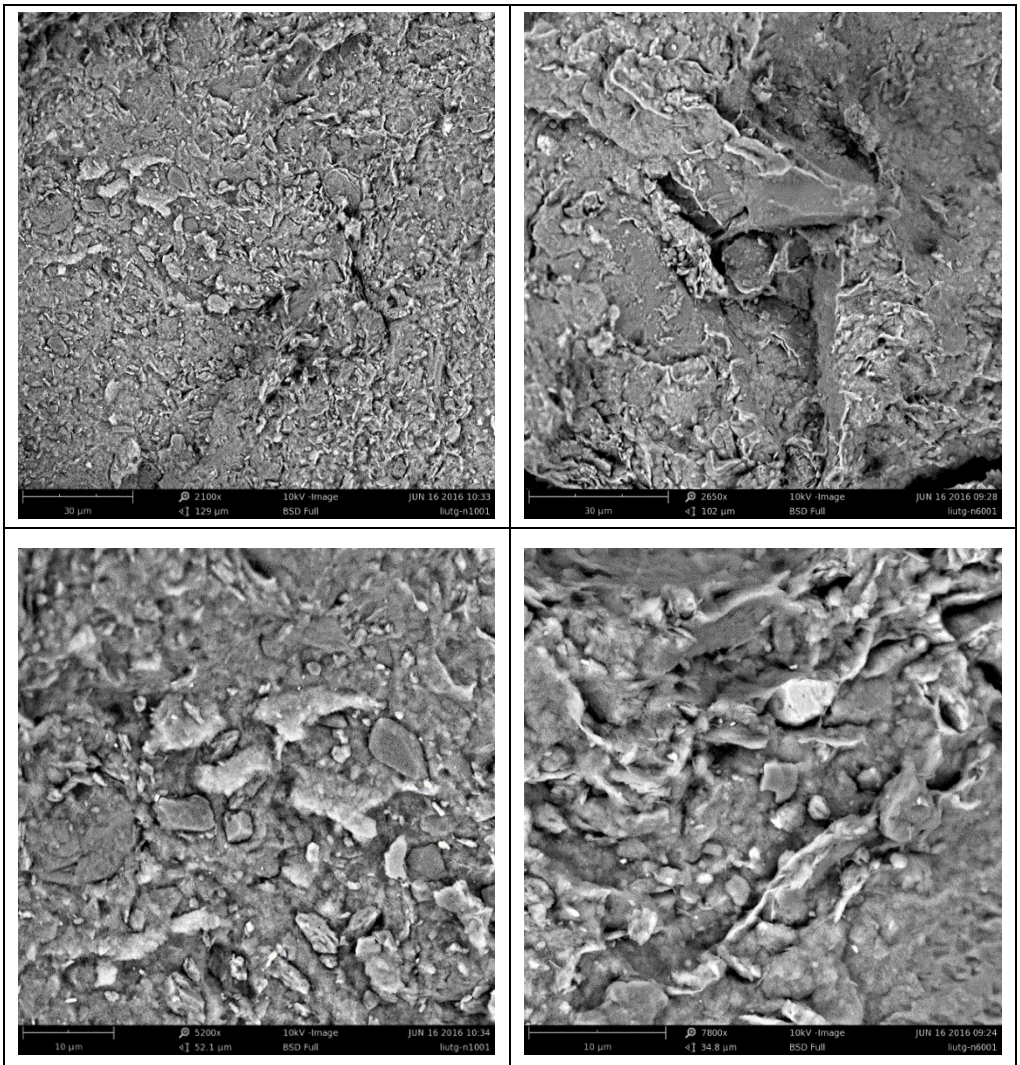

(1) G1N01: 15% sand	*(2) G4N02: 60% sand*

Figure.A.3 Microstructure of surface obtained through the SEM

Appendix 5: Photos of the synthetic clay "*Gx*" through *CT* scan

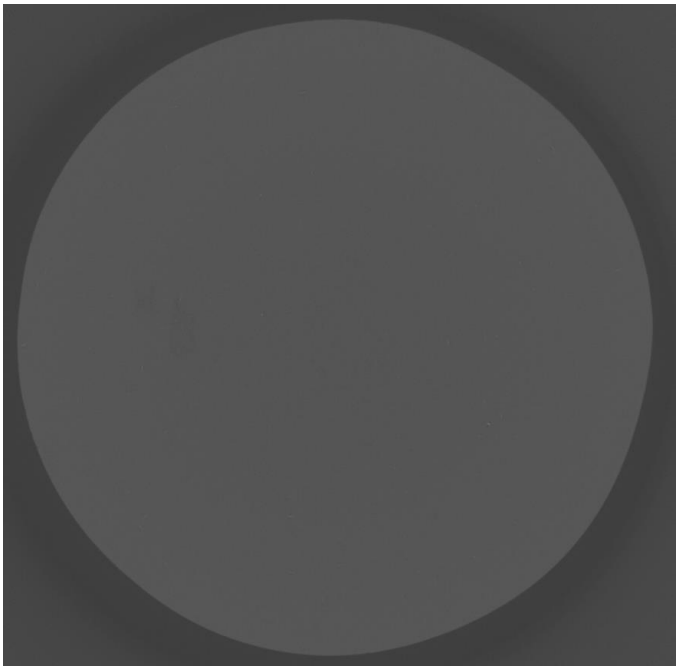

(a) Resolution of 26um for a pixel

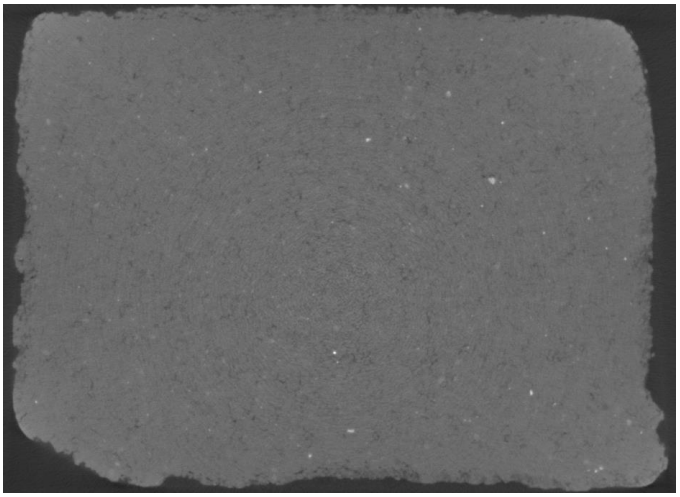

(b) Resolution of 10um for a pixel

Figure.A.4 Microstructure photos of one section through the CT scan

References

[1] Abou-Chakra G.A., Cormery F., Shao J.F., Kondo D. 2009. A multiscale modeling of damage and time-dependent behavior of cohesive rocks. International Journal for Numerical and Analytical Methods in Geomechanics. 33(5): 567-589.

[2] Adamson A. and Jostov M. 2006 Perspectives for the mining of oil shale and limestone with surface miner in Estonia. ISCSM Aachen. 1-6.

[3] Ahn H. and Jo H. 2009. Influence of exchangeable cations on hydraulic conductivity of compacted bentonite. Applied Clay Science. 44: 144-150.

[4] Al-Mukhtar M., Q Y., Alcover J.F., Bergaya F. 1999. Oedometric and water-retention behavior of highly compacted unsaturated smectites. Canadian Geotechnical Journal. 36: 675-684.

[5] Athy L.F. 1930. Density, porosity, and compaction of sedimentary rocks. American Association of Petroleum Geologists-Bulletin. 14(1): 1-24.

[6] Aubertin M. and Li L. 2004. A porosity-dependent inelastic criterion for engineering materials. International Journal of Plasticity. 20: 2179-2208.

[7] Auriault J.L. and Sanchez-Palencia E. 1977. Etude du comportement macroscopique d'unm milieu poreux sature deformable. Journal de Mecanique. 16: 575-603.

[8] Badrul Alam A.K.M., Niioka M., Fujii Y., Kodama J.I. 2014. Effects of confining pressure on the permeability of three rock types under compression. International Journal of Rock Mechanics and Mining Sciences. 65: 49-61.

[9] Bai B.J., Elgmati M., Zhang H., Wei M.Z. 2013. Rock characterization of Fayetteville shale gas plays. Fuel. 105: 645-652.

[10] Bai B. and Su Z.Q. 2012. Thermal responses of saturated silty clay during repeated heating-cooling processes. Transport in Porous Media. 93(1): 1-11.

[11] Baille W., Tripathy S., Schanz T. 2010. Swelling pressures and one-dimensional compressibility behavior of bentonite at large pressure. Applied Clay Science. 48(3): 324-333.

[12] Banthia B.S., M.S. King, Fatt I. 1965. Ultrasonic shear wave velocities in rocks subjected to simulated overburden pressure and internal pore pressure. Geophysics. 30(1): 117-121.

[13] Bandis S., Lumsden A.C., Barton N.R. 1981. Experimental studies of scale effects on the shear behavior of rock joints. International Journal of Rock Mechanics and Mining Sciences & Geomechanics Abstracts. 18(1): 1-21.

[14] Barden L., McGown A., Collins K. 1973. The collapse mechanism in partly saturated soil. Engineering Geology. 7(1): 49-60.

[15] Barthelemy J.F., Dormieux L. 2003. Determination of the macroscopic strength criterion of a porous medium by nolinear homogenization. Comptes Rendus Mecanique. 331: 271-277.

[16] Bennethum L.S., Murad M.A., Cushman J.H. 1997. Modified Darcy's law, Terzaghi's effective stress principle and Fick's law for swelling clay soils. Computers and Geotechnics. 20(3-4): 245-266.

[17] Berner E., Longuemare P., Vincke O. 2004. Poroelastic parameters of Meuse/Haut Marne argillites: effect of loading and saturation states. Applied Clay Science. 26: 366-369.

[18] Bianca S. 2008. The effect of montmorillonite nano-clay on mechanical and barrier properties of mung bean starch films. Thesis. Clemson University.

[19] Bikong C., Hoxha D., Shao J.F. 2015. A micro-macro model for time-dependent behavior of clayey rocks due to anisotropic propagation of microcracks. International Journal of Plasticity. 69: 73-88.

[20] Biot M.A. 1941. General theory of three0dimensional consolidation. Journal of Applied Physics. 12: 155-164.

[21] Biot M.A. 1955. Theory of elasticity and consolidation for a porous anisotropic solid. Journal of Applied Physics. 26: 182-185.

[22] Biot M.A. 1956a. Theory of propagation of elastic waves in a fluid-saturated solid, 1, Low frequency range. Journal of the Acoustical Society of America. 28(2): 168-178.

[23] Biot M.A. 1956b. Theory of propagation of elastic waves in a fluid-saturated solid, 2, Higher frequency range, Journal of the Acoustical Society of America. 28(2): 179-191.

[24] Blondel A. 2014. Developpement des methods geophysiques electriques pour la caracterisation des sites et sols pollues aux hydrocarbures. these de doctorat de L'universite Michel de Montaigne.

[25] Bolt G.H. 1956. Physicochemical analysis of the compressibility of pure clays. Geotechnique. 6:86-93.

[26] Bornert M., Vales F., Gharbi H., Nguyen Minh D. 2010. Multiscale full-field strain measurements for micromechanical investigations of the hydro-mechanical behavior of clayey rocks. Strain. 46: 33-46.

[27] Bornert M., Bretheau, T. Gilormini P. 2001. Homogeneisation en mecanique des

materiaux 1: materiaux aleatoires elastidques et milieu periodiques. Hermes Sciences Europe Ltd.

[28] Brace W.F., Walsh J.B., Frangos W.T. 1968. Permeability of granite under high pressure. Journal of Geophysical Research. 73(6): 2225-2236.

[29] Brandt H. 1955. A study of the speed of sound in porous granular material, ASME Journal of Applied mechanics. 22: 479-486.

[30] Brendan C. 2014. The consolidation and strength behavior of mechanically compressed fine-grained sediments. Thesis. Massachusetts Institute of Technology.

[31] Brooker E.W. and Ireland H.O. 1965. Earth pressures at rest related to stress history. Can. Geotech. J. 2: 1-15.

[32] Charlier R., Collin F., Pardoen B., Talandier J., Radu J.P., Gerard P. 2013. An unsaturated hydro-mechanical modelling of two in-situ experimental in Callovo-Oxfordian argillite. Engineering Geology. 165(24): 46-63.

[33] Chen Z.H. 1993. Consolidation theory of unsaturated soil based on the theory of mixture-II. Applied Mathematics and Mechanics. 14(8): 721-733.

[34] Coussy O. 1995. Mehcanis of porous continua. Wiley, New York.

[35] Davy C.A, Skoczylas F., Barnichon J.D., Lebon P. 2007. Physics and Chemistry of the Earth, Parts A/B/C. 32(8-14): 667-680.

[36] De Magistris F.S., Silvestri F., Vinale F. 1998. Physical and mechanical properties of a compacted silty sand with low bentonite fraction. Can. Geotech. J. 35: 909-925.

[37] Delage P. 2007. Microstructure feature in the behavior of engineered barriers for nuclear waste disposal. Exerimental Unsaturated Soil Mechanics. Springer. Berlin Heidelberg. 11-32.

[38] Delage P., Sultan N. and Cui Y.J. 2000. On the thermal consolidation of boom clay. Canadian Geotechnical Journal. 37: 343-354.

[39] Devapriya C., Wijeyesekera M.H., De Freita M.H. High-pressure consolidation of Kaolinite clay: geologic notes. American Association of Petroleum Geologists-Bulletin. 60(2): 293-298.

[40] Di Maio C., Snatoli L., Schiavone P. 2004. Volume change behavior of clays: the influence of mineral composition, pore fluid composition and stress state. Mechanics of Materials. 36: 435-451.

[41] Djeran-Maigre I., Tessier D., Grunberger D. Velde B., Vasseur G. Evolution of microstructures and of macroscopic properties of some clays during experimental

compaction. Marine and Petroleum Geology. 15(2): 109-128.

[42] Donald W. and Wilfred M. 1940. A theory of clay consolidation accounting for secondary compression. Journal of Mathematics and Physics. 19(1-4): 167-185.

[43] Dormieux L. Molinari A. Kondo D. 2002. Micromechanical approach to the behavior of poroelastic materials. Journal of the mechanics and Physics of Solids, 50: 2203-2231.

[44] Dutta J. and Mishra A.K. 2015. A study on the influence of inorganic salts on the behavior of compacted bentonites. Applied Clay Science. 116-117: 85-92.

[45] Eseme E., Littke R., Krooss B.M. 2006. Factors controlling the thermos-mechanical deformation of oil shales: implications for compaction of mudstones and exploitation. Marine and Petroleum Geology. 23(7): 715-734.

[46] Fabre G. and Pellet F. 2006. Creep and time-dependent damage in argillaceous rocks. International Journal of Rock Mechanics and Mining Sciences. 43(6): 950-960.

[47] Fan R.D., Du Y.J., Reddy K.R., Liu S.Y., Yang Y.L. 2014. Compressibility and hydraulic conductivity of clayey soil mixed with calcium bentonite for slurry wall backfill: initial assessment. Applied Clay Science. 101: 119-127.

[48] Ferrari A. and Laloui L. 2013. Advances in the testing of the hydro-mechanical behavior of shales. Multi-physical testing of Soils and Shales. Springer Series in Geomechanics and Geoengineering. pp: 57-68.

[49] Fityus S.G. and Buzzi O. 2009. The place of expansive clays in the framework of unsaturated soil mechanics. Applied Clay Science. 42: 150-155.

[50] Fortin J., Gueguen Y., Schubnel A. 2007. Effects of pore collapse and grain crushing on ultrasonic velocities and Vp/Vs. Journal of Geophysical Research. 112(B08207): 1-16.

[51] Gardner G.H.F., Wyllie M.R.J., Droschak D.M. 1965. Hysteresis in the velocity-pressure characteristics of rocks, Geophysics. 30(1): 111-116.

[52] Guery A.C. 2007. Contributions a la medolisation micromechanique du comportement non linearire de l'argilite du Callovo-Oxfordien. Thesis. Universite des Sciences et Technologies de Lille, France.

[53] Gueguen Y., Bouteca M. 2004. Mechanics of Fluid-Saturated Rocks. International Geophysics Series. Elsevier Academic Press.

[54] Guo T.F., Faleskog J. Shih C.F. 2008. Continuum modeling of a porous solid with pressure-sensitive dilatant matrix. Journal of the Mechanics and Physics of Solids. 56: 2188-2122.

[55] Gurson A.L. 1977. Continuum theory of ductile rupture by void nucleation and growth: Part I-yield criteria and flow rules for porous ductile media. Journal of Engineering Materials and Technology. 99: 2-15.

[56] Hamilton E.L. 1976. Variations of density and porosity with depth in deep-sea sediments. Journal of Sedimentary petrology. 46(2): 280-300.

[57] Han B., Xie S.Y., Shao J.F. 2016. Experimental investigation on mechanical behavior and permeability evolution of a porous limestone under compression. Rock Mechanics and Rock Engineering. 49(9): 3425-3435.

[58] Hayen R., Van Balen K., Van Gemert D. 2005. The mechanical behavior of mortars in triaxial compression. Structural Analysis of Historical Construction. Modena, Lourenco & Roca (eds). Taylor & Francis Group, London.

[59] Hofstetter G., Simo J.C., Taylor R.L. 1993. A modified cap model: closet point solution algorithms. Computers and Structures 46(2): 203-214.

[60] Homand S., Shao J.F. 2000. Mechanical behavior of a porous chalk and water/chalk interaction. Part II: numerical modelling. Oil &Gas Science and Technology. 55: 599-609.

[61] Hou Z.M., 2003. Mechanical and hydraulic behavior of rock salt in the excavation disturbed zone around underground facilities. Internal Journal of Rock Mechanics and Mining Sciences. 40: 725-735.

[62] Hoxha A., Giraud F., Homand C.A. 2007. Saturated and unsaturated behavior modelling of Meuse-Haute/Marne argillite. International Journal of Plasticity. 23(5): 733-766.

[63] Hsieh P.A., Tracy J.V., Neuzil C.E., Bredehoeft J.D., Silliman S.E. 1981. A transient laboratory method for determining the hydraulic properties of ‘tight’ rocks – I. Theory, International Journal of Rock Mechanics and Mineral Sciences and Geomechanics Abstracts. 18(3): 245-252.

[64] Hu D.W., Zhang F., Shao J.F., Gatmiri B. 2014a. Influence of Mineralogy and water content on the mechanical properties of argillite. Rock Mechanics and Rock Engineering. 47: 157-166.

[65] Hu D.W., Zhang F., Shao J.F. 2014b. Experimental study of poromechanical behavior of saturated claystone under triaxial compression. Acta Geotechnica. 9: 207-214.

[66] Huang Y., Shen W.Q., Shao J.F., Abou-Chakra G.A., Jia Y. 2014. Multi-scale modelling of time-dependent behavior of claystones with a viscoplastic compressible porous matrix. Mechanics of Materials. 79: 25-34.

[67] Hupers A. and Kopf A.J. 2009. The thermal influence on the consolidation state of underthrust sediments from the Nankai margin and its implications for excess pore pressure. 286(1-2): 324-332.

[68] Issen K.A. 2002. The influence of constitutive models on localization conditions for porous rock. Engineering Fracture Mechanics. 69: 1891-1906.

[69] Jiang T., Xu W.Y., Shao J.F. 2015. Multiscale study of the nonlinear behavior of heterogeneous clayey rocks based on the FFT method. Rock Mechanics and Rock Engineering. 48(2): 417-426.

[70] Karig D.E. and Hou G. 1992. High-stress consolidation experiments and their geologic implications. Journal of Geophysical Research. 97(B1): 289-300.

[71] Kim H.S., Cho G.C., Lee J.Y., Kim S.J. 2013. Geotechnical and geophysical properties of deep marine fine-grained sediments recovered during the second Ulleung Basin gas hydrate expedition, East Sea, Korea. Marine and Petroleum Geology. 47: 56-65.

[72] Kim H., Kwon H., Lee J., Cho N., Kim H. 2012. Thermal conductivity measurement of saturated clayey mixtures using oedometer consolidation and constant rate of strain consolidation tests. The Journal of Engineering Geology. 22(3): 275-281.

[73] Kurz K.H., Grosse C.U., Reinhardt H.W. 2005. Strategies for reliable automatic onset time picking of acoustic emissions and of ultrasound signals in concrete. Ultrasonics. 43: 538-546.

[74] Lado M. and Ben-Hur M. 2004. Soil mineralogy effects on seal formation, runoff and soil loss. Applied Clay Science. 24: 209-224.

[75] Lade P.V. 1977. Elastoplastic stress-strain theory for cohesionless soil with curved yield surface. International of Journal of Solids Structures. 13: 1019-1035.

[76] Lade P.V. and Kim M.K. 1995. Single hardening constitutive model for soil, rock and concrete. International Journal of Solids Structure. 1995. 32: 1963-1978.

[77] Lambe T.W. 1951. Soil testing for engineers, John Wiley, New York.

[78] Lambe T.W. and Whitman R.V. 1969. Soil Mechanics. John Wiley, New York.

[79] Larive E.2002. Etude experimentale des roches a tres faible permeabilite par la mise en oeuvure d'un permeabetre de precision. These a l'Universite Montpellier II.

[80] Lee J.M. and Shackelford C.D. 2005. Impact of bentonite quality on hydraulic conductivity of geosynthetic clay liners. Journal of Geotechnical and Geoenvironmental Engineering. 131(1): 64-77.

[81] Li W. 1999. Variation of pore water pressure and volume strain of saturated clayey soil under high pressure compression test. Chinese Journal of Geotechnical Engineering. 21(6): 666-669.

[82] Li W., Zhang Z., Sun R., Wang W., Li X. 2006. High pressure K0 creep experiment and the anisotropy of microstructure of deep buried clay. Chinese Journal of Geotechnical Engineering. 28(10): 1185-1190.

[83] Lide D.R. 2004. Handbook of Chemistry and Physics. CRC Press.

[84] Lin L., Shao J.F., Dijmedo K. 2011. A two scale model of porous rocks with Drucker-Prager matrix: application to a sandstone. Mechanics Research Communications 38(8): 602-606.

[85] Lin J., Xie S.Y., J.F. Shao, Kondo D. 2012. A micromechanical modeling of ductile behavior of a porous chalk: formulation, identification, and validation. International of Journal of Numerical and Analytical Methods in Geomechanics. 36(10): 1245-1263.

[86] Liu W., Li Y.P., Yang C.H., Daemen J.J.K., Yang Y., Zhang G.M. 2015. Permeability characteristics of mudstone cap rock and interlayers in bedded salt formations and tightness assessment for underground gas storage caverns. Engineering Geology. 193(2): 212-223.

[87] Liu Z.B., Shao J.F., Liu T.G., Xie S.Y., Conil N. 2016. Gas permeability evolution mechanism during creep of a low permeable claystone. Applied Clay Science. 129:47-53.

[88] Liu Z.B., Xie S.Y., Secq J., Shao J.F. 2014. Experimental investigation of mechanical behaviors of argillite from Angola under various loading condition. Rapport de Fin de Contrat. Total FR00007150:1-52.

[89] Liu Z.B., Xie S.Y., Shao J.F., Conil N. 2015. Effects of deviatoric stress and structural anisotropy on compressive creep behavior of a clayey rock. Applied Clay Science. 114: 491-496.

[90] Liu Z.B., Shao J.F., Xie S.Y., Secq J. 2015. Gas permeability evolution of clayey rocks in process of compressive creep test. Material Letters. 139: 422-425.

[91] Loto C.A. and Adebayo H. 1990. Effects of variation in water content, clay fraction and sodium carbonate additions on the synthetic moulding properties of Igbokoda clay and silica sand. Applied Clay Science. 5: 165-181.

[92] Magara K. 1980. Comparison of porosity-depth relationship of shale and sandstone. Journal of Petroleum Geology. 3(2): 175-185.

[93] Maghous S., Dormieux L. Barthelemy J.F. 2009. Micromechanical approach to the

strength properties of friction geomaterials. European Journal of Mechanics A/Solids. 28: 179-188.

[94] Malkawi A.I.H., Alawneh A.S., Abu-Safaqah O.T. 1999. Effects of organic matter on the physical and the physicochemical properties of an illitic soil. Applied Clay Science. 14(5-6): 257-278.

[95] Malecot Y., Daudeville L., Dypray F., Poinard C., Buzaud E. 2010. Strength and damage of concrete under high triaxial loading. European Journal of Environmental and Civil Engineering. 14(6-7): 777-803.

[96] Marcial D., Delage P., Cui Y.J. 2002. On the high stress compression of bentonites. Canadian Geotechinical Journal. 39(4): 812-820.

[97] Masri M., Sibai M., Shao J.F., Mainguy M. 2014. Experimental investigation of the effect of temperature on the mechanical behavior of Tournemire shale. International Journal of Rock Mechanics and Mining Sciences. 70: 185-191.

[98] Martin P.L., Barcala J.M., Huertas F. 2006. Large-scale and long-term coupled thermos-hydro-mechanic experiments with bentonite: the FEBEX mock-up test. Journal of Iberian Geology. 32(2): 259-282.

[99] Meerea P.A. and Mulchrone K.F. 2003. The effect of sample size on geological strain estimation from passively deformed clastic sedimentary rocks. Journal of Structural Geology. 25: 1587-1595.

[100] Mishra A.K, Ohtsubo M., Li L.L., Higashi T., Park J. 2009. Effect of salt of various concentrations on liquid limit, and hydraulic conductivity of different soil-bentonite mixtures. Environmental Geology. 57(5):1145-1153.

[101] Mishra A., Ohtsubo M., Li L., Higashi T. 2011. Controlling factors of the swelling of various bentonites and their correlations with the hydraulic conductivity of soil-bentonite mixtures. Applied Clay Science. 52(1-2): 78-84.

[102] Mondol N.H., Bjorlykke K., Jahren J., Hoeg K. 2007. Experimental mechanical compaction of clay mineral aggregates-- changes in physical properties of mudstones during burial. Marine and Petroleum Geology. 24(5): 289-311.

[103] Monfared M., Delage P., Sunlem J., Mohajerani M., Tange A.M., De Laure E. 2011. A new hollow cylinder triaxial cell to study the behavior of geo-materials with low permeability. International Journal of Rock Mechanics and Mining Sciences. 48:637-649.

[104] Monte J.L. and Krizek R.J. 1976. One-dimensional mathematical model for large-strain consolidation. Geotechnique. 26(3): 495-510.

[105] Mori T. and Tanaka K. 1973. Average stress in a matrix and average elastic energy

of materials with misfitting inclusions. Acta Metallurgica et Materialia. 42(7): 597-629.

[106] Mowar S., Zaman M., Steams D.W., Roegiers J.C. 1996. Micro-mechanisms of pore collapse in limestone. Journal of Petroleum Science and Engineering. 15(2-4): 221-235.

[107] Neuzil C.E., Cooley C., Silliamn S.E., Bredehoeft J.D., Hsieh P.A. 1981. A transient laboratory method for determining the hydraulic properties of 'tight' rocks – II. Application, International Journal of Rock Mechanics and Mineral Sciences and Geomechanics Abstract. 18: 253-258.

[108] Nyakairu G.W.A. and Koeberl C. 2001 Mineralogical and chemical composition and distribution of rare earth elements in clay-rich sediments from central Uganda. Geochemical Journal. 35: 13-28.

[109] Oscar C., Valdiviezo M., Ruben N.L. 2014. Dynamic characterization of shale systems by dispersion and attenuation of P- and S-waves considering their mineral composition and rock maturity. Journal of Petroleum Science and Engineering. 122: 420-427.

[110] Panet M., Fourmaintraux D. 2004. La mecanique des roches appliquee aux ouvrages du genie-civil. CRC press.

[111] Park K., Lee J., Yoon H., Kim D. 2016. Hydraulic and thermal conductivities of Kaolin-Silica mixtures under different consolidation stresses. Marine Georesources & Geotechnology. 34(6): 532-541.

[112] Pereira J.P., De Freita M.H. 1993. Mechanisms of shear failure in artificial fractures of sandstone and their implication for models of hydromechanical coupling. Rock Mechanics and Rock Engineering. 26(3): 195-214.

[113] Prashant A. 2004. Three-dimensional mechanical behavior of kaolin clay with controlled microfabric using true triaxial testing. Thesis. University of Tennessee-Knoxville.

[114] Rendulic L. 1935. Der hydrodynamische spannungsangleich in zentral entwasserten Tonzylindren. Wasserwirt. Tech. 2: 250-253 & 269-273.

[115] Robinet J.C. 2008. Mineralogie, porosite et diffusion des solutes dans l'argilite du Callovo-Oxfordien de Bure (Meuse, Haut-Marne, France) de l'echelle centimetrique a micrometrique. These. Laboratoire Hydrogeologie, argiles, sols et alterations. Universite de Poitiers, Poitiers.

[116] Robinet J.C., Sardini P., Coelho D., Parneix J.C., Pret D., Sammartino S., Boller E., Altmann S. 2012. Effects of mineral distribution at mesoscopic scale on solute diffusion in a clay-rich rock: example of the Callovo-Oxfrodian mudstone (Bure,

France). Water Resources Research. 48(5): 1-17.

[117] Shackelford C., Sevick G., Eykholt G. 2010. Hydraulic conductivity of geosynthetic clay liners to tailings impoundment solutions. Geotextiles and Geomembranes. 135(12): 1941-1956.

[118] Shang X.Y., Zhou G.Q., Kuang L.F, Cai W. 2014. Compressibility of deep clay in east china subjected to a wide range of consolidation stresses. Canadian Geotechnical Journal. 51: 1-7.

[119] Shen W.Q. 2011 Modelisations micro-macro du comportement mecanique des materiaux poreux ductiles: application a l'argillite du Callovo-Oxfordien. Thesis. University of Lille 1, France.

[120] Shen W.Q., Shao J.F., Kondo D. Gatmiri B. 2012. A micro-macro model for clayey rocks with a plastic compressible porous matrix. International Journal of Plasticity. 36: 64-85.

[121] Shen W.Q., Kondo D., Dormieux L., Shao J.F. 2013. A closed-form three scale model for ductile rocks with a plastically compressible porous matrix. Mechanics of Materials. 59: 73-86.

[122] Shen W.Q. and Shao J.F. 2016a. An elastic-plastic model for porous rocks with two populations of voids. Computers and Geotechnics. 76: 194-200.

[123] Shen W.Q. and Shao J.F. 2016b. An incremental micro-macro model for porous geomaterials with double porosity and inclusion. International Journal of Plasticity. 83: 37-54.

[124] Shima S. and Oyane M. 1976. Plasticity theory for porous metals. International of Journal of Mechanical Science. 18: 285-291.

[125] Skempton A.W. 1969. The consolidation of clays by gravitational compaction. Quarterly Journal of the Geological Society. 125: 373-411.

[126] Sleeman R. and Eck T.V. 1999. Robust automatic p-phase picking: An online implementation in the analysis of broadband seismogram recordings. Physics of the Earth and Planetary Interiors. 113: 265-275.

[127] Soe A.K.K, Osada M., Win T.T.N. 2010. Drying-induced deformation behavior of Shirahama sandstone in no loading regime. Engineering Geological. 114: 423-432.

[128] Sone H. and Zoback M.D. 2010. Strength, creep and frictional properties of gas shale reservoir rocks. American Rock Mechanics Association. Pages (5)

[129] Sone H. and Zobakc M.D. 2013. Mechanical properties of shale-gas reservoir rocks-part 1: static and dynamic elastic properties and anisotropy. Geophysics.

78(5): D381-D392.

[130] Sridharan A., and Jayadeva M.S. 1982. Double layer theory and compressibility of clays. Geothenique. 32(2): 133-144.

[131] Srodori J., Drits V.A., McCarty D.K., Hsieh J.C.C. Eberl D.D. 2001. Quantitative X-Ray diffraction analysis of clay-bearing rocks from random preparations. Clays and Clay Minerals. 49(6): 514-528.

[132] Suarez-Rivera F.R., Cook N.G.W., Cooper G.A., Zheng Z. 1990. Indentation by pore collapse in porous rocks. American Rock Mechanics Association. The 31th U.S. Symposium on Rock Mechanics, Golden, Colorado.

[133] Suquet P. 1995. Overall properties of nonlinear composites: a modified secant moduli approach and its link with Ponte Castaneda's nonlinear variational procedure. Comptes Rendus de L'Academie des Sciences. Paris. IIB, 320: 563-571.

[134] Terzaghi K. 1925. Principles of soil mechanics. IV—settlement and consolidation of clay. Engineering News-Record. 95(3): 874-878.

[135] Terzaghi K. 1943. Theoretical soil mechanics. New York: John Wiley and Sons, INC. pp. 265-296.

[136] Todd T. and Simmons G.1972. Effect of pore pressure on the velocity of compressional waves in low-porosity rocks. Journal of Geophysical research. 77(20): 3731-3743.

[137] Trimmer D.A. 1981. Design criteria for laboratory measurements of low permeability rocks. Geophysical Research Letters. 8(9): 973-975.

[138] Tripathy S. and Schanz T. 2007. Compressibility behavior of clays at large pressures. Canadian Geotechnical Journal. 44(3): 355-362.

[139] Turan A., Hincheberger S.D., EI Naggar M.H. 2009. Mechanical characterization of an artificial clay. Journal of Geotechnical and Geoenvironmental Engineering. 134(2): 280-290.

[140] Xie S.Y. and Shao J.F. 2006, Elatoplastic deformation of a porous rock and water interaction. International Journal of Plasticity. 22: 2195-2225.

[141] Xie S.Y. and Shao J.F. 2012. Experimental investigation and poroplastic modeling of saturated porous geomaterials. International Journal of Plasticity. 39: 27-46.

[142] Vasseur G. 1995. Evolution of structural and physical parameters of clays during experimental compaction. Marine and Petroleum Geology. 12(8): 941-954.

[143] Velde B. 1996. Compaction trends of clay-rich deep sea sediments. Marine

Geology. 133: 193-201.

[144] Vales F., Nguyen M.D., Gharbi H., Rejeb A. 2004. Experimental study of the influence of the degree of saturation on physical and mechanical properties in Tournemire shale (France). Applied Clay Science. 26: 197-207.

[145] Walsh J.B. 1965. The effect of cracks on the compressibility of rock. Journal of geophysical Research. 70(2): 381-389.

[146] Wang Q. 2012. Hydro-mechanical behavior of bentonite-based materials used for high-level radioactive waste disposal. Thesis. Universite Paris-Est.

[147] Wang Q., Tang A.M., Cui Y.J., Delage P., Barnichon, J.D. 2013. The effects of technological voids on the hydro-mechanical behavior of compacted bentonite-sand mixture. Soils and foundations. 53(2): 232-245.

[148] Wong R.H.C., Chau K.T., Tang C.A., Lin P. 2001. Analysis of crack coalescence in rock-like materials containing three flaws-Part I: Experimental approach. International Journal of Rock Mechanics and Mining Sciences. 38(7): 909-924.

[149] Xue Q., Zhang Q., LIU L. 2012. Impact of high concentration solutions on hydraulic properties of geosynthetic clay liner materials. Materials. 5(11): 2326-2341.

[150] Yang S.Q., Jiang Y.Z., Xu W.Y., Chen X.Q. 2008. Experimental investigation on strength and failure behavior of pre-cracked marble under conventional triaxial compression. International Journal of Solids and Structures. 45: 4796-4819.

[151] Yilmaz I. and Marchalko M. 2014. The effect of different types of water on the swelling behavior of expansive clays. Bulletin of Engineering Geology and the Environment. 73(4): 1049-1062

[152] Yven B., Sammartino S., Gegraud Y., Homand F., Villieras F. 2007. Mineralogy, texture and porosity of Callovo-Oxfordian argillites of the Meuse/Haute-Marne region (Eastern Paris Basin). Memoires de la Societe Geologique de France. 178: 73-90.

[153] Yun T.S., Santamarina J.C., Ruppel C. 2007. Mechanical properties of sand, silt, and clay containing tetrahydrofuran hydrate. Journal of Geophysical research. 112: B04106 (1-13)

[154] Zeng T., Shao J.F., Xue W.Y. 2014. Multiscale modeling of cohesive geomaterials with a polycrystalline approach. Mechanics of Materials. 69(1): 132-145.

[155] Zhang C.L. and Rothfuchs T. 2004. Experimental study of the hydro-mechanical behavior of the Callovo-Oxfordian argillite. Applied Clay Science. 26(1-4): 325-336.

[156] Zhang F. 2011. Comportement mecanique des argilites de MHM-influences de la saturation, de la composition mineralogique et de la temperature. Thesis. Universite Lille 1- Sciences et Technologies, Lille, France.

[157] Zhang F., Xie S.Y., Hu D.W., Shao J.F., Gatmiri B. 2012. Effect of water content and structural anisotropy on mechanical property of claystone. Applied Clay Science. 69: 79-86.

[158] Zhang M., Takahashi M., Morin R.H. 2000. Evolution and application of the transient-pulse technique for determining hydraulic properties of low permeability rocks – part 1: theoretical evaluation. ASTM Geothenical Testing Journal, 23(1): 83-90.

[159] Zhou H., Bian H.B., Jia Y., Shao J.F. 2013. Elastoplastic damage modeling the mechanical behavior of rock-like materials considering confining pressure dependency. Mechanics Research Communications. 53: 1-8.

[160] Zhu W., Baud P., Wong T.F. 2010. Micromechanics of cataclastic pore collapse in limestone. Journal of Geophysical Research Solid Earth. 115(B4): 4405-4421.

[161] Zhu W., Wong T.F. 1997. The transition from brittle faulting to cataclastic flow: permeability evolution. Journal of Geophysical Research. 102: 3027-3041.

[162] Zhu W., Montesi L.G.J., Wong T.F. 1997. Shear-enhanced compaction and permeability reduction: triaxial extension tests on porous sandstone. Mechanics of Materials. 25: 199-214.